Copyright

by

Daniel Ray Popp

2004

UTrAp 2.0: Linearized Buckling Analysis of Steel Trapezoidal Girders

by

Daniel Ray Popp, B.S.C.E.

Thesis

Presented to the Faculty of the Graduate School of

The University of Texas at Austin

in Partial Fulfillment

of the Requirements

for the Degree of

Master of Science in Engineering

The University of Texas at Austin

May 2004

UTrAp 2.0: Linearized Buckling Analysis of Steel Trapezoidal Girders

Approved by
Supervising Committee:

Eric B. Williamson

Joseph A. Yura

to my family

for my Lord

Acknowledgements

I would like to express my sincere gratitude and appreciation to Professor Eric Williamson, who supervised this research project. He no doubt rues the day he gave me an office just across the hall from his, allowing me to bother him incessantly with questions. Each one has been answered patiently, with never a hint of exasperation. He has given me guidance on many topics, from engineering to life in general. Thank you, Dr. Williamson, for your mentorship. Gratitude is also due Dr. Joseph Yura, who contributed a great deal to my research and encouraged me along the way.

My research would not have been possible without the prior efforts of Cem Topkaya, the original author of UTrAp. He promptly answered every question I had about the program and gave me many ideas for its improvement. I also wish to thank my friend and fellow graduate student Widianto, whose constant cheer is always an encouragement. He assisted me with the program verification and was generally indispensable. Dilip Maniar was also a great help to me in many ways, and I am thankful to him. The generous funding of the Texas Department of Transportation is also acknowledged.

Finally, I thank both of my families. I am especially thankful to Jill, who will soon be my wife, for her love and support during the entire project and for her belief in me. And not least, I thank God, who fulfilled His promise to establish my thoughts.

May 7, 2004

Abstract

UTrAp 2.0: Linearized Buckling Analysis of Steel Trapezoidal Girders

Daniel Ray Popp, M.S.E.

The University of Texas at Austin, 2004

Supervisor: Eric B. Williamson

Steel trapezoidal box-girder bridges have been gaining popularity due to their aesthetic appeal and structural efficiency. The completed closed section resists torsion very efficiently, making it an attractive choice for curved bridges. Under construction loading, however, the section is open or pseudo-closed, offering very little torsional capacity. Thus, the construction stage is critical in the response of these systems.

The stability of a girder in the construction process is of particular concern. Numerous failures of individual brace members have been observed, and global buckling failures have occurred in two bridges under construction in the past several years, one of which resulted in loss of life. In order to provide a tool for understanding and predicting the buckling behavior of steel trapezoidal girders, the elastic analysis program UTrAp has been modified to include a buckling analysis capability. UTrAp 2.0 performs a linearized buckling analysis, using the finite element model developed previously. Geometric nonlinearity is

included, but material nonlinearity is not taken into account. The program finds the buckling load as a scalar multiple of the applied load, assuming linear-elastic behavior. Included in the output are deflections and rotations of the girder to assist a designer in visualizing the buckled shape. A comparison with the results of general finite element software shows that UTrAp 2.0 accurately predicts the linearized buckling load.

Table of Contents

List of Tables ..... **xi**

List of Figures ..... **xii**

CHAPTER 1 INTRODUCTION **1**

1.1 Background 1

1.2 Previous Work 4

1.3 Scope 5

1.4 Organization 6

CHAPTER 2 BUCKLING ANALYSIS FORMULATION **8**

2.1 Types of Structural Analysis 8

2.1.1 Elastic Critical Load Analysis 9

2.2 Element Formulations 9

2.2.1 Shell Element Elastic Stiffness 10

2.2.2 Shell Element Geometric Stiffness 13

2.2.3 Truss Element Elastic Stiffness 16

2.2.4 Truss Element Geometric Stiffness 16

2.2.5 Spring Element Stiffness 21

2.2.6 Web Stiffener Element Elastic Stiffness 21

2.2.7 Web Stiffener Element Geometric Stiffness 25

2.3 Summary 26

CHAPTER 3 THE EIGENPROBLEM 27

3.1 Eigenproblems Mathematically 27

3.1.1 Eigenproblem Example 28

3.1.2 Solution Methods 30

3.2 Eigenproblems in Buckling Analysis 31

3.2.1 Solving the Generalized Eigenproblem 32

3.3 Eigenproblem Software 35

3.3.1 ARPACK 36

3.4 Summary 40

CHAPTER 4 PROGRAM VERIFICATION 41

4.1 Theory 41

4.2 Finite-Element Software 45

4.2.1 Model 1 Girder 45

4.3 Case Study of Marcy Bridge Collapse 49

4.3.1 Comparison with ANSYS 53

4.4 Summary 53

CHAPTER 5 UTRAP 2.0 USER'S GUIDE 55

5.1 Capabilities and Limitations 55

5.1.1 Straight versus Curved Girders 56

5.2 Graphical User Interface 57

5.2.1 Example Problem Definition 57

5.2.2 UTrAp 2.0 Menus 58

5.2.3 Buckling Analysis Output 84
5.3 Other Issues 88
5.4 Summary 88
CHAPTER 6 GLOBAL INSTABILITY 89
6.1 Buckling 89
6.2 Lateral Torsional Buckling of a Trapezoidal Section 90
6.2.1 Example of Determining Critical Stress 97
6.2.2 Non-uniform Moment Loading 101
6.3 Top Lateral Bracing 103
6.3.1 Example of Determining Critical Stress with Top Lateral Bracing 107
6.4 Summary 109
CHAPTER 7 CONCLUSIONS AND FUTURE RESEARCH 111
7.1 Conclusions 111
7.1.1 Lateral Torsional Buckling 113
7.2 Further Research 113
Appendix A Eigensolver References 115
References 116
Vita 121

List of Tables

Table 3.1: Eigensolver mode comparison 38

Table 6.1: C_b factors for trapezoidal box-girder bridges 102

List of Figures

Figure 1.1: Cross-section of a steel trapezoidal box girder (US Steel, 1978) 1
Figure 1.2: Local failure of bracing member during construction (Chen, 2002) ... 2
Figure 1.3: Collapse of pedestrian bridge near Marcy, New York
(Utica Observer-Dispatch) 3
Figure 2.1: Nine-noded shell element (Topkaya, 2002) 10
Figure 2.2: Web stiffeners and internal brace 22
Figure 2.3: Web stiffener element 23
Figure 2.4: Predicted web stiffener deflections 25
Figure 3.1: Comparison of eigensolver modes 39
Figure 4.1: First plate buckling mode from UTrAp 2.0 44
Figure 4.2: Second plate buckling mode from UTrAp 2.0 44
Figure 4.3: Third plate buckling mode from UTrAp 2.0 44
Figure 4.4: ANSYS buckled shape for 50´ Model 1 girder 46
Figure 4.5: UTrAp 2.0 buckled shape for 50´ Model 1 girder 47
Figure 4.6: Section dimensions of Marcy pedestrian bridge 50
Figure 4.7: UTrAp 2.0 model of Marcy pedestrian bridge 51
Figure 4.8: UTrAp buckled cross-section of Marcy bridge 52
Figure 4.9: Marcy bridge buckled shape from ANSYS 53
Figure 5.1: Geometric Properties form 59
Figure 5.2: Plate Properties form 61
Figure 5.3: Internal and external brace types 63
Figure 5.4: Top lateral brace types 63

Figure 5.5: Internal Braces tab 65
Figure 5.6: Top Lateral Braces tab 65
Figure 5.7: Web Stiffeners tab 66
Figure 5.8: Support Locations form 67
Figure 5.9: Stud Properties form 68
Figure 5.10: Pour Sequence form 70
Figure 5.11: UTrAp 2.0 main window 71
Figure 5.12: Linear Analysis screen 72
Figure 5.13: Buckling Analysis screen 73
Figure 5.14: Table of incremental deflections 74
Figure 5.15: Diagram of incremental deflections 75
Figure 5.16: Table of incremental shear values 76
Figure 5.17: Diagram of incremental shear values 77
Figure 5.18: Table of incremental normal stress values 78
Figure 5.19: Diagram of incremental normal stresses 79
Figure 5.20: Visualization of incremental normal stresses on cross-section 80
Figure 5.21: Table of incremental axial forces in internal braces 81
Figure 5.22: Chart of incremental axial forces in internal braces 82
Figure 5.23: Analysis Summary form 83
Figure 5.24: Deflections just prior to buckling 86
Figure 5.25: Buckled Shape form 87
Figure 6.1: Shear center of a trapezoidal cross-section 91
Figure 6.2: Notation for flange integration 93

Figure 6.3: Notation for web integration 95
Figure 6.4: Properties of Model 1 girder 98
Figure 6.5: Predicted critical buckling stresses versus length for Model 1 girder 100
Figure 6.6: Open section girder with struts 103
Figure 6.7: Top lateral bracing systems 104
Figure 6.8: Trapezoidal girder plan view with and without top lateral bracing. 105
Figure 6.9: Top lateral bracing for Model 1 girder 107

CHAPTER 1
Introduction

"The beginning is the most important part of the work."

- Plato

1.1 BACKGROUND

Since being introduced in the United States in the early 1960s, steel box-girder bridges have grown in popularity. Hundreds of these structures have been built over the last four decades, including several dozen in the state of Texas. The torsional rigidity of the completed section makes it ideal for curved bridges such as those in large highway interchanges. A box girder's clear expression of structural function enhances the bridge's aesthetic appeal, an increasingly important aspect of design.

Steel box girders typically utilize sloping webs in order to decrease the width of the bottom flange, leading to the designation "trapezoidal". A cross-section of a typical steel trapezoidal box-girder bridge is shown in Figure 1.1.

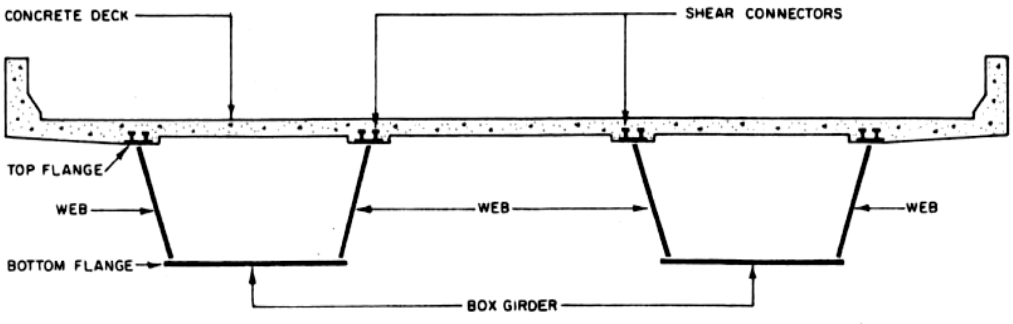

Figure 1.1 Cross-section of a steel trapezoidal box girder (US Steel, 1978)

Shear connectors on the top flanges of the girders allow the concrete deck to act compositely with the steel girder, resulting in a very stiff completed section that is more than adequate for carrying live loads during its service life. However, during construction, the steel section alone must resist the loads, which are due primarily to the dead weight of the concrete during the deck pour. Thus, the construction phase is often critical in the design of steel trapezoidal box-girder bridges.

Figure 1.2 Local failure of bracing member during construction (Chen, 2002)

A majority of the problems that have occurred with steel box-girder bridges have taken place during construction, including all of the overall failures. Three major collapses occurred during construction three decades ago including those in 1970 at Milford Haven, Wales and West Gate, as well as the one in Koblenz, Germany in 1971. These failures led to a revision of the governing

design philosophies to include a consideration of ultimate buckling strength. Trapezoidal box-girder bridges have more recently experienced a variety of problems during construction, ranging from buckling of bracing members, as shown in Figure 1.2, to complete collapse, as in the case of the pedestrian bridge near Marcy, New York, shown in Figure 1.3. All of these failures are related to stability, not yield strength. Current design specifications do not adequately address stability, which clearly can be a governing design criterion.

Figure 1.3 Collapse of pedestrian bridge near Marcy, New York (Utica Observer-Dispatch)

1.2 PREVIOUS WORK

The steel box girder construction failures in the early 1970s led to more research on the behavior of these structural systems during construction. McDonald et al. (1976) tested box sections with top lateral bracing, analyzed using the equivalent box section method that had been introduced by Dabrowski (1968). A report by United States Steel (1978) detailed common construction difficulties and provided guidelines for design. Branco and Green (1985) studied the elastic response of steel box girders with various bracing configurations to construction loading.

Nonlinear behavior of steel box girders was also a particular focus of research after the series of collapses. Galambos (1998) noted that after the failures, emphasis was shifted from elastic critical loads to inelastic buckling strengths for ultimate design. Experiments were performed by Corrado and Yen (1973) and others to determine the ultimate behavior characteristics of steel box girders. Dowling (1975) and Thimmhardy (1991) studied the buckling of steel box girders with initial imperfections. Salahuddin (1994) discussed the design of box girder bridges by nonlinear theory, giving a design procedure involving longitudinally-stiffened flanges.

A majority of the literature encountered tends to separate construction considerations from stability considerations. The construction phase has been studied almost exclusively from a strength standpoint, not considering stability. Studies of completed girders have included nonlinearity, and many tests have been performed to determine their ultimate capacity. Stability during construction, however, has rarely been considered, and is usually left for the contractor to handle. Sennah and Kennedy (2001), in a state-of-the-art review of the design of curved steel box-girder bridges, stated:

> *The current North American codes as well as the published literature do not provide the design engineer with adequate information on the behavior of the unshored straight and curved box-girder bridges during the construction phase. Further research work is required using 3D finite-element analysis to investigate the behavior of straight and curved box girders at this phase and avoid possible failure.*

This advice gains new urgency from the recent failures of steel trapezoidal box-girder bridges.

Much of the recent research involving steel trapezoidal box-girder bridges has taken place at The University of Texas at Austin. Studies of the buckling behavior of steel trapezoidal box girders were performed by Gilchrist (1997) and Chen (1999). The work by Gilchrist involved laboratory testing of scale models and finite-element buckling analysis in which the box girders were treated as two independent I-girders with continuous bottom flange bracing. Chen continued the work by Gilchrist, examining the effect of top lateral bracing on the buckling of steel box girders. Here again the trapezoidal sections were treated as two half-girders for the purposes of buckling analysis. Recent construction problems, including the Marcy bridge collapse, have shown that this simplification may be inappropriate for certain types of box-girder bridges.

1.3 SCOPE

The work presented in this thesis was part of TxDOT research project No. 0-4307 “Steel Trapezoidal Girders: State-of-the-Art.” The purpose of this portion of the project was to develop software to perform stability analyses of steel trapezoidal box-girder bridges. The software developed for the current study was

based on an existing linear-elastic finite-element analysis program that explicitly models the steel section, the concrete deck, and the partially composite action present during the placement of the concrete. The original program, UTrAp, was developed at The University of Texas at Austin by Cem Topkaya and Eric Williamson as part of a previous research project (Topkaya 2002).

As a method of predicting stability, an elastic critical load analysis capability was added to the existing UTrAp program. This approach, also known as Euler buckling analysis, gives the load at which a secondary load path becomes mathematically possible. The revised program, named UTrAp 2.0, is employed in a preliminary investigation of the stability of trapezoidal box girders. Special attention is given to the Marcy pedestrian bridge, being an actual example of a stability-related failure during construction. Conclusions are drawn based on these studies, and recommendations are given to assist the designer in assuring the stability of steel trapezoidal box-girder bridges during construction.

1.4 ORGANIZATION

Chapter two of this thesis presents the theory behind the finite element analysis in UTrAp 2.0. To add the buckling analysis capability, the necessary nonlinear stiffness matrices were formed for each type of element, as described in the chapter. Additions to the linear analysis procedures in the original program are also documented.

In chapter three, a procedure for finding the elastic critical buckling load is presented. The mathematical formulation is known as the eigenproblem. Solution methods are discussed, and the method of choice is explained along with details of the program implementation.

The verification process for UTrAp 2.0 is described in the fourth chapter. Buckling loads obtained from the program are compared with simple theory, commercial finite element software, and observations from the Marcy bridge collapse. Chapter five documents the capabilities and limitations of UTrAp 2.0 and provides guidance for the user.

Chapter six presents an analytical method for determining the critical buckling stress in a straight, simply-supported trapezoidal girder. The developed formulation is evaluated by considering the performance of the Marcy bridge and results predicted using finite element analyses. Lateral torsional buckling of the entire cross-section of a girder is investigated using both the derived equation and UTrAp 2.0.

Conclusions drawn from the research are presented in the final chapter. The work done with the completed program has been somewhat limited in scope, leaving much to be explored in future research. Recommendations for additional work are given.

CHAPTER 2
Buckling Analysis Formulation

"Equations are just the boring part of mathematics."

- Stephen Hawking

The objective of this research project was to add buckling analysis capabilities to an existing linear analysis finite element program. In this chapter, structural analysis options that are available are presented along with the explanation for the approach implemented in UTrAp 2.0. The finite element modeling process used by UTrAp is explained, and both the linear and nonlinear stiffness formulations for each type of finite element implemented in UTrAp 2.0 are presented.

2.1 TYPES OF STRUCTURAL ANALYSIS

Structural analysis can be performed on a number of levels, ranging from simple, approximate analyses to complex, more accurate analyses. The method of analysis chosen depends on the desired information about the structure being modeled. For structural response at service loads, a first-order linear elastic analysis is almost always adequate. If information about the buckling characteristics of the structure is desired, an elastic critical load analysis can be performed, giving the load at which an alternate load path becomes mathematically valid. An inelastic critical load analysis is similar, but includes the possibility of nonlinear material behavior. Also available to the analyst are second-order elastic and inelastic methods, which are much more computationally demanding but more capable of predicting actual behavior.

In UTrAp 2.0, an elastic critical load analysis is performed. The steel trapezoidal box girders analyzed by the program are formed from thin plates which tend to buckle at stresses much lower than the yield stress. Material nonlinearity is thus not of great concern and is not considered in the program.

2.1.1 Elastic Critical Load Analysis

In a general linear analysis, equilibrium of the structure is found in the original, undeformed configuration, with the displacements assumed to be infinitesimal. For stability analysis, equilibrium is enforced in the deformed position. Because a change in the configuration of the structure being analyzed is considered, this type of structural analysis is known as *geometrically nonlinear analysis*. It is also possible to consider material nonlinearity, but for an elastic critical load analysis, material behavior is assumed to be linear and elastic.

In order to perform a geometrically nonlinear analysis, an additional matrix must be added to the elastic stiffness matrix. This matrix, known as the *geometric stiffness matrix*, is a function of both the geometry of the structure and the stresses in the members. As with the elastic stiffness matrix, local geometric stiffness matrices are assembled into the global geometric stiffness matrix for the structure, which is then used in the eigenproblem. The formulation and solution of the elastic critical analysis eigenproblem is presented in Chapter 3.

2.2 ELEMENT FORMULATIONS

UTrAp forms a mathematical representation of a bridge structure using various finite elements. The concrete deck and the steel plates that form the girders are both modeled with shell elements. Bracing members, including internal braces, external braces, and top lateral braces, are modeled with truss elements. Spring elements are used to model the shear studs, capturing the

variable composite action between the concrete deck and the girder that is possible during construction. Each type of element is formulated individually and assembled into the overall structural model. This section presents the formulations for both the elastic stiffness matrix and the geometric stiffness matrix of each element type.

2.2.1 Shell Element Elastic Stiffness

UTrAp employs a nine-noded, isoparametric shell element developed by Ahmad, Irons, and Zienkiewicz (1970) and shown in Figure 2.1. Details of this formulation are given in Topkaya (2002). The shell element is mapped from the *x*, *y*, and *z* coordinates into material coordinates ξ, η and ζ. At each node, a right-handed triplet of unit vectors is defined, with V_2 along the length of the bridge, V_3 through the thickness of the element, and V_1 orthogonal to V_2 and V_3.

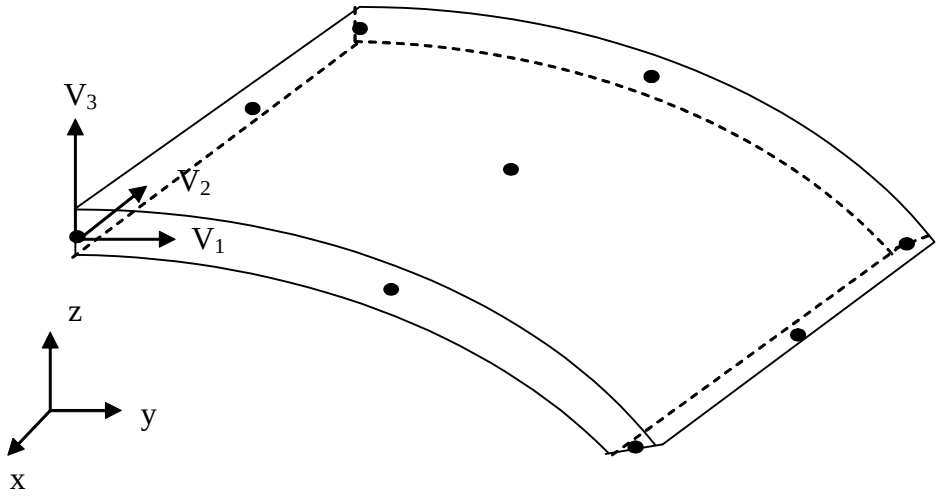

Figure 2.1 Nine-noded shell element (Topkaya, 2002)

The geometry $\boldsymbol{x}$ of the element can be interpolated as follows:

$$\boldsymbol{x}(\xi,\eta,\zeta) = \sum_{i=1}^{9}\left[\left(\boldsymbol{x}_i + \zeta\frac{h}{2}\boldsymbol{V}_3\right)N_i(\xi,\eta)\right] \tag{2.1}$$

where $\boldsymbol{x_i}$ is a vector of the *x*-*y*-*z* coordinates at node *i*, *h* is the constant shell thickness, and $N_i(\xi,\eta)$ are the Lagrangian shape functions found in Bathe (1982).

Deformations are defined by three displacement degrees of freedom, *u*, *v*, and *w*, along with two rotational degrees of freedom, α and β, defined as the rotations about the $\boldsymbol{V_1}$ and $\boldsymbol{V_2}$ axes, respectively. The displacement field $\boldsymbol{u}$ is defined as follows:

$$\boldsymbol{u}(\xi,\eta,\zeta) = \sum_{i=1}^{9}\left[\left(\boldsymbol{u}_i + \zeta\frac{h}{2}(-\alpha_i\boldsymbol{V}_2 + \beta_i\boldsymbol{V}_1)\right)N_i(\xi,\eta)\right] \tag{2.2}$$

where $\boldsymbol{u_i}$ is the vector of displacements at node *i*. The number of degrees of freedom is reduced from six to five by neglecting the "drilling" degree of freedom, that is, rotations about a vector normal to the shell surface. These rotations, being in the plane of the element, are small and store relatively little strain energy. Accordingly, they can be disregarded without sacrificing accuracy in the solution.

Another simplification is the basic shell assumption that the stress normal to any lamina is zero. The full 6 x 6 rigidity matrix in local coordinates has one row and one column of zeros, and can be reduced to

$$\boldsymbol{D}^{local} = \frac{E}{\left(1-\upsilon^2\right)}\begin{bmatrix} 1 & \upsilon & 0 & 0 & 0 \\ & 1 & 0 & 0 & 0 \\ & & \dfrac{1-\upsilon}{\upsilon} & 0 & 0 \\ & sym. & & \dfrac{1-\upsilon}{2k} & 0 \\ & & & & \dfrac{1-\upsilon}{2k} \end{bmatrix} \tag{2.3}$$

where *k* is the bulk modulus of the material.

The global rigidity matrix is calculated as follows:

$$\boldsymbol{D} = \boldsymbol{R}^{\boldsymbol{T}} \boldsymbol{D}^{\boldsymbol{local}} \boldsymbol{R} \tag{2.4}$$

where the rotation matrix is formed from the direction cosines:

$$\boldsymbol{R} = \begin{bmatrix} t_{1x}^{\,2} & t_{1y}^{\,2} & t_{1z}^{\,2} & t_{1x}t_{1y} & t_{1x}t_{1z} & t_{1y}t_{1z} \\ t_{2x}^{\,2} & t_{2y}^{\,2} & t_{2z}^{\,2} & t_{2x}t_{2y} & t_{2x}t_{2z} & t_{2y}t_{2z} \\ t_{3x}^{\,2} & t_{3y}^{\,2} & t_{3z}^{\,2} & t_{3x}t_{3y} & t_{3x}t_{3z} & t_{3y}t_{3z} \\ 2t_{1x}t_{2x} & 2t_{1y}t_{2y} & 2t_{1z}t_{2z} & t_{1x}t_{2y}+t_{1y}t_{2x} & t_{1x}t_{2z}+t_{1z}t_{2x} & t_{1y}t_{2z}+t_{1z}t_{2y} \\ 2t_{1x}t_{3x} & 2t_{1y}t_{3y} & 2t_{1z}t_{3z} & t_{1x}t_{3y}+t_{1y}t_{3x} & t_{1x}t_{3z}+t_{1z}t_{3x} & t_{1y}t_{3z}+t_{1z}t_{3y} \\ 2t_{2x}t_{3x} & 2t_{2y}t_{3y} & 2t_{2z}t_{3z} & t_{2x}t_{3y}+t_{2y}t_{3x} & t_{2x}t_{3z}+t_{2z}t_{3x} & t_{2y}t_{3z}+t_{2z}t_{3y} \end{bmatrix} \tag{2.5}$$

The $\boldsymbol{B}$ matrix relates strains to nodal parameters $\boldsymbol{a}$:

$$\boldsymbol{\varepsilon_0} = \boldsymbol{B}\boldsymbol{a} \tag{2.6}$$

with

$$\boldsymbol{\varepsilon_0} = \left\{ \frac{\partial u}{\partial x} \quad \frac{\partial v}{\partial y} \quad \frac{\partial w}{\partial z} \quad \frac{\partial v}{\partial z}+\frac{\partial w}{\partial y} \quad \frac{\partial w}{\partial x}+\frac{\partial u}{\partial z} \quad \frac{\partial u}{\partial y}+\frac{\partial v}{\partial x} \right\}^{\boldsymbol{T}} \tag{2.7}$$

$$\boldsymbol{a} = \left\{ u_1 \quad v_1 \quad w_1 \quad \alpha_1 \quad \beta_1 \quad u_2 \quad \ldots \right\}^{\boldsymbol{T}} \tag{2.8}$$

The elastic stiffness matrix can now be defined according to the following equation:

$$\boldsymbol{K} = \int_V \boldsymbol{B}^{\boldsymbol{T}} \boldsymbol{D}\boldsymbol{B}\, dV \tag{2.9}$$

where V is the volume of the element. This integration is performed numerically using Gaussian quadrature with three points in the ξ and η directions and two points in the ζ direction. Accordingly, the stiffness matrix is computed by Eq. (2.10):

$$\boldsymbol{K} = \sum_{ip=1}^{18} \boldsymbol{B}^{\boldsymbol{T}} \boldsymbol{D}\boldsymbol{B} \det(\boldsymbol{J}) w(ip) \tag{2.10}$$

In the above expression, det($\boldsymbol{J}$) is the determinant of the Jacobian matrix and *w(ip)* is the weighting factor at the integration point.

2.2.2 Shell Element Geometric Stiffness

For stability analysis, the original shell element formulation must be extended to include nonlinear geometry. The general three-dimensional strain vector can be divided into infinitesimal and large displacement components:

$$\boldsymbol{\varepsilon} = \boldsymbol{\varepsilon}_0 + \boldsymbol{\varepsilon}_L \tag{2.11}$$

where the infinitesimal strain $\boldsymbol{\varepsilon}_0$ is defined in Eq. (2.6). The nonlinear strain terms can be written using a new matrix $\boldsymbol{A}$:

$$\boldsymbol{\varepsilon}_L = \frac{1}{2}\begin{bmatrix} \boldsymbol{\theta}_x^T & \boldsymbol{0} & \boldsymbol{0} \\ \boldsymbol{0} & \boldsymbol{\theta}_y^T & \boldsymbol{0} \\ \boldsymbol{0} & \boldsymbol{0} & \boldsymbol{\theta}_z^T \\ \boldsymbol{0} & \boldsymbol{\theta}_z^T & \boldsymbol{\theta}_y^T \\ \boldsymbol{\theta}_z^T & \boldsymbol{0} & \boldsymbol{\theta}_x^T \\ \boldsymbol{\theta}_y^T & \boldsymbol{\theta}_x^T & \boldsymbol{0} \end{bmatrix} \begin{Bmatrix} \boldsymbol{\theta}_x \\ \boldsymbol{\theta}_y \\ \boldsymbol{\theta}_z \end{Bmatrix} = \frac{1}{2}\boldsymbol{A}\boldsymbol{\theta} \tag{2.12}$$

where

$$\boldsymbol{\theta}_x^T = \begin{bmatrix} \frac{\partial u}{\partial x} & \frac{\partial v}{\partial x} & \frac{\partial w}{\partial x} \end{bmatrix} \tag{2.13}$$

$$\boldsymbol{\theta}_y^T = \begin{bmatrix} \frac{\partial u}{\partial y} & \frac{\partial v}{\partial y} & \frac{\partial w}{\partial y} \end{bmatrix} \tag{2.14}$$

$$\boldsymbol{\theta}_z^T = \begin{bmatrix} \frac{\partial u}{\partial z} & \frac{\partial v}{\partial z} & \frac{\partial w}{\partial z} \end{bmatrix} \tag{2.15}$$

Taking the variation of Eq. (2.12) and using the fact that $\delta\boldsymbol{A}\boldsymbol{\theta} = \boldsymbol{A}\delta\boldsymbol{\theta}$ (see Zienkiewicz 1977),

$$\delta\boldsymbol{\varepsilon}_L = \frac{1}{2}\delta\boldsymbol{A}\boldsymbol{\theta} + \frac{1}{2}\boldsymbol{A}\delta\boldsymbol{\theta} = \boldsymbol{A}\delta\boldsymbol{\theta} \tag{2.16}$$

The $\boldsymbol{G}$ matrix relates the derivatives of the displacement functions to the nodal parameters $\boldsymbol{a}$:

$$\boldsymbol{\theta} = \boldsymbol{G}\boldsymbol{a} \tag{2.17}$$

In expanded form, Eq. (2.17) becomes

$$\begin{Bmatrix} \frac{\partial u}{\partial x} \\ \frac{\partial v}{\partial x} \\ \frac{\partial w}{\partial x} \\ \frac{\partial u}{\partial y} \\ \frac{\partial v}{\partial y} \\ \frac{\partial w}{\partial y} \\ \frac{\partial u}{\partial z} \\ \frac{\partial v}{\partial z} \\ \frac{\partial w}{\partial z} \end{Bmatrix} = \left[\begin{array}{cccc:c:c} \frac{\partial N_1}{\partial x} & 0 & 0 & -\frac{h}{2}V_{2x}\left(\zeta\frac{\partial N_1}{\partial x}+N_1\frac{\partial \zeta}{\partial x}\right) & \frac{h}{2}V_{1x}\left(\zeta\frac{\partial N_1}{\partial x}+N_1\frac{\partial \zeta}{\partial x}\right) & \frac{\partial N_2}{\partial x} & \cdots \\ 0 & \frac{\partial N_1}{\partial x} & 0 & -\frac{h}{2}V_{2y}\left(\zeta\frac{\partial N_1}{\partial x}+N_1\frac{\partial \zeta}{\partial x}\right) & \frac{h}{2}V_{1y}\left(\zeta\frac{\partial N_1}{\partial x}+N_1\frac{\partial \zeta}{\partial x}\right) & 0 & \cdots \\ 0 & 0 & \frac{\partial N_1}{\partial x} & -\frac{h}{2}V_{2z}\left(\zeta\frac{\partial N_1}{\partial x}+N_1\frac{\partial \zeta}{\partial x}\right) & \frac{h}{2}V_{1z}\left(\zeta\frac{\partial N_1}{\partial x}+N_1\frac{\partial \zeta}{\partial x}\right) & 0 & \cdots \\ \hdashline \frac{\partial N_1}{\partial y} & 0 & 0 & -\frac{h}{2}V_{2x}\left(\zeta\frac{\partial N_1}{\partial y}+N_1\frac{\partial \zeta}{\partial y}\right) & \frac{h}{2}V_{1x}\left(\zeta\frac{\partial N_1}{\partial y}+N_1\frac{\partial \zeta}{\partial y}\right) & \frac{\partial N_2}{\partial y} & \cdots \\ 0 & \frac{\partial N_1}{\partial y} & 0 & -\frac{h}{2}V_{2y}\left(\zeta\frac{\partial N_1}{\partial y}+N_1\frac{\partial \zeta}{\partial y}\right) & \frac{h}{2}V_{1y}\left(\zeta\frac{\partial N_1}{\partial y}+N_1\frac{\partial \zeta}{\partial y}\right) & 0 & \cdots \\ 0 & 0 & \frac{\partial N_1}{\partial y} & -\frac{h}{2}V_{2z}\left(\zeta\frac{\partial N_1}{\partial y}+N_1\frac{\partial \zeta}{\partial y}\right) & \frac{h}{2}V_{1z}\left(\zeta\frac{\partial N_1}{\partial y}+N_1\frac{\partial \zeta}{\partial y}\right) & 0 & \cdots \\ \hdashline \frac{\partial N_1}{\partial z} & 0 & 0 & -\frac{h}{2}V_{2x}\left(\zeta\frac{\partial N_1}{\partial z}+N_1\frac{\partial \zeta}{\partial z}\right) & \frac{h}{2}V_{1x}\left(\zeta\frac{\partial N_1}{\partial z}+N_1\frac{\partial \zeta}{\partial z}\right) & \frac{\partial N_2}{\partial z} & \cdots \\ 0 & \frac{\partial N_1}{\partial z} & 0 & -\frac{h}{2}V_{2y}\left(\zeta\frac{\partial N_1}{\partial z}+N_1\frac{\partial \zeta}{\partial z}\right) & \frac{h}{2}V_{1y}\left(\zeta\frac{\partial N_1}{\partial z}+N_1\frac{\partial \zeta}{\partial z}\right) & 0 & \cdots \\ 0 & 0 & \frac{\partial N_1}{\partial z} & -\frac{h}{2}V_{2z}\left(\zeta\frac{\partial N_1}{\partial z}+N_1\frac{\partial \zeta}{\partial z}\right) & \frac{h}{2}V_{1z}\left(\zeta\frac{\partial N_1}{\partial z}+N_1\frac{\partial \zeta}{\partial z}\right) & 0 & \cdots \end{array}\right] \begin{Bmatrix} u_1 \\ v_1 \\ w_1 \\ \alpha_1 \\ \beta_1 \\ \hdashline u_2 \\ \cdots \end{Bmatrix}$$

It follows that

$$\delta\boldsymbol{\varepsilon}_{\boldsymbol{L}} = \boldsymbol{A}\boldsymbol{G}\delta\boldsymbol{a} = \boldsymbol{B}_{\boldsymbol{L}}\delta\boldsymbol{a} \tag{2.18}$$

and

$$\boldsymbol{B}_{\boldsymbol{L}} = \boldsymbol{A}\boldsymbol{G} \tag{2.19}$$

$$\boldsymbol{B}_{\boldsymbol{L}}{}^{\boldsymbol{T}} = \boldsymbol{G}^{\boldsymbol{T}}\boldsymbol{A}^{\boldsymbol{T}} \tag{2.20}$$

$$\delta\boldsymbol{B}_{\boldsymbol{L}}{}^{\boldsymbol{T}} = \boldsymbol{G}^{\boldsymbol{T}}\delta\boldsymbol{A}^{\boldsymbol{T}} \tag{2.21}$$

The geometric stiffness matrix can be defined as follows:

$$\boldsymbol{K}_{\sigma}\delta\boldsymbol{a} = \int_{V}\delta\boldsymbol{B}_{\boldsymbol{L}}{}^{\boldsymbol{T}}\boldsymbol{\sigma}\,\mathrm{d}V = \int_{V}\boldsymbol{G}^{\boldsymbol{T}}\delta\boldsymbol{A}^{\boldsymbol{T}}\boldsymbol{\sigma}\,\mathrm{d}V \tag{2.22}$$

where the vector of initial stresses is

$$\boldsymbol{\sigma} = \begin{Bmatrix} \sigma_x & \sigma_y & \sigma_z & \tau_{xy} & \tau_{xz} & \tau_{yz} \end{Bmatrix}^T \tag{2.23}$$

It can be verified that

$$\delta \boldsymbol{A}^T \boldsymbol{\sigma} = \begin{bmatrix} \sigma_x \boldsymbol{I}_3 & \tau_{xy} \boldsymbol{I}_3 & \tau_{xz} \boldsymbol{I}_3 \\ & \sigma_y \boldsymbol{I}_3 & \tau_{yz} \boldsymbol{I}_3 \\ sym. & & \sigma_z \boldsymbol{I}_3 \end{bmatrix} \delta \boldsymbol{\theta} = \boldsymbol{M} \delta \boldsymbol{\theta} \tag{2.24}$$

where

$$\boldsymbol{I}_3 = \begin{bmatrix} 1 & 0 & 0 \\ 0 & 1 & 0 \\ 0 & 0 & 1 \end{bmatrix} \tag{2.25}$$

The matrix $\boldsymbol{M}$ depends on the initial stress vector $\boldsymbol{\sigma}$, which must be in global coordinates. The stresses in local coordinates are found from the elastic analysis:

$$\boldsymbol{\sigma}_{local} = \begin{Bmatrix} \sigma_x' & \sigma_y' & \sigma_z' & \tau_{xy}' & \tau_{xz}' & \tau_{yz}' \end{Bmatrix}^T \tag{2.26}$$

Note that σ_z' must be zero according to the shell assumption. The local stresses are rotated to the global coordinate system using the matrix found in Eq. (2.5):

$$\boldsymbol{\sigma} = \boldsymbol{R}^T \boldsymbol{\sigma}_{local} \tag{2.27}$$

Using the relationship

$$\delta \boldsymbol{\theta} = \boldsymbol{G} \delta \boldsymbol{a} \tag{2.28}$$

along with Eqs. (2.22) and (2.24), the geometric stiffness matrix in global coordinates is

$$\boldsymbol{K}_\sigma = \int_V \boldsymbol{G}^T \boldsymbol{M} \boldsymbol{G} \mathrm{d}V \tag{2.29}$$

Evaluated numerically as with the elastic stiffness matrix, Eq. (2.29) becomes

$$\boldsymbol{K}_\sigma = \sum_{ip=1}^{18} \boldsymbol{G}^T \boldsymbol{M} \boldsymbol{G} \det(\boldsymbol{J}) w(ip) \tag{2.30}$$

where det(**J**) and *w(ip)* are the same as in Eq. (2.10).

2.2.3 Truss Element Elastic Stiffness

UTrAp uses a standard 3-dimensional, 2-noded truss element. The familiar elastic stiffness matrix in local coordinates is

$$\boldsymbol{K} = \frac{EA}{L}\begin{bmatrix} 1 & 0 & 0 & -1 & 0 & 0 \\ 0 & 0 & 0 & 0 & 0 & 0 \\ 0 & 0 & 0 & 0 & 0 & 0 \\ -1 & 0 & 0 & 1 & 0 & 0 \\ 0 & 0 & 0 & 0 & 0 & 0 \\ 0 & 0 & 0 & 0 & 0 & 0 \end{bmatrix} \tag{2.31}$$

where E is the modulus of elasticity, A is the cross-sectional area, and L is the element length.

2.2.4 Truss Element Geometric Stiffness

Although the geometric stiffness matrix for a simple truss element is readily found in many references, its derivation is given below to illustrate the process followed for all element types. The general procedure is the same as that given for the shell element above.

The geometry of a two-noded truss element is defined by its nodal coordinates and assumed shape functions:

$$\begin{Bmatrix} x \\ y \\ z \end{Bmatrix} = \begin{bmatrix} N_1 & 0 & 0 & N_2 & 0 & 0 \\ 0 & N_1 & 0 & 0 & N_2 & 0 \\ 0 & 0 & N_1 & 0 & 0 & N_2 \end{bmatrix} \begin{Bmatrix} x_1 \\ y_1 \\ \cdots \\ z_2 \end{Bmatrix} \tag{2.32}$$

Likewise, the displacements are related to the nodal parameters:

$$\begin{Bmatrix} u \\ v \\ w \end{Bmatrix} = \begin{bmatrix} N_1 & 0 & 0 & N_2 & 0 & 0 \\ 0 & N_1 & 0 & 0 & N_2 & 0 \\ 0 & 0 & N_1 & 0 & 0 & N_2 \end{bmatrix} \begin{Bmatrix} u_1 \\ v_1 \\ \cdots \\ w_2 \end{Bmatrix} \tag{2.33}$$

or

$$\boldsymbol{u} = \boldsymbol{N}\boldsymbol{a} \tag{2.34}$$

where $\boldsymbol{N}$ is a vector of the shape functions, assumed to be linear for a truss element:

$$\begin{aligned} N_1(\xi) &= \frac{1}{2}(1-\xi) \\ N_2(\xi) &= \frac{1}{2}(1+\xi) \end{aligned} \tag{2.35}$$

Total strain is defined in Eq. (2.11), where the terms are as follows:

$$\boldsymbol{\varepsilon_0} = \begin{Bmatrix} \dfrac{\partial u}{\partial x} \\ \dfrac{\partial v}{\partial y} \\ \dfrac{\partial w}{\partial z} \end{Bmatrix} \tag{2.36}$$

$$\boldsymbol{\varepsilon_L} = \begin{Bmatrix} \dfrac{1}{2}\left[\left(\dfrac{\partial u}{\partial x}\right)^2 + \left(\dfrac{\partial v}{\partial x}\right)^2 + \left(\dfrac{\partial w}{\partial x}\right)^2\right] \\ \dfrac{1}{2}\left[\left(\dfrac{\partial u}{\partial y}\right)^2 + \left(\dfrac{\partial v}{\partial y}\right)^2 + \left(\dfrac{\partial w}{\partial y}\right)^2\right] \\ \dfrac{1}{2}\left[\left(\dfrac{\partial u}{\partial z}\right)^2 + \left(\dfrac{\partial v}{\partial z}\right)^2 + \left(\dfrac{\partial w}{\partial z}\right)^2\right] \end{Bmatrix} \tag{2.37}$$

The nonlinear strain terms above can be written in the form of Eq. (2.12). The $\boldsymbol{G}$ matrix is defined by Eq. (2.17), which can be expanded as follows:

$$\begin{Bmatrix} \frac{\partial u}{\partial x} \\ \frac{\partial v}{\partial x} \\ \frac{\partial w}{\partial x} \\ \frac{\partial u}{\partial y} \\ \frac{\partial v}{\partial y} \\ \frac{\partial w}{\partial y} \\ \frac{\partial u}{\partial z} \\ \frac{\partial v}{\partial z} \\ \frac{\partial w}{\partial z} \end{Bmatrix} = \begin{bmatrix} \frac{\partial N_1}{\partial x} & 0 & 0 & \frac{\partial N_2}{\partial x} & 0 & 0 \\ 0 & \frac{\partial N_1}{\partial x} & 0 & 0 & \frac{\partial N_2}{\partial x} & 0 \\ 0 & 0 & \frac{\partial N_1}{\partial x} & 0 & 0 & \frac{\partial N_2}{\partial x} \\ \frac{\partial N_1}{\partial y} & 0 & 0 & \frac{\partial N_2}{\partial y} & 0 & 0 \\ 0 & \frac{\partial N_1}{\partial y} & 0 & 0 & \frac{\partial N_2}{\partial y} & 0 \\ 0 & 0 & \frac{\partial N_1}{\partial y} & 0 & 0 & \frac{\partial N_2}{\partial y} \\ \frac{\partial N_1}{\partial z} & 0 & 0 & \frac{\partial N_2}{\partial z} & 0 & 0 \\ 0 & \frac{\partial N_1}{\partial z} & 0 & 0 & \frac{\partial N_2}{\partial z} & 0 \\ 0 & 0 & \frac{\partial N_1}{\partial z} & 0 & 0 & \frac{\partial N_2}{\partial z} \end{bmatrix} \begin{Bmatrix} u_1 \\ v_1 \\ w_1 \\ u_2 \\ v_2 \\ w_2 \end{Bmatrix} \tag{2.38}$$

where

$$\frac{\partial N_1}{\partial x} = \frac{\partial N_1}{\partial \xi}\frac{\partial \xi}{\partial x} \tag{2.39}$$

Because a truss element by definition has no shear stresses, the $\boldsymbol{M}$ matrix becomes

$$\boldsymbol{M} = \begin{bmatrix} \sigma_x \boldsymbol{I}_3 & 0 & 0 \\ & \sigma_y \boldsymbol{I}_3 & 0 \\ sym. & & \sigma_z \boldsymbol{I}_3 \end{bmatrix} \tag{2.40}$$

and the matrix product $\boldsymbol{G}^T \boldsymbol{M} \boldsymbol{G}$ from Eq. (2.29) expands to

$$
\begin{bmatrix}
-\frac{1}{2}\frac{\partial\xi}{\partial x}\sigma_x & 0 & 0 & -\frac{1}{2}\frac{\partial\xi}{\partial y}\sigma_y & 0 & 0 & -\frac{1}{2}\frac{\partial\xi}{\partial z}\sigma_z & 0 & 0 \\
0 & -\frac{1}{2}\frac{\partial\xi}{\partial x}\sigma_x & 0 & 0 & -\frac{1}{2}\frac{\partial\xi}{\partial y}\sigma_y & 0 & 0 & -\frac{1}{2}\frac{\partial\xi}{\partial z}\sigma_z & 0 \\
0 & 0 & -\frac{1}{2}\frac{\partial\xi}{\partial x}\sigma_x & 0 & 0 & -\frac{1}{2}\frac{\partial\xi}{\partial y}\sigma_y & 0 & 0 & -\frac{1}{2}\frac{\partial\xi}{\partial z}\sigma_z \\
\frac{1}{2}\frac{\partial\xi}{\partial x}\sigma_x & 0 & 0 & \frac{1}{2}\frac{\partial\xi}{\partial y}\sigma_y & 0 & 0 & \frac{1}{2}\frac{\partial\xi}{\partial z}\sigma_z & 0 & 0 \\
0 & \frac{1}{2}\frac{\partial\xi}{\partial x}\sigma_x & 0 & 0 & \frac{1}{2}\frac{\partial\xi}{\partial y}\sigma_y & 0 & 0 & \frac{1}{2}\frac{\partial\xi}{\partial z}\sigma_z & 0 \\
0 & 0 & \frac{1}{2}\frac{\partial\xi}{\partial x}\sigma_x & 0 & 0 & \frac{1}{2}\frac{\partial\xi}{\partial y}\sigma_y & 0 & 0 & \frac{1}{2}\frac{\partial\xi}{\partial z}\sigma_z
\end{bmatrix}
\boldsymbol{G}
$$

$$
=\begin{bmatrix}
\frac{1}{4}\left(\frac{\partial\xi}{\partial x}\right)^2\sigma_x+\frac{1}{4}\left(\frac{\partial\xi}{\partial y}\right)^2\sigma_y+\frac{1}{4}\left(\frac{\partial\xi}{\partial z}\right)^2\sigma_z & 0 & 0 & \cdots \\
0 & \frac{1}{4}\left(\frac{\partial\xi}{\partial x}\right)^2\sigma_x+\frac{1}{4}\left(\frac{\partial\xi}{\partial y}\right)^2\sigma_y+\frac{1}{4}\left(\frac{\partial\xi}{\partial z}\right)^2\sigma_z & 0 & \cdots \\
0 & 0 & \frac{1}{4}\left(\frac{\partial\xi}{\partial x}\right)^2\sigma_x+\frac{1}{4}\left(\frac{\partial\xi}{\partial y}\right)^2\sigma_y+\frac{1}{4}\left(\frac{\partial\xi}{\partial z}\right)^2\sigma_z & \cdots \\
-\frac{1}{4}\left(\frac{\partial\xi}{\partial x}\right)^2\sigma_x-\frac{1}{4}\left(\frac{\partial\xi}{\partial y}\right)^2\sigma_y-\frac{1}{4}\left(\frac{\partial\xi}{\partial z}\right)^2\sigma_z & 0 & 0 & \cdots \\
0 & -\frac{1}{4}\left(\frac{\partial\xi}{\partial x}\right)^2\sigma_x-\frac{1}{4}\left(\frac{\partial\xi}{\partial y}\right)^2\sigma_y-\frac{1}{4}\left(\frac{\partial\xi}{\partial z}\right)^2\sigma_z & 0 & \cdots \\
0 & 0 & -\frac{1}{4}\left(\frac{\partial\xi}{\partial x}\right)^2\sigma_x-\frac{1}{4}\left(\frac{\partial\xi}{\partial y}\right)^2\sigma_y-\frac{1}{4}\left(\frac{\partial\xi}{\partial z}\right)^2\sigma_z & \cdots
\end{bmatrix}
$$

If the truss element lies along the x-axis, ξ is defined as follows:

$$\left.\begin{array}{l} x = 0 \rightarrow \xi = -1 \\ x = L \rightarrow \xi = 1 \end{array}\right\} \rightarrow \xi = \frac{2}{L}x - 1$$

$$\frac{\partial \xi}{\partial x} = \frac{2}{L}$$

The (1,1) term in the geometric stiffness matrix is therefore

$$K_{G11} = \int_V \frac{1}{4}\left(\frac{\partial \xi}{\partial x}\right)^2 \sigma_x + \frac{1}{4}\left(\frac{\partial \xi}{\partial y}\right)^2 \sigma_y + \frac{1}{4}\left(\frac{\partial \xi}{\partial z}\right)^2 \sigma_z dV = \int_V \frac{1}{4}\left(\frac{2}{L}\right)^2 \sigma_x dV$$

because σ_y and σ_z are zero. The volume is simply the area multiplied by the length, which gives

$$\int_0^L \frac{1}{L^2} \sigma_x A_x dx$$

The stress multiplied by the area is the axial force in the member, leading to

$$K_{G11} = \frac{F_x}{L}$$

The remaining terms can be calculated in a similar fashion, resulting in the entire geometric stiffness matrix for a two-noded truss element:

$$\boldsymbol{K_G} = \frac{F_x}{L}\begin{bmatrix} 1 & 0 & 0 & -1 & 0 & 0 \\ 0 & 1 & 0 & 0 & -1 & 0 \\ 0 & 0 & 1 & 0 & 0 & -1 \\ -1 & 0 & 0 & 1 & 0 & 0 \\ 0 & -1 & 0 & 0 & 1 & 0 \\ 0 & 0 & -1 & 0 & 0 & 1 \end{bmatrix} \tag{2.41}$$

which agrees with that given by McGuire et al. (2000) and other references on the subject. As noted above, the derivation for a truss element geometric stiffness matrix was done to provide an example of the process, which is the same for the other elements, including the shells.

2.2.5 Spring Element Stiffness

A standard three-dimensional, two-noded spring element is used for the shear stud elements in UTrAp 2.0. The elastic stiffness matrix as given in Topkaya (2002) is

$$\boldsymbol{K} = \begin{bmatrix} K_1 & 0 & 0 & -K_1 & 0 & 0 \\ 0 & K_2 & 0 & 0 & -K_2 & 0 \\ 0 & 0 & K_3 & 0 & 0 & -K_3 \\ -K_1 & 0 & 0 & K_1 & 0 & 0 \\ 0 & -K_2 & 0 & 0 & K_2 & 0 \\ 0 & 0 & -K_3 & 0 & 0 & K_3 \end{bmatrix} \tag{2.42}$$

where K_1, K_2, and K_3 are the stiffness values in the three global directions. Because the shear studs serve only to connect the deck and the top flange elements, accounting for geometric nonlinearity of the studs does not influence the buckling load. Therefore, the stud elements are not added to the global geometric stiffness matrix, and no local geometric stiffness formulation is needed.

2.2.6 Web Stiffener Element Elastic Stiffness

Steel trapezoidal box-girder bridges typically have internal cross frames or diaphragms along their length in order to prevent cross-sectional distortion. In addition, web stiffeners are added at the internal brace locations to prevent the local forces due to the brace members from buckling the web. A typical cross-section with web stiffeners and an internal brace is shown in Figure 2.2. The brace members are typically angle sections or structural tees joined by a gusset plate at the center and either bolted or welded to the web stiffeners, which are generally formed from steel plate.

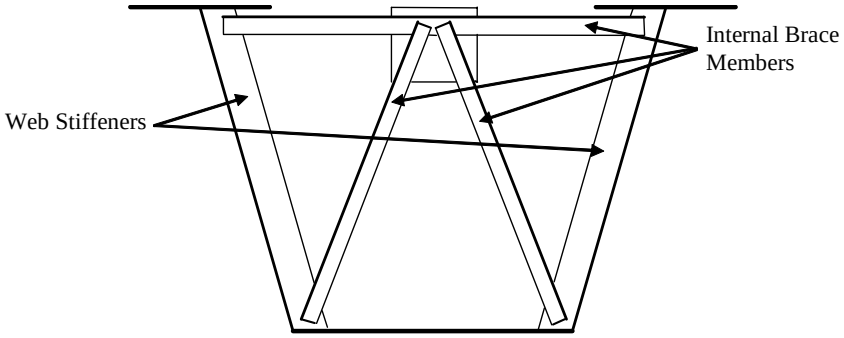

Figure 2.2 Web stiffeners and internal brace

The original version of UTrAp models the internal brace members as truss elements, and can accurately predict the axial forces in the members. However, it does not include any representation of the web stiffeners. For the elastic analysis, this modeling approach is sufficient, as the results given by the program are in agreement with both other finite element programs and field data from actual bridges. After modifying the original program to include a buckling analysis, it was observed that the lower buckling modes all involved web bending, usually near the internal brace locations. Without web stiffeners, the web itself has to carry the forces from the truss action of the brace members along with the remaining stresses due to the loads, leading to buckling behavior dominated by local web bending. In order to predict the buckling response of the girders more accurately, it was deemed necessary to add web stiffeners to the model.

Beam elements were chosen to model the web stiffeners, which are designed to resist both axial forces and bending moments. Because the original version of UTrAp contained no beam elements, a new formulation was required. In order to integrate the new beam element with the existing model, five degrees of freedom were used at each node. Nine-noded elements were required to match the number of nodes in the web. The resulting web stiffener element is shown in Figure 2.3.

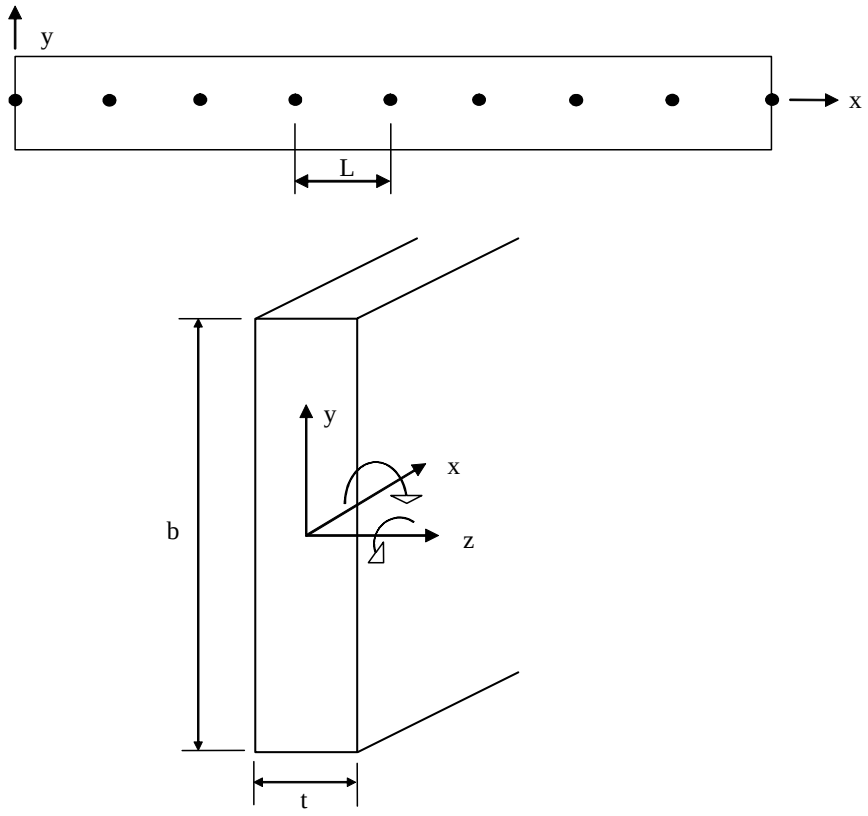

Figure 2.3 Web stiffener element

In Figure 2.3, *b* and *t* are the width and thickness of the web stiffener, respectively, and *L* is the distance between nodes in the webs. As shown in the figure, the web stiffener element has three translational degrees of freedom and two rotational degrees of freedom: one about the x-axis, which corresponds to α in the shell formulation, and the other about the z-axis, which corresponds to β. Without a rotational degree of freedom about the y-axis, the stiffness matrix for the web stiffener element cannot be assembled directly from the two-noded stiffness matrices of the beam elements that comprise it because the degrees of freedom in the y-direction are not independent. This difficulty was avoided by

first forming the stiffness matrix for a two-noded beam element with six degrees of freedom per node:

$$\boldsymbol{K} = \begin{bmatrix}
\frac{EA}{L} & 0 & 0 & 0 & 0 & 0 & -\frac{EA}{L} & 0 & 0 & 0 & 0 & 0 \\
0 & \frac{12EI_z}{L^3} & 0 & 0 & \frac{6EI_z}{L^2} & 0 & 0 & -\frac{12EI_z}{L^3} & 0 & 0 & \frac{6EI_z}{L^2} & 0 \\
0 & 0 & \frac{12EI_y}{L^3} & 0 & 0 & -\frac{6EI_y}{L^2} & 0 & 0 & -\frac{12EI_y}{L^3} & 0 & 0 & -\frac{6EI_y}{L^2} \\
0 & 0 & 0 & \frac{GJ}{L} & 0 & 0 & 0 & 0 & 0 & -\frac{GJ}{L} & 0 & 0 \\
0 & \frac{6EI_z}{L^2} & 0 & 0 & \frac{4EI_z}{L} & 0 & 0 & -\frac{6EI_z}{L^2} & 0 & 0 & \frac{2EI_z}{L} & 0 \\
0 & 0 & -\frac{6EI_y}{L^2} & 0 & 0 & \frac{4EI_y}{L} & 0 & 0 & \frac{6EI_y}{L^2} & 0 & 0 & \frac{2EI_y}{L} \\
-\frac{EA}{L} & 0 & 0 & 0 & 0 & 0 & \frac{EA}{L} & 0 & 0 & 0 & 0 & 0 \\
0 & -\frac{12EI_z}{L^3} & 0 & 0 & -\frac{6EI_z}{L^2} & 0 & 0 & \frac{12EI_z}{L^3} & 0 & 0 & -\frac{6EI_z}{L^2} & 0 \\
0 & 0 & -\frac{12EI_y}{L^3} & 0 & 0 & \frac{6EI_y}{L^2} & 0 & 0 & \frac{12EI_y}{L^3} & 0 & 0 & \frac{6EI_y}{L^2} \\
0 & 0 & 0 & -\frac{GJ}{L} & 0 & 0 & 0 & 0 & 0 & \frac{GJ}{L} & 0 & 0 \\
0 & \frac{6EI_z}{L^2} & 0 & 0 & \frac{2EI_z}{L} & 0 & 0 & -\frac{6EI_z}{L^2} & 0 & 0 & \frac{4EI_z}{L} & 0 \\
0 & 0 & -\frac{6EI_y}{L^2} & 0 & 0 & \frac{2EI_y}{L} & 0 & 0 & \frac{6EI_y}{L^2} & 0 & 0 & \frac{4EI_y}{L}
\end{bmatrix} \tag{2.43}$$

Eight of these elements were then assembled into one superelement stiffness matrix, comprised of nine nodes and fifty-four degrees of freedom. The six extra degrees of freedom were condensed out, leaving the desired forty-five degrees of freedom. This stiffness matrix was implemented into UTrAp.

To test the web stiffener formulation, a UTrAp model was formed with very thin vertical webs. The top and bottom of the web stiffener were pinned, and a load was applied horizontally at the midheight of the stiffener. Figure 2.4 shows the horizontal deflections of the web stiffener given by UTrAp along with the deflections predicted by beam theory. The two are in very close agreement, showing that the 5-DOF web stiffener element formulation is sufficiently accurate.

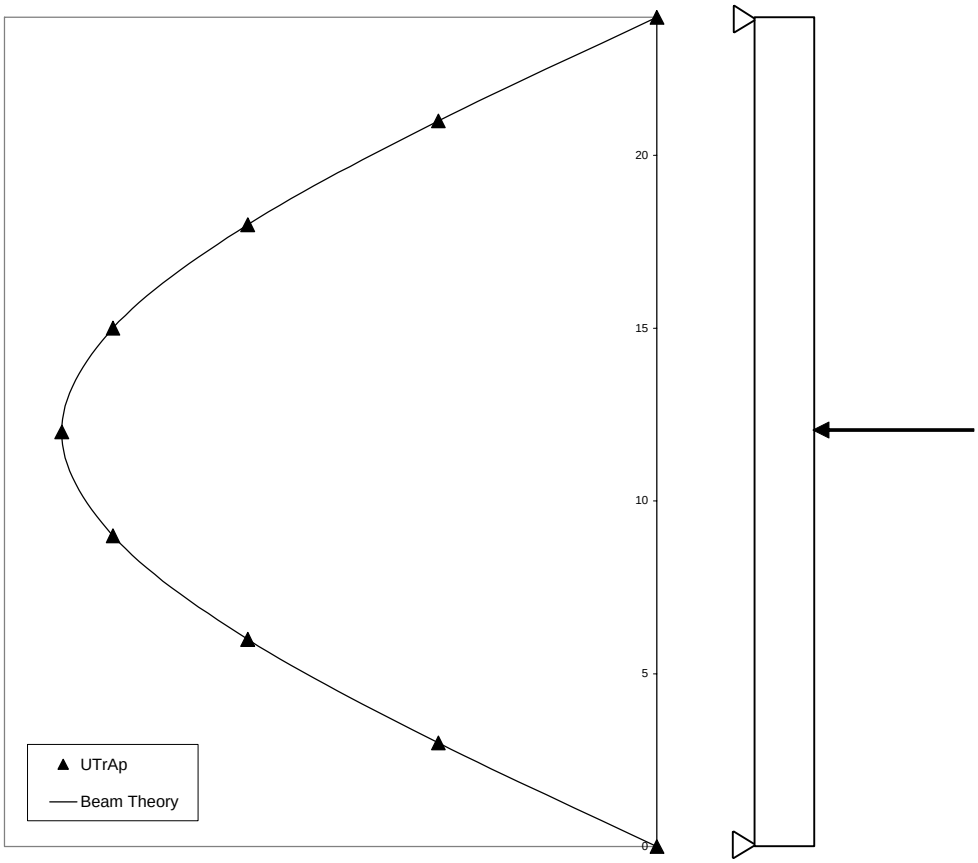

Figure 2.4 Predicted web stiffener deflections

2.2.7 Web Stiffener Element Geometric Stiffness

As mentioned previously, the box girders analyzed in UTrAp are formed from thin steel plates, which can buckle at low stress levels. The web stiffeners have much smaller width-to-thickness ratios than the webs and flanges, and thus are not of primary concern for buckling considerations. Accounting for geometric nonlinearities in the web stiffeners will not significantly affect the buckling load computed for the bridge being modeled in UTrAp. Therefore, the geometric

stiffness matrices of the web stiffener elements have not been formulated and are not included in the global geometric stiffness matrix.

2.3 SUMMARY

Each element type found in UTrAp 2.0 has been presented in this chapter, and the formulations for the elastic and the geometric stiffness matrices have been given. A geometric stiffness formulation for the shell elements used in the program was not found in the literature, so one has been developed. Beam elements have been introduced to model the web stiffeners found in trapezoidal girders.

Using the stiffness matrices from this chapter, an elastic critical load analysis can be performed. The following chapter explains the use of the eigenproblem in elastic critical load analysis, giving both the theory and the practical implementation of the solution.

CHAPTER 3
The Eigenproblem

"Do not worry about your difficulties in Mathematics. I can assure you mine are still greater." - *Albert Einstein*

All matrices have as properties both eigenvalues and corresponding eigenvectors, named for the German *eigen* meaning "characteristic." These characteristic values play an important roll in a wide range of fields, from chemistry to physics to engineering. In structural engineering, eigenproblems commonly arise in dynamic analyses, where they provide the vibrational frequencies of structures, and in stability analyses, where they are used to determine the buckling response of a structure. In this chapter, eigenproblems will first be approached from a mathematical perspective. The application of eigenproblems to a buckling analysis will then be presented, followed by a discussion of general solution methods and the particular method of solution chosen for implementation in UTrAp.

3.1 EIGENPROBLEMS MATHEMATICALLY

A *standard* eigenproblem in mathematics takes the form

$$\boldsymbol{A}\boldsymbol{x} = \lambda\boldsymbol{x} \tag{3.1}$$

where $\boldsymbol{A}$ is the matrix of interest, $\boldsymbol{x}$ is the eigenvector, and λ is the eigenvalue. This equation can be rearranged as

$$(\boldsymbol{A} - \lambda\boldsymbol{I})\boldsymbol{x} = \boldsymbol{0} \tag{3.2}$$

where $\boldsymbol{I}$ is the identity matrix. In order for Eq. (3.2) to hold, the determinant of $(\boldsymbol{A} - \lambda \boldsymbol{I})$ must be zero, or

$$\left|\boldsymbol{A} - \lambda \boldsymbol{I}\right| = 0 \tag{3.3}$$

Many fairly simple solution techniques, some of which are discussed later in this chapter, are available for this form of the eigenproblem.

A second common mathematical form is the *generalized* eigenproblem:

$$\boldsymbol{A}\boldsymbol{x} = \lambda \boldsymbol{B}\boldsymbol{x} \tag{3.4}$$

where $\boldsymbol{A}$ and $\boldsymbol{B}$ are both matrices of order n. Rearranging Eq. (3.4) gives

$$(\boldsymbol{A} - \lambda \boldsymbol{B})\boldsymbol{x} = \boldsymbol{0} \tag{3.5}$$

In the case where $\boldsymbol{B} = \boldsymbol{I}$, Eq. (3.5) reduces to standard form. If $\boldsymbol{B}$ is not equal to the identity matrix, a variety of techniques can be used to convert this equation to standard form, allowing a more straightforward solution technique to be employed.

3.1.1 Eigenproblem Example

In order to illustrate the computation of eigenvalues and eigenvectors, a simple example will be adapted from Fletcher (1972). Let

$$\boldsymbol{A} = \begin{bmatrix} -1 & 2 & 2 \\ -8 & 7 & 4 \\ -13 & 5 & 8 \end{bmatrix} \tag{3.6}$$

and

$$\boldsymbol{A}\boldsymbol{x} = \boldsymbol{A}\begin{Bmatrix} x_1 \\ x_2 \\ x_3 \end{Bmatrix} = \begin{bmatrix} -x_1 + 2x_2 + 2x_3 \\ -8x_1 + 7x_2 + 4x_3 \\ -13x_1 + 5x_2 + 8x_3 \end{bmatrix} \tag{3.7}$$

From Eq. (3.1), the resulting vector must be a scalar multiple of the original, implying

$$\begin{aligned} -x_1 + 2x_2 + 2x_3 &= \lambda x_1 \\ -8x_1 + 7x_2 + 4x_3 &= \lambda x_2 \\ -13x_1 + 5x_2 + 8x_3 &= \lambda x_3 \end{aligned} \tag{3.8}$$

which, rearranged, leads to

$$\begin{aligned} (-1-\lambda)x_1 + 2x_2 + 2x_3 &= 0 \\ -8x_1 + (7-\lambda)x_2 + 4x_3 &= 0 \\ -13x_1 + 5x_2 + (8-\lambda)x_3 &= 0 \end{aligned} \tag{3.9}$$

A theorem of linear algebra (found in Fletcher and elsewhere) states that a set of linear homogeneous equations like those in Eq. (3.9) has a solution in which the unknowns are not all zero if and only if the determinant of the coefficients on the left-hand side is zero. Thus,

$$\begin{vmatrix} -1-\lambda & 2 & 2 \\ -8 & 7-\lambda & 4 \\ -13 & 5 & 8-\lambda \end{vmatrix} = 0 \tag{3.10}$$

which can be written

$$\left|(\boldsymbol{A} - \lambda \boldsymbol{I})\right| = 0 \tag{3.11}$$

Expanding the determinant results in the characteristic equation:

$$\lambda^3 - 14\lambda^2 + 63\lambda - 90 = 0 \tag{3.12}$$

Solving Eq. (3.12) gives the eigenvalues:

$$\lambda = 3,\ 5,\ \text{and}\ 6$$

Substituting any of these eigenvalues into Eq. (3.9) above gives the corresponding eigenvector. For example, using the first eigenvalue,

$$\begin{aligned} (-1-3)x_1 + 2x_2 + 2x_3 &= 0 \\ -8x_1 + (7-3)x_2 + 4x_3 &= 0 \\ -13x_1 + 5x_2 + (8-3)x_3 &= 0 \end{aligned}$$

These equations are by nature not independent, meaning that the values of x_1, x_2, and x_3 can only be specified by their relative ratios. Thus

$$x_1 : x_2 : x_3 = 0 : 1 : -1$$

Eigenvectors can therefore be scaled by any number and remain valid. Note that

$$\boldsymbol{A}\boldsymbol{x} = \boldsymbol{A}\begin{bmatrix} 0 \\ 1 \\ -1 \end{bmatrix} = \begin{bmatrix} 0 \\ 3 \\ -3 \end{bmatrix} = 3\begin{bmatrix} 0 \\ 1 \\ -1 \end{bmatrix} = \lambda \boldsymbol{x}$$

as expected. The eigenvectors corresponding to the second and third eigenvalues can be found in a similar manner.

3.1.2 Solution Methods

While calculating the eigenvalues of a small matrix such as the one above can be a straightforward task, large eigenproblems present a much greater challenge. Over the last two centuries, a great deal of effort has been expended on finding new and improved methods for solving eigenproblems. An excellent overview of the history of eigenvalue computations is given by Golub and van der Vorst (2000). Considering the large number of papers published each year involving eigenproblems, a complete overview of the literature is impractical, but the main methods and important developments can be chronicled.

One of the pioneers of eigenvalue computation was Jacobi, who in 1846 developed a method for diagonalizing a symmetric matrix, allowing efficient computation of the eigenvalues. The Jacobi method today forms the basis for many popular algorithms. Of the same vintage is the Power iteration method, no longer used in its original form due to slow convergence. Many modern methods, such as the inverse iteration, the QR-method, and the Krylov method, use Power iteration in some form. A comprehensive listing of references for these and other solution methods is given by Golub and van der Vorst (2000).

With the advent of the digital computer, the area of eigenvalue computations began to flourish. In the mid-1950's, the Householder method was

developed, along with the Lanczos algorithm. The latter has endured as a method of choice, and has been implemented in various forms in a variety of subsequent methods and algorithms. It was also during this time that Arnoldi created a reduction algorithm for non-symmetric matrices, the precursor to the method used by UTrAp.

The developments of the following two decades are discussed in *The Symmetric Eigenproblem* by Parlett (1998), an authoritative work originally published in 1980 and republished as a classic. The QR method, based on Power iteration, is explored, along with Rayleigh-Ritz procedures, Krylov methods, and subspace iteration. Since this time, a major focus of research has been the refinement of these and other methods for use in computational routines. Dongarra and Walker (1995) provide a guide to the various software packages developed for the solution of eigenproblems.

3.2 EIGENPROBLEMS IN BUCKLING ANALYSIS

For a standard, linear structural analysis, the familiar equation relating forces and displacements is

$$\boldsymbol{K}\boldsymbol{u} = \boldsymbol{f} \tag{3.13}$$

where $\boldsymbol{K}$ is the linear elastic stiffness matrix, $\boldsymbol{u}$ is a vector containing the displacements, and $\boldsymbol{f}$ is a vector of the static forces on the structure. This equation includes the assumption that the stiffness of the structure is independent of the forces applied. As the forces approach the buckling load, however, the stiffness becomes nonlinear, that is, dependent on the forces. To account for this aspect of response, a nonlinear analysis can be performed, the simplest of which is an Euler or bifurcation buckling analysis. In this approach, the total stiffness matrix is generalized, giving

$$\left[\boldsymbol{K} + \lambda \boldsymbol{K}_g\right] \boldsymbol{u} = \lambda \boldsymbol{f} \tag{3.14}$$

in which $\boldsymbol{K_g}$ is alternately known as the differential stiffness matrix or, more commonly, the *geometric stiffness matrix* and is a function of the forces on the structure. Buckling occurs when the generalized stiffness matrix becomes singular, that is, when λ is an eigenvalue of

$$\boldsymbol{K}\boldsymbol{x} = -\lambda \boldsymbol{K}_g \boldsymbol{x} \tag{3.15}$$

In this formulation, λ is the factor of safety against buckling and $\boldsymbol{x}$ is the buckling mode shape. The form of Eq. (3.15) differs from the generalized eigenproblem only in the sign of λ.

Implicit in the above formulation is the assumption that displacements prior to buckling remain infinitesimal, allowing the geometric stiffness matrix to be scaled by the eigenvalue as the load increases. This assumption may not be valid for certain analysis cases in which displacements do not remain small. To properly model the structural behavior in those circumstances, a large-displacement nonlinear analysis must be performed. Such an analysis is generally not necessary for plate buckling problems, and is not included in this research.

3.2.1 Solving the Generalized Eigenproblem

In the solution of the generalized buckling eigenproblem shown in Eq. (3.15), a variety of approaches can be taken. This section presents two of the more common approaches used for buckling analysis.

3.2.1.1 Inverse Reciprocal Approach

A straightforward technique is to interchange $\boldsymbol{K}$ and $\boldsymbol{K_g}$ and compute the largest negative eigenvalues of

$$\boldsymbol{K}_g \boldsymbol{x} = \mu \boldsymbol{K}\boldsymbol{x} \tag{3.16}$$

where

$$\mu = -\frac{1}{\lambda} \tag{3.17}$$

This approach, described by Grimes et al. (1994), is known as the inverse reciprocal approach. The problem can be transformed into the standard eigenproblem by pre-multiplying both sides by $\boldsymbol{K}^{-1}$:

$$\boldsymbol{K}^{-1}\boldsymbol{K}_g\boldsymbol{x} = \mu\boldsymbol{x} \tag{3.18}$$

Thus, the matrix of interest from Eq. (3.1) is

$$\boldsymbol{A} = \boldsymbol{K}^{-1}\boldsymbol{K}_g \tag{3.19}$$

and the original eigenvalues can be found from Eq. (3.17).

In the problem at hand, as with typical structural analysis problems, the elastic stiffness matrix is positive definite and invertible, while the geometric stiffness matrix may be neither. Thus, this method avoids inverting what may be a singular geometric stiffness matrix. In addition, the largest eigenvalues of the transformed matrix are sought, a task well-suited for common algorithms.

3.2.1.2 Spectral Transformation

Another approach to work around a possibly indefinite geometric stiffness matrix is to shift the range of desired eigenvalues, known as the eigenvalue spectrum. This strategy is known as *spectral transformation*, first explored by Ericsson and Ruhe (1980). Various shifts are possible, including the two shown below.

Expressing the eigenvalues as

$$\lambda = \sigma + \frac{1}{\upsilon} \tag{3.20}$$

the generalized problem becomes

$$\boldsymbol{K}\boldsymbol{x} = -\left(\sigma + \frac{1}{\upsilon}\right)\boldsymbol{K}_g\boldsymbol{x} \tag{3.21}$$

Rearranging Eq. (3.21) leads to

$$\left[\boldsymbol{K} - \sigma\left(-\boldsymbol{K}_g\right)\right]\boldsymbol{x} = \frac{1}{\upsilon}\left(-\boldsymbol{K}_g\right)\boldsymbol{x} \tag{3.22}$$

and finally

$$\upsilon\boldsymbol{x} = \left[\boldsymbol{K} - \sigma\left(-\boldsymbol{K}_g\right)\right]^{-1}\left(-\boldsymbol{K}_g\right)\boldsymbol{x} \tag{3.23}$$

Thus, in terms of the standard eigenproblem shown in Eq. (3.1),

$$\boldsymbol{A} = \left[\boldsymbol{K} - \sigma\left(-\boldsymbol{K}_g\right)\right]^{-1}\left(-\boldsymbol{K}_g\right) \tag{3.24}$$

After solving the standard eigenproblem, the original eigenvalues can be found from Eq. (3.20). This approach is known as the shift-invert method.

An alternate shifting strategy given by Bostic (1993) is to let

$$\lambda = \sigma\frac{\upsilon}{1-\upsilon} \tag{3.25}$$

which, when substituted into Eq. (3.15), yields

$$\boldsymbol{K}\boldsymbol{x} = -\sigma\frac{\upsilon}{1-\upsilon}\boldsymbol{K}_g\boldsymbol{x} \tag{3.26}$$

Multiplying both sides of this equation by (1-υ) gives

$$\boldsymbol{K}\boldsymbol{x} - \boldsymbol{K}\upsilon\boldsymbol{x} = -\sigma\upsilon\boldsymbol{K}_g\boldsymbol{x} \tag{3.27}$$

and

$$\boldsymbol{K}\boldsymbol{x} = \left[\boldsymbol{K} - \sigma\boldsymbol{K}_g\right]\upsilon\boldsymbol{x} \tag{3.28}$$

To arrive at the standard eigenproblem form, it is necessary to pre-multiply both sides by the inverse of $\boldsymbol{K} - \sigma\boldsymbol{K}_g$, finally giving

$$\left[\boldsymbol{K} - \sigma\boldsymbol{K}_g\right]^{-1}\boldsymbol{K}\boldsymbol{x} = \upsilon\boldsymbol{x} \tag{3.29}$$

which corresponds to the standard form of Eq. (3.1). Therefore, in the buckling problem,

$$\boldsymbol{A} = \left[\boldsymbol{K} - \sigma\boldsymbol{K}_g\right]^{-1}\boldsymbol{K} \tag{3.30}$$

This method is known as the buckling approach, and is often preferred for buckling problems.

The difficulty with spectral transformation is choosing an appropriate shift value. Without prior knowledge of the buckling behavior of a structure, the choice would be arbitrary. A poorly chosen shift value, far from the actual eigenvalues sought, could result in a large increase in computation time and a decrease in accuracy for iterative solvers. In a buckling problem, however, the eigenvalues of interest are expected to be close to one, the value separating stability and instability. Setting the shift value near unity will result in efficient solution for typical stability problems.

3.3 EIGENPROBLEM SOFTWARE

To date, a large number of algorithms and programs have been developed to solve eigenproblems. Sorensen (2002) lists a sampling of these, including Lanczos, SRRIT, ARNCHEB, LOBPCG, Laso, SVDpack, IRBL, JDQR, and ARPACK. Each is available for no cost online. A listing of the locations where these programs may be found is given in Appendix A. A researcher is left to choose from among these and many others the most efficient package for their particular problem.

In a comprehensive overview of eigenvalue computation developments, Golub et al. (2000) state that “at present, ARPACK seems to be the default choice for large sparse eigenproblems.” ARPACK is also one of the most recently developed solvers, and thus incorporates the most efficient routines existing today. For these reasons, ARPACK was chosen as the eigensolver for the UTrAp buckling analysis.

3.3.1 ARPACK

ARPACK (short for ARnoldi PACKage), developed at Rice University by R.B. Lehoucq, D.C. Sorensen, and C. Yang, contains a collection of Fortran77 subroutines for solving large-scale eigenvalue problems. It is based on the implicitly restarted Arnoldi method, originally developed by Sorenson (1995). A user's guide (Lehoucq et al. 1998), written by the software developers, explains the underpinnings and the use of ARPACK.

The ARPACK software has the capacity to handle both standard and generalized eigenproblems involving single or double precision values, both real and complex, in symmetric or non-symmetric matrices. For the generalized case, various drivers are included to implement shift-invert strategies, as explained below. The program uses what is known as reverse communication, allowing the user to select an optimum matrix storage format.

3.3.1.1 Implementation of ARPACK

ARPACK is available online through the Rice University website (see appendix for reference). Also available online in PDF format is the user's manual. For generalized eigenproblems, such as for a buckling analysis, a shift-invert strategy is recommended based upon the use of a sparse-direct matrix factorization, which already existed in the original version of UTrAp.

3.3.1.1.1 Reverse Communication

ARPACK relies on an indirect method of transferring the necessary matrix values. Called *reverse communication*, this method allows the user to supply subroutines for expressing their applications in vector form as the solution of a system of equations, instead of directly specifying the matrix values. This approach allows any storage format to be used and results in significant computational savings as well. In UTrAp, the reverse communication interface

allowed the existing matrix storage format to be used without modification in the eigenproblem solution.

3.3.1.1.2 Solution Modes

To solve the generalized eigenproblem, ARPACK offers four modes of operation: regular inverse, shift-invert, buckling, and Cayley transformation. The Cayley spectral transformation is designed for finding extreme eigenvalues, not eigenvalues near the origin, so it is not considered in this research project. The remaining three are viable alternatives, and each has been tested in UTrAp.

Regular inverse mode, corresponding to the inverse reciprocal approach previously described, is the most direct method of solving an eigenproblem. It does not incorporate a shift, and thus avoids the accompanying difficulties. The smallest eigenvalues will be found by this mode, even if they are negative or otherwise far from the expected values.

The shift-invert mode in ARPACK, corresponding to Eqs. (3.20) to (3.24) above, proves very unstable when used for a buckling analysis. When tested with small-order matrices, this mode fails to provide accurate results for a number of cases. Indefinite geometric stiffness matrices and negative eigenvalues are not handled correctly. For these reasons, this mode is not used in UTrAp.

A third ARPACK solution mode, corresponding to the buckling mode described in Eqs. (3.25) through (3.30), employs a spectral transformation, making it useful for finding eigenvalues near a specified shift. This mode gives good results on small matrices with known eigenvalues, but the purpose of UTrAp is to find unknown eigenvalues of large matrices. Unless the shift value is below the lowest eigenvalue, the eigenvalues returned will not be those of interest. The lowest eigenvalues are easily missed, with no indication of this

omission. To avoid this limitation, the shift value can be set close to zero so that only negative eigenvalues will be omitted.

In order to choose an eigensolver mode for UTrAp, the regular inverse mode and the buckling mode were compared in a buckling analysis of a small single-girder bridge in UTrAp. The shift value for the buckling mode was set at 0.02, and solver tolerances were varied between 10^{-8} and 10^{-2}. Table 3.1 shows the values obtained in the comparison.

Table 3.1 Eigensolver mode comparison

	Regular Inverse Mode		**Buckling Mode**	
Tolerance	Time (s)	Error	Time (s)	Error
10^{-8}	2.17	0.0000000%	2.00	0.0000001%
10^{-7}	2.11	0.0000000%	1.84	0.0000147%
10^{-6}	2.08	0.0000000%	1.42	0.5241094%
10^{-5}	1.92	0.0000000%	1.27	2.6114868%
10^{-4}	1.89	0.0000000%	1.25	2.6114868%
10^{-3}	1.75	0.0000006%	1.25	2.6114868%
10^{-2}	1.41	0.5142611%	1.25	2.6114868%

The values from Table 3.1 are plotted in Figure 3.1. Solution time (left axis) is shown by solid lines, and percent error (right axis) is shown by dashed lines. The buckling mode is consistently faster, but its accuracy decreases rapidly with the changing tolerance. The accuracy also depends on the choice of the shift value. If a shift can be chosen close to the lowest eigenvalue, the buckling mode solver will be both accurate and efficient. Without prior knowledge of the eigenvalues, however, this approach is impractical. Alternatively, the regular inverse mode is somewhat slower, but maintains good accuracy even at large

tolerances and is not dependent on a shift value. Because accuracy is more critical than the solution time, the regular inverse mode is used in UTrAp.

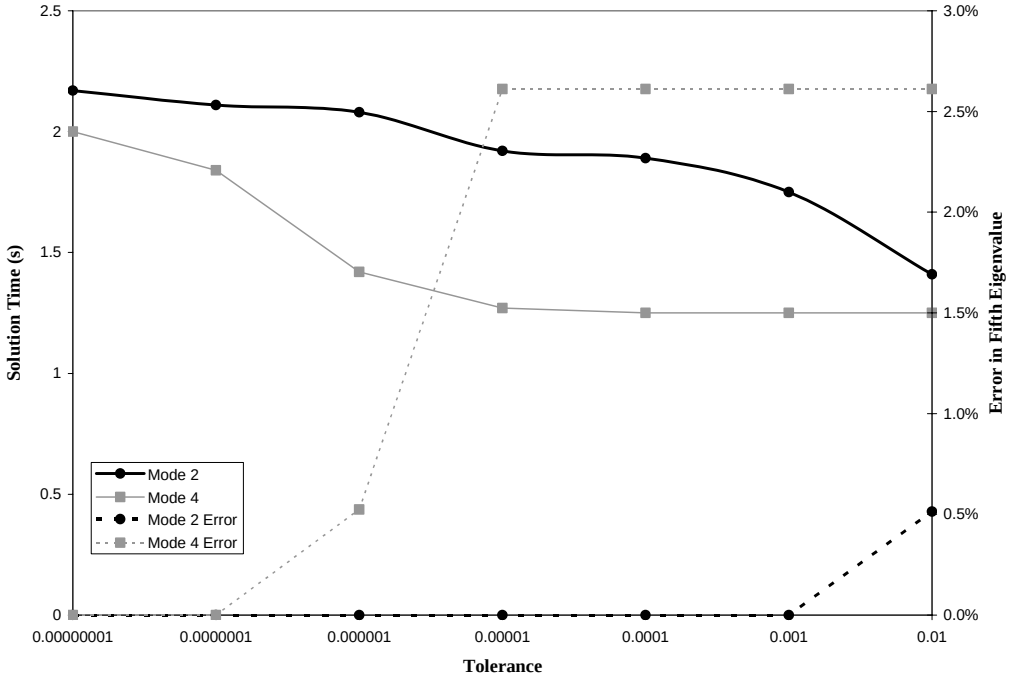

Figure 3.1 Comparison of eigensolver modes

3.3.1.1.3 Eigensolver Verification

To verify that the program calculates correct eigenvalues, a pair of simple test matrices was created. Both the elastic stiffness matrix and the geometric stiffness matrix were defined to be of order ten, with non-zero terms only on the diagonal, sub-diagonal, and super-diagonal. The eigenvalues of the generalized eigenproblem involving these two matrices were found both with the UTrAp solver and with Mathcad. Excellent agreement between the two was achieved for both the regular inverse mode and the buckling mode, confirming that the ARPACK solver functions correctly within UTrAp.

3.4 SUMMARY

The mathematical underpinnings of an elastic critical load analysis have been presented in this chapter. The eigenproblem, as it is known, has many other applications, and has received much attention from mathematicians and programmers over the years. In UTrAp, the buckling analysis eigenproblem is solved using ARPACK, a recently developed group of subroutines. ARPACK has proven to be both accurate and efficient within UTrAp 2.0.

CHAPTER 4
Program Verification

"By far the best proof is experience."

- Sir Francis Bacon

One of the most important steps in developing any structural analysis software is verification: does the program give trustworthy results? Verification is especially important for nonlinear programs such as UTrAp 2.0, where it is difficult to have a sense of whether the results are correct. In this chapter, the procedure followed for verifying the accuracy of UTrAp 2.0 results is presented. Computed values from UTrAp are compared with theoretical predictions, results from other finite element software, and an actual buckling failure of a steel trapezoidal box-girder bridge during construction. Each method verifies the results from UTrAp 2.0, showing that the program gives accurate predictions of the buckling characteristics of steel trapezoidal box girders.

4.1 THEORY

Perhaps the simplest and most familiar form of instability is named for Leonhard Euler, the famous Swiss mathematician who in 1757 developed his theory of buckling. Euler buckling, also known as classical or eigenvalue buckling, describes the behavior of a slender column that has reached a critical load. At loads above this value, any slight disturbance will cause the column to deflect laterally and lose capacity. The critical load for Euler buckling is found by solving the differential equation that results from analyzing the column in the

deformed configuration. The derivation is given in many textbooks on structural analysis, including that by Craig (2000), and is not repeated here.

For a column pinned at both ends, the possible buckling loads are given by the equation

$$P_n = \frac{n^2 \pi^2 EI}{L^2} \tag{4.1}$$

in which E is Young's elastic modulus, I is the moment of inertia of the section about the weak axis, L is the length of the column, and n is any positive integer. The critical load is given by the smallest value of n, i.e., $n = 1$:

$$P_{cr} = \frac{\pi^2 EI}{L^2} \tag{4.2}$$

The value in Eq. (4.2) is the Euler buckling load. Corresponding to this critical load is the buckling mode shape, given by

$$y(x) = A \sin\left(\frac{\pi x}{L}\right) \tag{4.3}$$

where x is the coordinate along the member, y is the coordinate perpendicular to the weak axis (in the direction of the displacement), and A is the amplitude of the displacement. The nature of the problem is such that A is arbitrary, that is, the amplitude cannot be found from the solution of the differential equation. This outcome is analogous to the eigenproblem, in which the magnitude of the eigenvector components cannot be found. The Euler buckling load is therefore equivalent to the eigenvalue of this problem, and the buckling mode shape corresponds to the eigenvector.

To verify that UTrAp 2.0 correctly predicts the Euler buckling load of a simple column, a test was run to simulate plate buckling. Because UTrAp models an entire trapezoidal section and is not easily modified to remove parts of the girder, the webs and top flanges of the test girder were made very thin. The

geometric stiffness matrices for only the elements in the bottom flange were assembled, preventing the thin plates in the webs and top flanges from buckling. This modeling approach left the bottom flange as the dominant member, simulating a single plate. Both ends of the flange were pinned to prevent lateral movement, and an axial compressive force was applied.

The bottom flange in this analysis had a width of 40 inches, a thickness of 2 inches, and a length of 240 inches. The moment of inertia about the weak axis is therefore

$$I_y = \frac{1}{12} bt^3 = \frac{1}{12}(40)(2)^3 = 26.67 \text{ in}^4$$

The Euler buckling load is found using Eq. (4.2):

$$P_{cr} = \frac{\pi^2 E I_y}{L^2} = \frac{\pi^2 (29600)(26.67)}{240^2} = 135.25 \text{ kips}$$

A buckling analysis was performed within UTrAp 2.0 with a compressive force of 100 kips applied to the bottom flange. The first eigenvalue for this problem is computed to be 1.366, which corresponds to a buckling load of 136.6 kips, less than 1% greater than predicted by theory. The buckling mode shape is predicted to be a single sine wave, as shown in Eq. (4.3). UTrAp's buckling mode shape is shown in Figure 4.1 below.

The first buckling mode shape from UTrAp agrees with the prediction, as does the critical buckling load. The latter is slightly greater than predicted by theory, due to the discretization inherent in the finite element method. The twenty-foot plate is divided into only ten elements along the length, resulting in a higher buckling load than would be expected of an actual plate. The second eigenvalue calculated by UTrAp is 2.036, corresponding to the eigenvector shown in Figure 4.2. The plate did not exhibit Euler buckling, but rather torsional buckling. This form of buckling involves a rotation about the longitudinal axis,

and occurs only in very slender sections that are symmetric about both axes, as in the case of a thin plate.

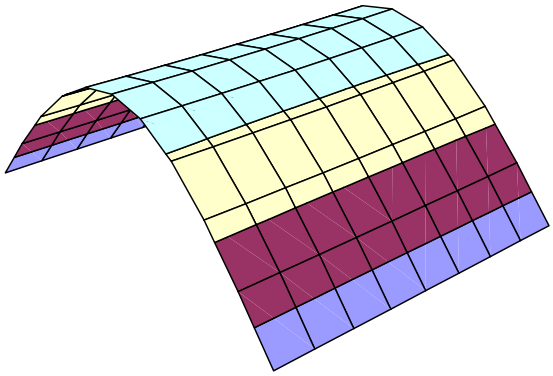

Figure 4.1 First plate buckling mode from UTrAp 2.0

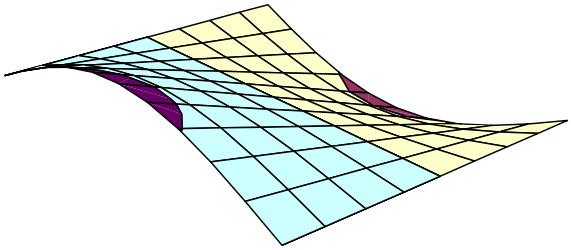

Figure 4.2 Second plate buckling mode from UTrAp 2.0

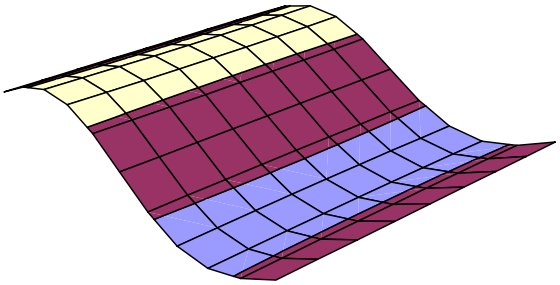

Figure 4.3 Third plate buckling mode from UTrAp 2.0

The buckling mode corresponding to the third eigenvalue of 5.611 is shown in Figure 4.3. This mode is the second Euler buckling mode, given by letting $n = 2$ in Eq. (4.1):

$$P_n = \frac{4\pi^2 EI}{L^2} = 541 \text{ kips}$$

The UTrAp value is 3.7% greater than the theoretical value. The greater discrepancy than in the first mode is again explained by the coarse discretization, which becomes more important in the higher buckling modes where the plate exhibits more curvature. This observation is confirmed by looking at the fifth eigenvalue, which corresponds to the third Euler buckling mode (n = 3). The theoretical value is 1217.25 kips, while the UTrAp value is 1316.9 kips, 8.2% too high. With a finer discretization, the higher buckling modes would agree more closely with the theoretical values. Even with only ten elements along the length, however, the first buckling mode given by UTrAp agreed very well with buckling theory, demonstrating that the program gives accurate results for plate buckling.

4.2 FINITE-ELEMENT SOFTWARE

Although verifying that UTrAp 2.0 correctly handles plate buckling has some use, it does not imply that the program can correctly handle the more complex problem of trapezoidal box-girder buckling. The commercial finite-element analysis program ANSYS was used to perform buckling analyses of steel trapezoidal box girders, forming a basis for verifying the results from UTrAp.

4.2.1 Model 1 Girder

Before attempting to analyze longer and more complex girders, a simple model was built within ANSYS of the Model 1 girder used by Widianto (2003). The girder length was set at fifty feet and a load of 1 kip/foot was applied along the top flanges. Struts with a cross-sectional area of 4.0 in^2 were placed every ten

feet; no top lateral bracing or internal diaphragms were used. An elastic critical load analysis was performed within ANSYS, giving an eigenvalue of 6.37 and the buckled shape shown in Figure 4.4.

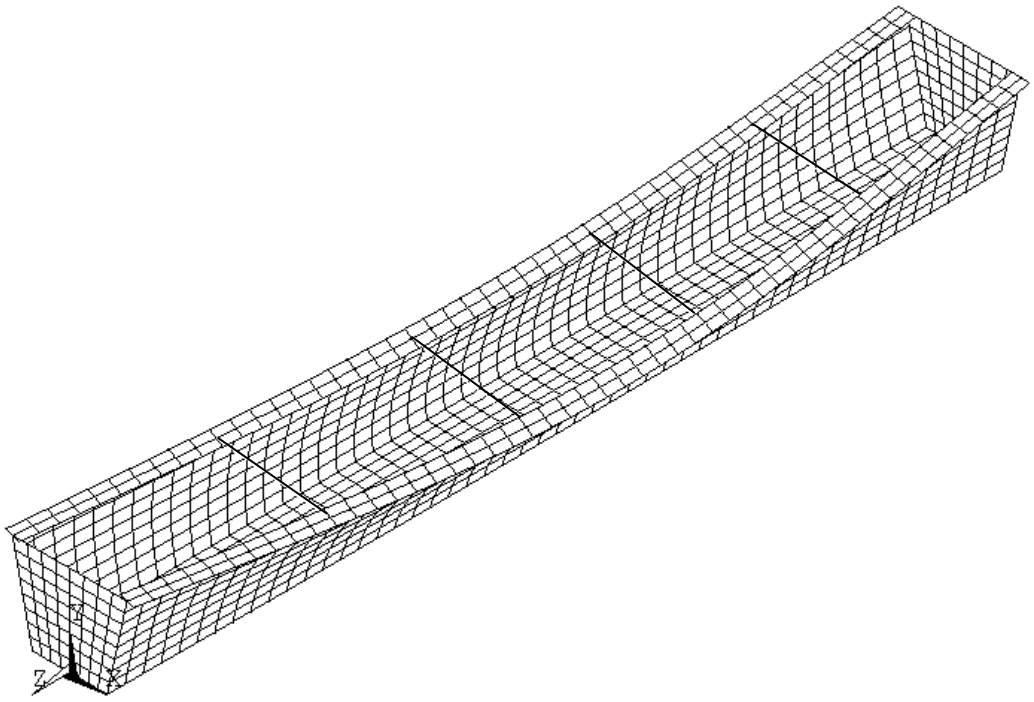

Figure 4.4 ANSYS buckled shape for 50´ Model 1 girder

UTrAp 2.0 was used to analyze the same girder under identical loading. The first eigenvalue given by UTrAp is 6.45, only 1.3% higher than the ANSYS value of 6.37. Differences between the analyses are discussed below. Because the current version of UTrAp does not offer three-dimensional post-processing capabilities and adding this feature would be difficult, UTrAp 2.0 slices the bridge into cross-sections, showing the two-dimensional deformed shape of each cross-section individually. Taken together, these cross-sections form a picture of the buckled shape of the girder, as shown in Figure 4.5. The cross-sections shown in Figure 4.5 are roughly at quarter points along the length of the girder.

12'

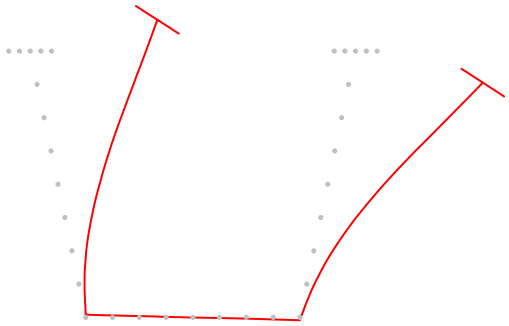

24'

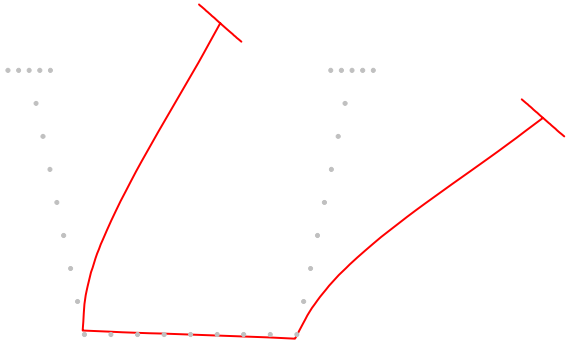

36'

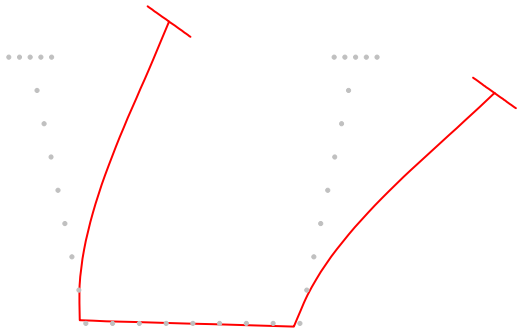

Figure 4.5 UTrAp 2.0 buckled shape for 50´ Model 1 girder

It is clear from comparing Figure 4.4 and Figure 4.5 that the buckled shapes provided by the two finite-element programs are very similar. In both, the lack of internal diaphragms allows the cross-section to deform, leading to lateral torsional buckling of each web and top flange without movement of the bottom flange, rather than buckling of the entire section. The struts force the top flanges to move in the same direction.

The small discrepancy between the eigenvalues from ANSYS and UTrAp is more than accounted for by differences in the models. In ANSYS, a plate was used at each end to model the support diaphragms; UTrAp uses a very stiff truss to model the diaphragms. The trusses only restrain relative movements of the intersections of the webs and flanges at the ends, whereas the plates restrain translations as well as rotations along the webs and bottom flange. In addition, a four-noded shell element was used in the ANSYS model, with four times as many shell elements as in UTrAp, which employs a nine-noded element. The result was two models with the same number of nodes, but different element formulations. Overall, however, these differences were insignificant, as the two programs gave similar results.

4.3 CASE STUDY OF MARCY BRIDGE COLLAPSE

UTrAp 2.0 has now been shown to agree with commercial finite element software, but its relation to performance under actual field conditions has not been demonstrated. The question remains: does UTrAp provide actual buckling characteristics of steel trapezoidal box girders? To answer this question, the Marcy pedestrian bridge is analyzed under actual loading conditions. This bridge buckled during the pouring of the concrete deck (Figure 1.3), presenting an opportunity to illustrate both the accuracy and the worth of UTrAp.

Figure 4.6 shows the section dimensions of the Marcy bridge. Dimensions were originally specified in metric units and are converted to inches in the figure below. The web thickness is constant over the length, while the top and bottom flanges each have a greater thickness at midspan. The bottom flange thickness changes 36.1 feet from each support, and the top flange thickness is increased 50.5 feet from each support. The span of the bridge is 170.6 feet.

Only internal diaphragms and struts are used in the Marcy bridge; no top lateral bracing is present. There are nine diaphragms spaces along the length of the girder, resulting in an internal diaphragm spacing of about 19 feet. Struts are placed at third points between internal diaphragms. All bracing members are L3x3x⅜ angles with a cross-sectional area of 2.11 in^2.

The concrete deck is 14 feet wide and 7.5 inches thick, with a dead weight including the haunches of 1.562 kips/ft. Additional dead weight from the permanent metal deck forms and the diaphragms adds 0.086 kips/ft. The total load applied to the girder is therefore 1.65 kips/ft, not including the self-weight of the girder, which is handled internally in UTrAp 2.0.

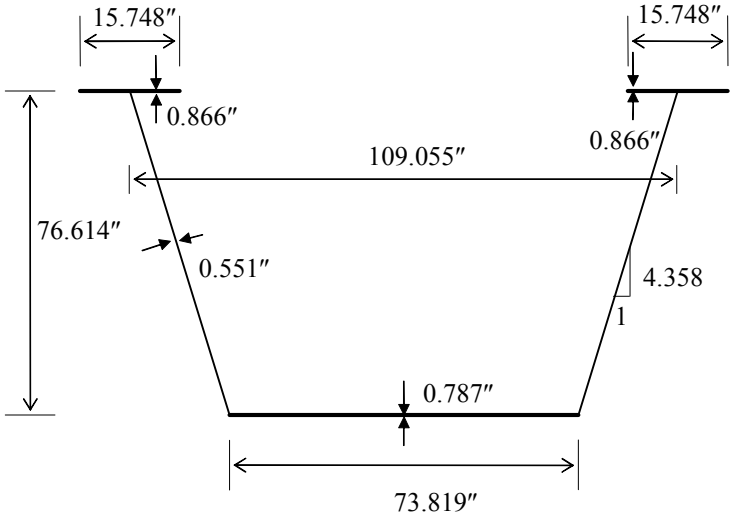

End Section Dimensions

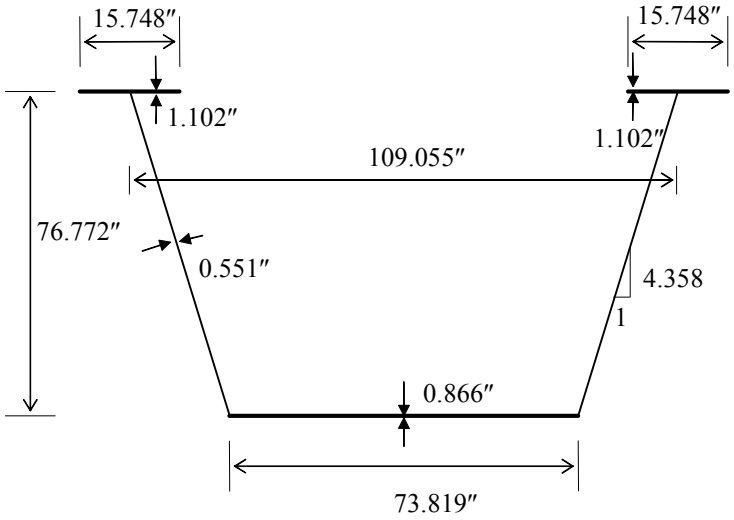

Midspan Section Dimensions

Figure 4.6 Section dimensions of Marcy pedestrian bridge

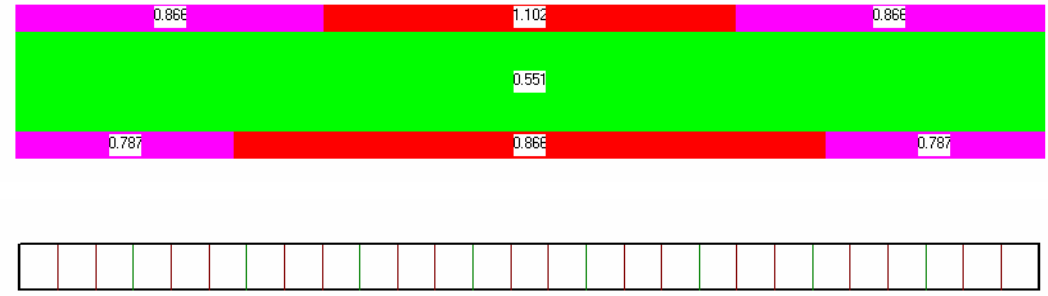

Figure 4.7 UTrAp 2.0 model of Marcy pedestrian bridge

Because UTrAp discretizes the bridge into finite elements, dimensions must be rounded within the program. Flange and web lengths must be multiples of two feet, the length of a shell element, and bracing members must join the girder at multiples of one foot, the distance between nodes along the bridge. Because of these requirements, the bridge as modeled by UTrAp is not precisely the same as the actual bridge, although it is acceptably close for analysis purposes. The Marcy bridge model in UTrAp 2.0 is shown in Figure 4.7. At the top of the figure are the dimensions of the top flanges, web, and bottom flange illustrated graphically; underneath is the plan view of the bridge. UTrAp displays the plan view of a bridge with a realistic length-to-width ratio.

Finding the length of deck that will cause buckling is an iterative procedure, requiring the user to input different deck lengths until the eigenvalue becomes 1.0. Using this process, UTrAp 2.0 predicts that the bridge will reach a critical buckling load when the concrete pour has extended 68 feet onto the bridge. The actual bridge failed when the concrete had reached approximately midspan, or 85 feet along the bridge. A cross-section of the buckled shape from UTrAp is shown in Figure 4.8.

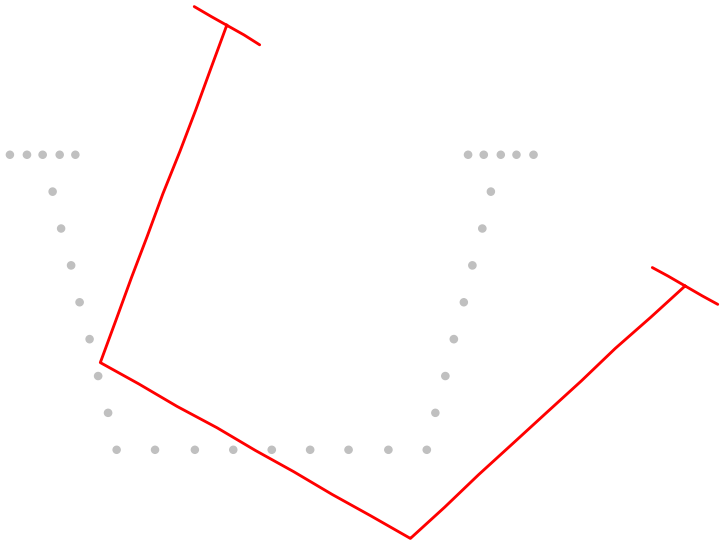

Figure 4.8 UTrAp buckled cross-section of Marcy bridge

Clearly, the predicted failure mode is lateral torsional buckling of the entire cross-section, which was the true failure mode observed in the field. UTrAp conservatively predicts failure at a pour length of 68 feet, less than the actual length of approximately 85 feet. This error is mainly due to the presence of permanent metal deck forms in the actual bridge, which serve to partially brace the top flanges, increasing the buckling load slightly. UTrAp does not account for the bracing effect of the metal decking, and thus the buckling loads will be generally slightly conservative. Nonetheless, the program predicts that buckling will occur--and indeed, the bridge buckled.

It should be mentioned that the second buckling mode given by UTrAp involves local bending of the webs. Unlike the first mode, this sort of failure would not be catastrophic. The load associated with this form of failure is approximately three and a half times that of the first mode. It is clear that lowest mode is the dominant mode of failure in this bridge.

4.3.1 Comparison with ANSYS

The Marcy pedestrian bridge was further analyzed with the ANSYS software. With a simple loading case of one kip per foot, the results from UTrAp 2.0 and ANSYS showed good agreement, further verifying the UTrAp answers. ANSYS work at the University of Houston also agreed with the modeling done for this thesis. A three-dimensional buckled shape from ANSYS is shown in Figure 4.9.

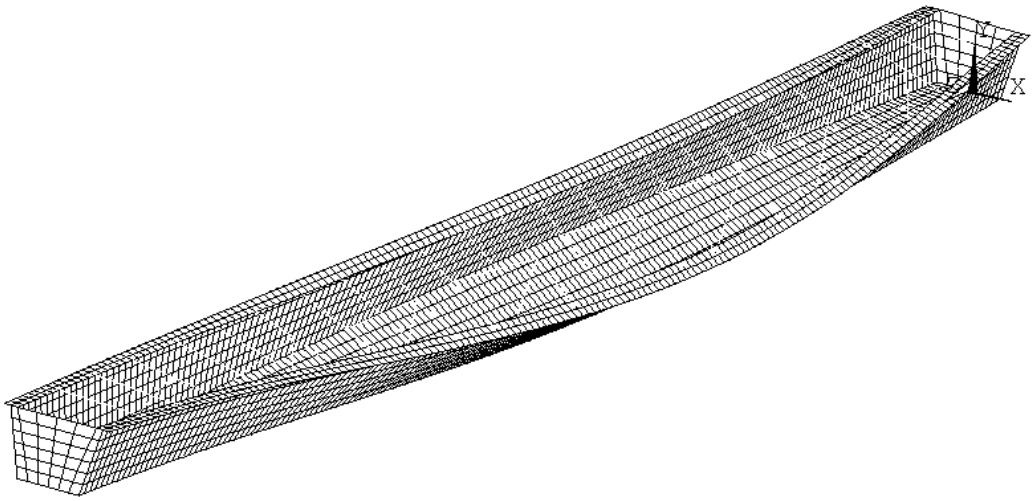

Figure 4.9 Marcy bridge buckled shape from ANSYS

The bridge is unmistakably exhibiting lateral torsional buckling, as is predicted by UTrAp and was seen in the field.

4.4 SUMMARY

In this chapter, the buckling loads given by UTrAp 2.0 have been shown to agree with basic theory, a commercial finite element program, and most importantly, with an actual instance of buckling failure in a trapezoidal box girder. In each of these comparisons, the buckling characteristics predicted by

UTrAp were accurate. Because buckling failures can be catastrophic and thus must be guarded against with a larger factor of safety than other forms of failure, slightly conservative estimates of the buckling load, such as those found for the Marcy bridge, are acceptable.

CHAPTER 5
UTrAp 2.0 User's Guide

"Programming today is a race between software engineers striving to build bigger and better idiot-proof programs, and the Universe trying to produce bigger and better idiots. So far, the Universe is winning." *- Rich Cook*

UTrAp 2.0 is a revised and expanded version of the program UTrAp, developed for the analysis of steel trapezoidal box-girder bridges during construction. The major new feature is the capability to perform buckling analyses, but various other improvements have been made, including the ability to add web stiffeners to the model and the inclusion of self-weight loading. Numerous changes have also been made to the user interface to increase the user-friendliness. This chapter presents a brief user's guide explaining the features of UTrAp 2.0. A complete user's guide will be included with the release version of the program.

5.1 CAPABILITIES AND LIMITATIONS

UTrAp 2.0 is intended to perform both linear analyses and linearized buckling analyses of straight or curved steel trapezoidal box-girder bridges under construction loading. The program is able to model the partially-composite behavior due to concrete curing during the bridge deck pours. UTrAp 2.0 is limited to elastic analyses, and does not account for nonlinear material behavior. There are no limits on stresses in the girder, which may therefore exceed the yield stress. In order for the UTrAp analysis to be valid, care must be taken by the designer to ensure that the bridge remains elastic under the given loading.

In addition, local buckling may not be captured by the UTrAp buckling analysis. Bracing members, which in reality are typically channels or angles, are modeled as truss members, which carry only axial force. This simplification prevents the buckling of individual truss members, which are defined by a straight line between two points.

Two methods for avoiding inaccuracies related to bracing members are suggested. The designer can ensure that each individual brace member will not buckle under its maximum expected load, obtained directly in a buckling analysis as explained below. If any bracing members are unable to carry their expected load, the UTrAp analysis will be inaccurate, because it assumes that bracing members will not buckle.

In the case of large brace forces where designing for elastic behavior would increase member size undesirably, an alternate procedure can be used to ensure accurate results. After running the initial buckling analysis and finding the forces in the bracing members, the user can remove from the model those braces which carry a high compressive force. In effect, this modeling approach treats those braces as having buckled and incapable of contributing to the overall stiffness of the girder being analyzed. A buckling analysis can then be performed on the revised model, showing the effects of the buckling (removal) of those members.

5.1.1 Straight versus Curved Girders

Section 4.6.1.2 of the AASHTO LRFD Bridge Specifications pertains to structures curved in plan. Subsection 1 states:

> *Segments of horizontally curved superstructures with torsionally stiff closed sections whose central angle*

subtended by a curved span or portion thereof is less than 12.0° may be analyzed as if the segment were straight.

Of note in this provision is that the superstructure must be torsionally stiff, as in the case of a composite trapezoidal girder. The UTrAp program, however, analyzes the girders during the concrete pour, when the sections are only partially closed, with a stiffness that could be one or two orders of magnitude less than that of the completed section. Accordingly, UTrAp 2.0 analyzes sections with any curvature, however small, as curved sections. Only in the case of a perfectly straight bridge will the program treat the girder as straight. The user can enter a value of zero for the radius of curvature, which the program will interpret as infinity.

5.2 GRAPHICAL USER INTERFACE

In UTrAp 2.0, bridge data is input by using the GUI (graphical user interface), and analyses are performed by a separate module invoked by the GUI. Results are viewed within the user interface. Presented here is a guide to the user interface, adapted from the original user's guide by Topkaya (2002). As features are explained, an example bridge is analyzed to illustrate the program's use.

5.2.1 Example Problem Definition

The Marcy pedestrian bridge is chosen to illustrate the use of the UTrAp 2.0 user interface. Information on the bridge is presented with the discussion of global instability in chapter four. The section dimensions are shown in Figure 4.7. In the interest of brevity, this information is not repeated here.

5.2.2 UTrAp 2.0 Menus

The graphical user interface of UTrAp has nine menus. This section describes each of these menus in detail and provides information regarding how data is supplied to UTrAp for the analysis of trapezoidal box-girder bridges. In addition, specific information needed to analyze the example bridge described above is provided.

File Menu: This menu is used for data management and has four submenus. Files are stored and retrieved using the following submenus:

New Project: Select this option to start a new bridge project. This option is only available when first starting UTrAp. To start a new project after working on another project, the user must exit and restart UTrAp.

Existing Project: This submenu opens an existing project. The UTrAp input project files have an extension of *.inp. When this submenu is invoked, an open file box will appear which is used to select the existing project file. This option is only available when first starting UTrAp.

Save Project: This submenu saves a project to the hard disk. It can be used to save the changes made to an existing project or the contents of a newly developed project. When this submenu is invoked, a save file box will appear which is used to name or rename the project file. As with any program, it is recommended that projects be saved on a regular basis while using UTrAp.

Exit: This submenu is used to exit the program. A confirmation box will offer a chance to save the project upon exiting.

Geometry Menu: Choosing this menu opens the form used to input the dimensions of the bridge. Values should be typed in the boxes provided. A

graphical representation of the cross section is displayed on the Geometric Properties form. After entering the required data, the user must press the Save Data button in order for the values to be stored in memory. Pressing the Save Data button stores the data and closes the form. If the user does not want to save the values, the Cancel button should be pressed. This process for saving data applies to the subsequent forms as well.

Example Problem: A new project is formed by choosing "New Project" from the File menu. The dimensions of the Marcy bridge are input into the Geometric Properties form, as shown in Figure 5.1.

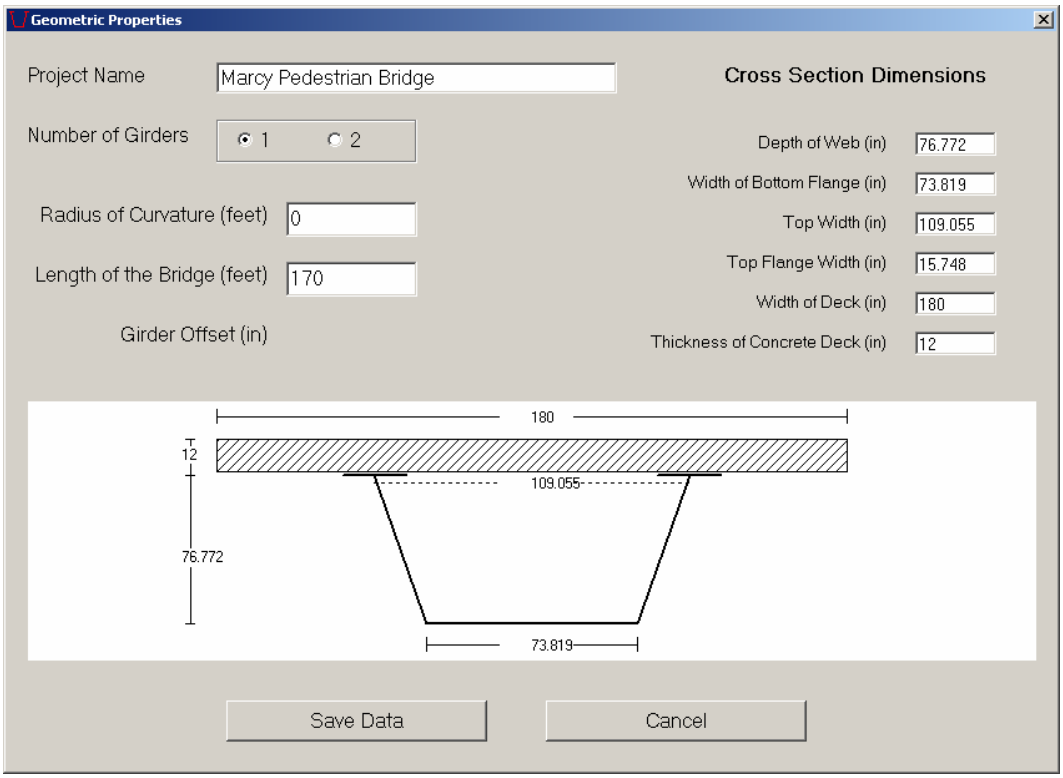

Figure 5.1 Geometric Properties form

Plate Properties Menu: This menu choice opens the Plate Properties form, which has three separate tabs for entering the web, bottom flange, and top flange properties. The lengths and corresponding thicknesses of the plates should be entered from the start to the end of the bridge. There are two buttons used to add and remove properties, as explained below.

Add: This button is used to add plate properties. A change in plate thickness requires the user to specify a new property. The user should enter the number of properties that will be needed to characterize the bridge. The number of rows in the table is increased by the number specified.

Remove: This button is used to remove plate properties. The property number to be removed should be specified in the box next to the Remove button.

Example Problem: In each tab, the number of properties is entered through use of the Add button. The user can enter the total number of plate properties in the box next to the Add button before it is pressed. Additional properties can be added as needed with the Add button. All plate properties are entered in a tabular format. The input for the bottom flange plate properties is given in Figure 5.2. Similar data are provided for the web and top flanges. Once all the necessary plate properties have been specified, the user must select the Save Data button in order to store the information in memory.

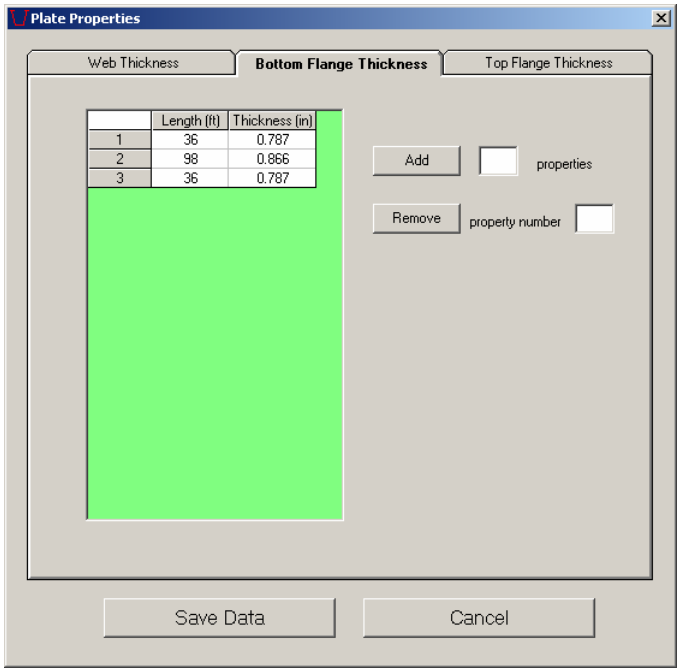

Figure 5.2 Plate Properties form

Bracing Menu: This selection opens the Bracing Properties form, which has four separate tabs for inputting the internal brace, external brace, top lateral brace, and web stiffener properties. The program currently offers only one type of both internal and external braces, which can be seen by clicking on the "Show Brace Types" button at the bottom of each tab. The location and member cross-sectional area are required for internal and external braces. The start location, end location, type, and area are required for the top lateral braces. In UTrAp 2.0, web stiffeners can also be added to the model by specifying their location, width, and thickness. Buttons are provided for adding and removing braces and stiffeners. Functions of the buttons are explained below.

Add: This button inserts braces or stiffeners. The number of rows in the table is increased by the number specified.

Equally Space: This button adds a specified number of braces or stiffeners at equally-spaced intervals between the two location values entered. The

location entered in the first box must be smaller than the location in the second box.

Match Internal Brace Locations: This button copies the internal brace locations into the web stiffener tab. Because internal braces are almost always accompanied by web stiffeners, this button simplifies the input process.

Remove: This button removes the brace or stiffener corresponding to the number entered.

Remove All Braces/Stiffeners: This button removes all braces or stiffeners in the tab.

Type: This button is displayed in the internal brace and external brace tabs. Because the current version of UTrAp offers only one type of both internal and external braces, this button is disabled and the braces are automatically set to type 1. The internal and external brace configurations can be seen by using the Show Internal/External Brace Types buttons.

Area: This button is used to assign the same cross-sectional area to all brace members. If all braces do not have the same cross-sectional area, the values for each brace can be entered directly into the table.

Width: This button appears only in the web stiffener tab, and is used to apply a constant width to all web stiffeners. Widths of individual stiffeners can also be specified directly in the table.

Thickness: Similar to the Width button, this button applies a constant thickness to all web stiffeners. Again, individual thicknesses can be entered directly.

Show Internal/External/Top Lateral Brace Types: These buttons are used to display the types of braces that can be specified in the program. When this button is pressed, a form that shows the geometry and types of braces is displayed on the screen. Figure 5.3 shows the types of internal and

external braces supported by the current version of the program. The two types of top lateral braces are shown in Figure 5.4.

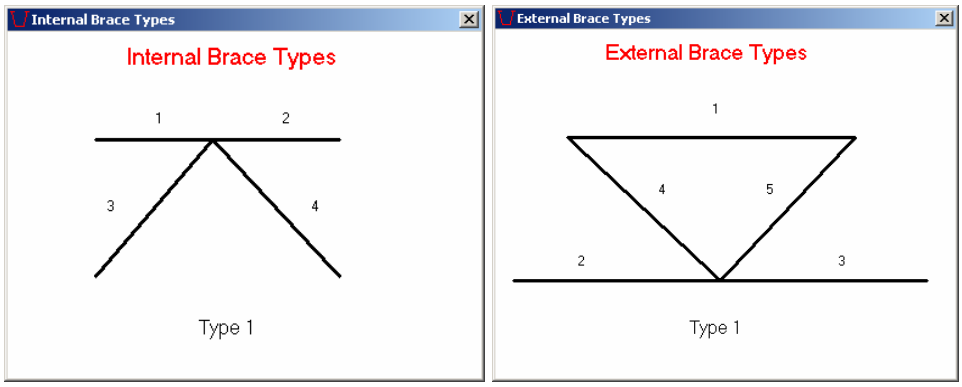

Figure 5.3 Internal and external brace types

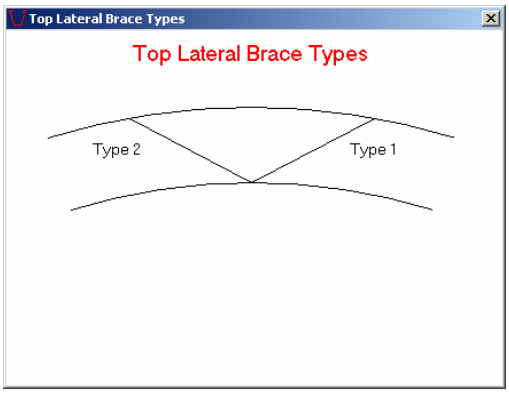

Figure 5.4 Top lateral brace types

All Type 1: This button, displayed only in the Top Lateral Braces tab, assigns Type 1 to all top lateral braces.

All Type 2: Similar to the previous button, this button assigns Type 2 to all top lateral braces.

Alternating Starting with Type 1: This button, displayed only in the Top Lateral Braces tab, assigns alternating types to consecutive braces. The first brace will be Type 1, the second Type 2, and so on.

Alternating Starting with Type 2: This button accomplishes the opposite of the previous button, starting with Type 2 braces instead of Type 1.

An X-type top lateral system can be handled by the program simply by specifying both Type 1 and Type 2 braces with the same start and end points. For each X-brace, two data lines with the same start and end location would be needed, one with a Type 1 brace and the other with a Type 2 brace. Struts can also be defined within the program. As shown in Figure 5.3, an internal brace includes a strut (members 1 and 2 in the figure). If a strut acts at location where an internal brace is not present, the user can simply specify the strut as a top lateral brace with identical start and end locations.

Example Problem: Eight internal braces are added using the Equally Space button, followed by eight pairs of web stiffeners added using the Match Internal Brace Locations button. The eighteen strut start locations are entered using the Equally Space button and are copied into the end locations. Areas and dimensions are entered using the Uniform Properties buttons. Figures 5.5 through 5.7 show the relevant tabs of the Bracing Properties form with the data for the example problem entered.

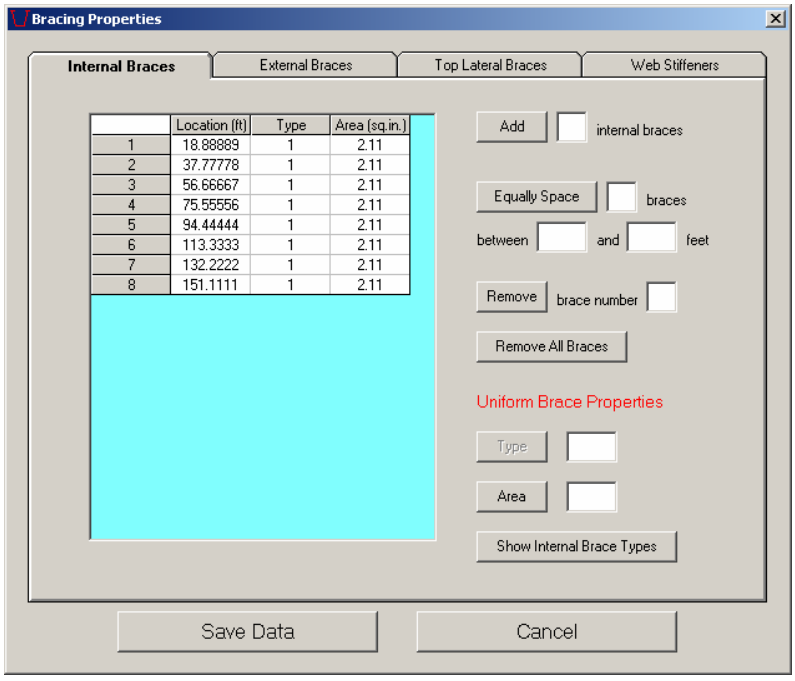

Figure 5.5 Internal Braces tab

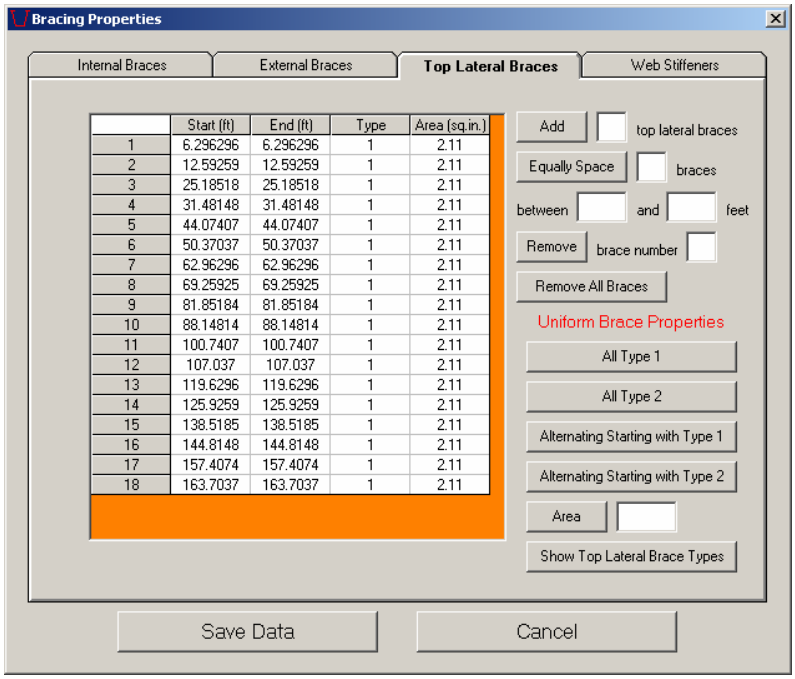

Figure 5.6 Top Lateral Braces tab

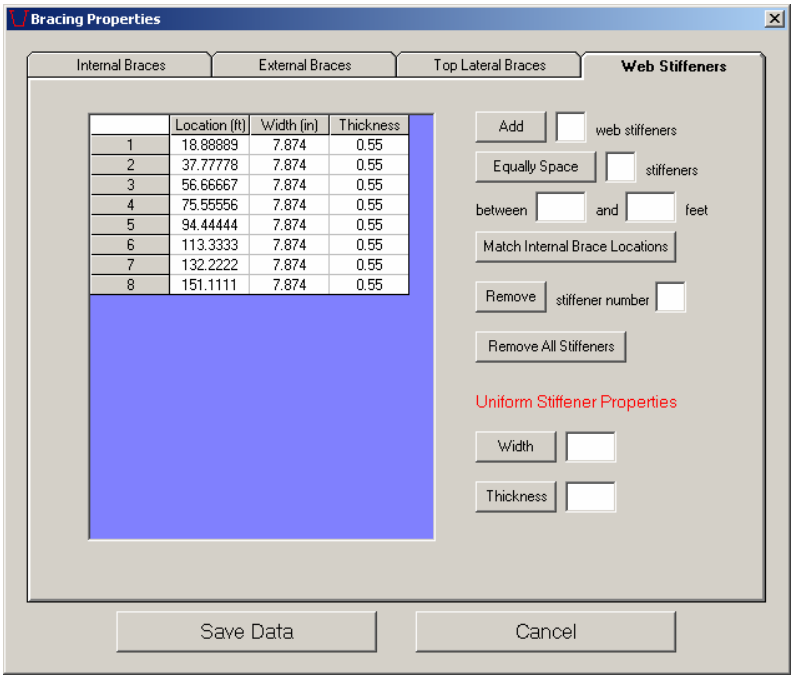

Figure 5.7 Web Stiffeners tab

Support Menu: This menu is used to input support locations. The program assumes the first support entered is pinned and the remainder are on rollers. The number of rows in the table is controlled by the Add and Remove buttons as explained below.

Add: This button is used to add the specified number of supports. The number of rows in the table is increased by the number entered.

Remove: This button is used to remove the specified support number.

Example Problem: Two supports are added to the table using the Add button. The bridge is simply-supported, so 0 feet and 170 feet are entered for the support locations. The support at 0 feet will be pinned, although the opposite end could be pinned by simply reversing the entries. Figure 5.8 shows the Support Locations form with the entered data.

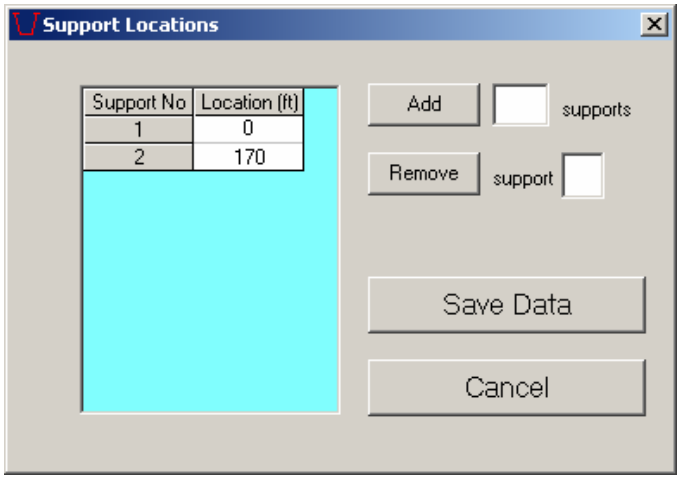

Figure 5.8 Support Locations form

Stud Menu: This menu is used to input stud properties in tabular form. The spacing of the studs along the length of the bridge and the number of studs per flange should be supplied to the program. The number of rows in the table is controlled by the Add and Remove buttons. Functions of these buttons are explained below.

Add: This button is used to add the specified number of properties.

Remove: This button is used to remove the specified property.

Example Problem: Stud spacing is constant along the length of the Marcy bridge, so only one row is added to the table using the Add button. A stud spacing of 24 inches is entered, and two studs per flange are specified. Figure 5.9 shows the Stud Properties form with the data entered.

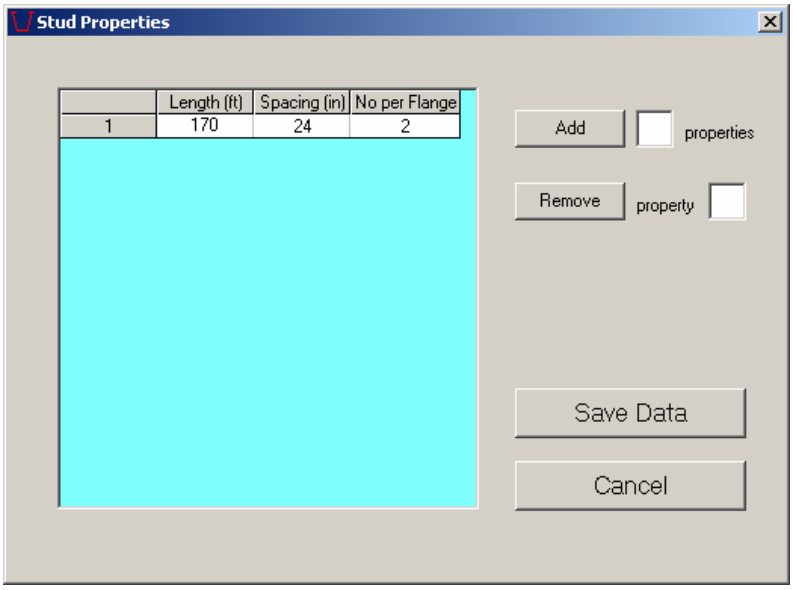

Figure 5.9 Stud Properties form

Pour Sequence Menu: This menu is used to input pour sequence analysis parameters in tabular form. The concrete deck can be divided into segments corresponding to each separate pour. Lengths of the deck segments are the same for all analyses. Independent analyses can be run for different loadings and deck segment stiffnesses. For each analysis, properties of the deck segments and loading on the segments are required input. Properties for a deck segment include the concrete stiffness and the stud stiffness. A new feature in UTrAp 2.0 is the ability to include the self-weight of the girder. This is accomplished by checking the "Include Self-Weight" box. Note that only the dead weight of the steel girder is added by the program, and not any weight from the concrete, bracing members, or other loads. The Pour Sequence table is controlled by four buttons, used to add and remove columns and rows as explained below.

Add Analysis Case: This button adds a new analysis case to the table. Three new columns are added to the right side of the table and are used to specify the concrete stiffness, the stud stiffness, and the load acting on the deck.

Remove Analysis Case: This button removes the specified analysis case. The three columns related to that analysis are removed from the table.

Add Deck Property After: As mentioned, the concrete deck can be divided into different pours, each with unique properties. This button adds a new deck property row to the table below the specified deck number. To specify the first deck, a value of zero should be used. The sum of the lengths of the deck properties must equal the total bridge length.

Remove Deck Property: This button removes the specified row of deck properties.

Example Problem: In this problem, the concrete deck is divided into two segments with lengths of 68 and 102 feet, respectively, for reasons explained in the previous chapter. The deck segments are added to the table by making use of the Add Deck Property After button. The two analysis cases to be performed are added to the table by using the Add Analysis Case button. In the first analysis, the dead weight from the forms and diaphragms of 0.086 kips/foot is added to both decks in addition to the self-weight of the girder. For the second analysis, the weight of the concrete slab and haunches of 1.562 kips/foot is applied only to the shorter deck segment. Figure 5.10 shows the Pour Sequence form with the Marcy bridge data.

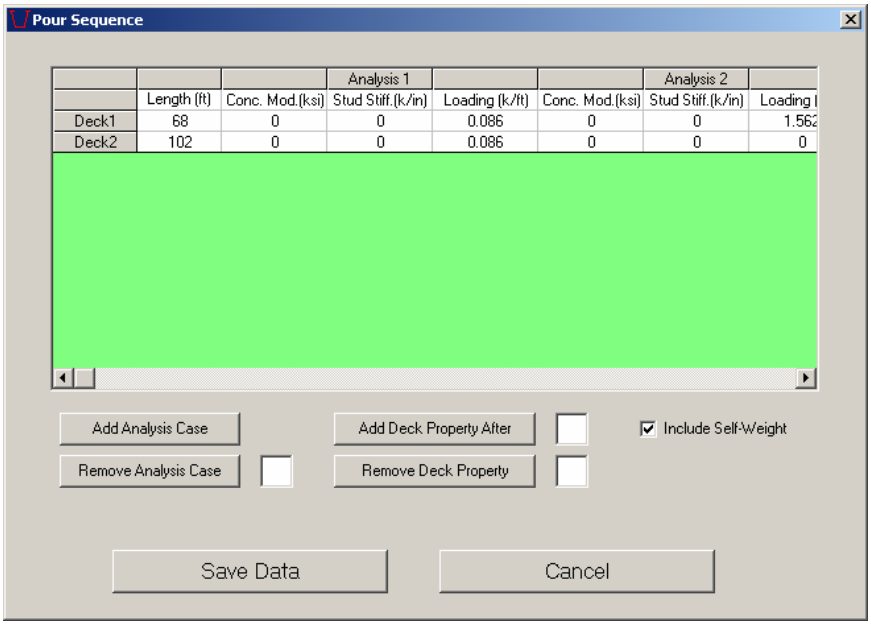

Figure 5.10 Pour Sequence form

Before running an analysis, the user can verify the bridge information by looking at the main window, which shows three figures representing the bridge properties. At the top, the plate thickness along the length is shown in an elevation view. The middle figure shows the deck numbers and relative lengths. The bottom figure is a plan view of the bridge, showing internal braces, external braces, and top lateral braces. Figure 5.11 shows the main window after all the information for the Marcy bridge has been provided.

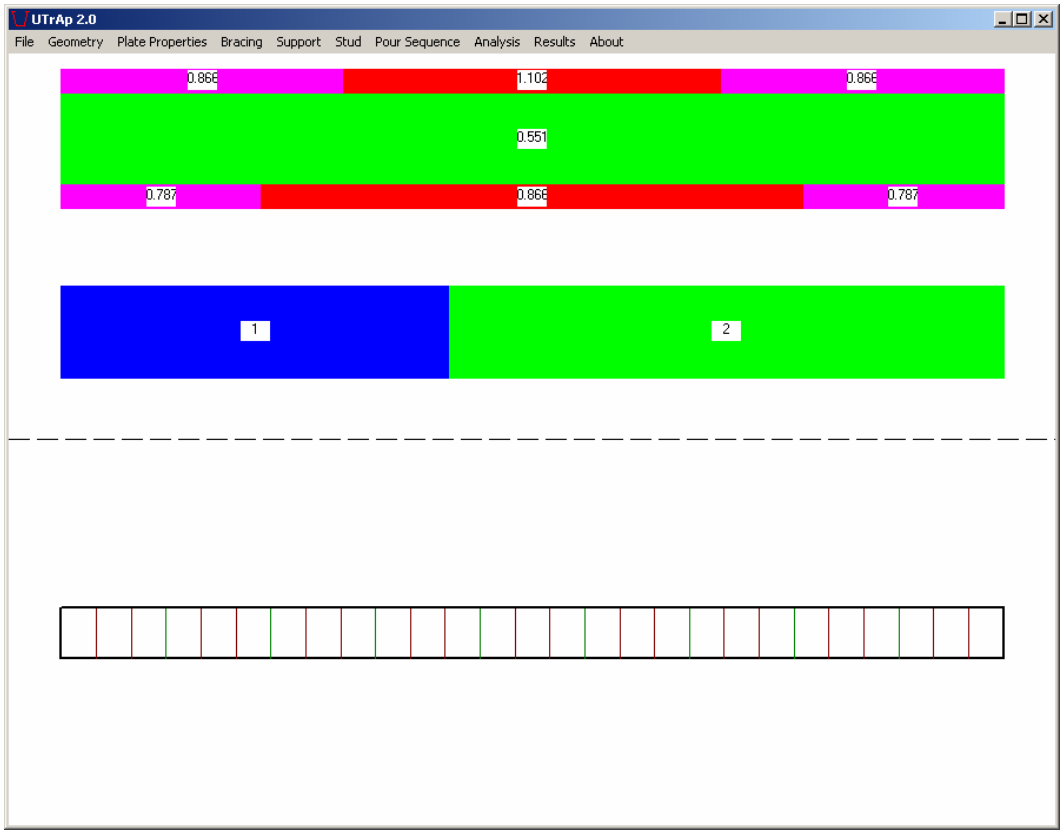

Figure 5.11 UTrAp 2.0 main window

Analysis Menu: The two submenus in this menu call the finite element analysis portion of UTrAp 2.0. When the user invokes either submenu, the program verifies that the bridge properties are consistently defined. For example, the length of all plates and decks should add up to the bridge length, and brace and support locations should be admissible. If any of the entries are missing or violate the geometric constraints, the program will give an error message. If all entries are permissible, the analysis module is called to perform the finite element analyses. The analysis module runs under the DOS environment. A user can monitor the progress of the analysis by observing the messages displayed in the DOS window, which closes automatically when the analysis is completed. The two options on the Analysis menu are explained below.

Linear Analysis Submenu: This submenu launches the linear analysis included in the original version of UTrAp. No nonlinear behavior of any sort will be considered. Figure 5.12 shows a representative linear analysis screen for the Marcy bridge.

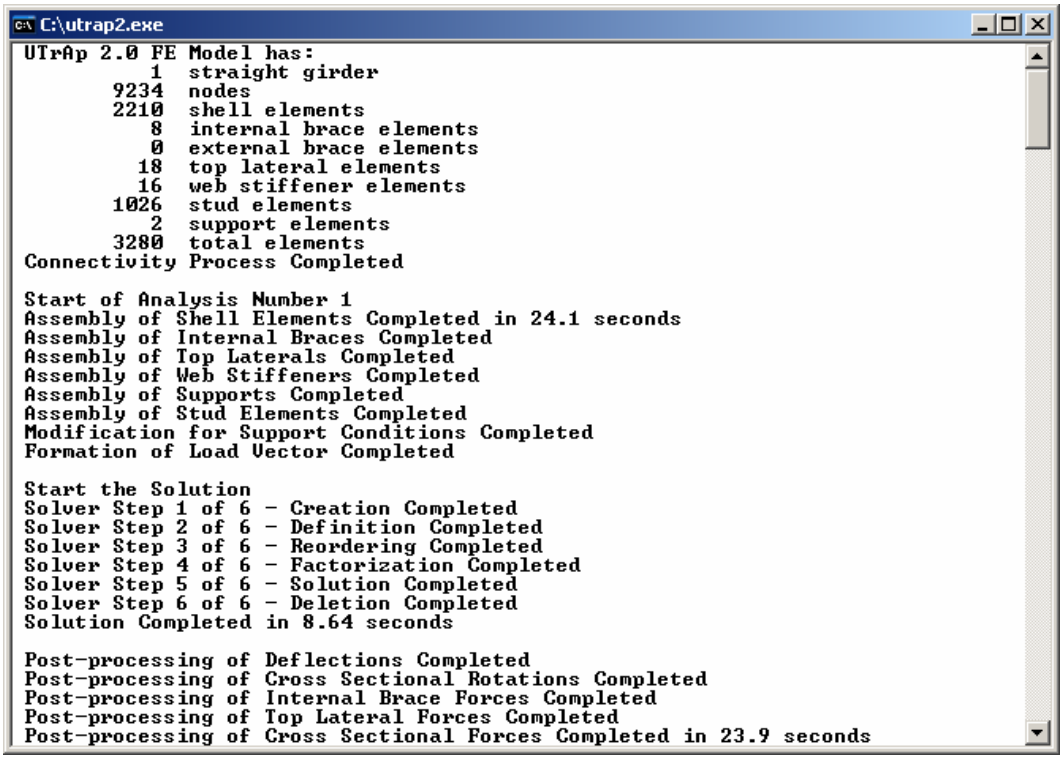

Figure 5.12 Linear Analysis screen

Buckling Analysis Submenu: This submenu starts a buckling analysis of the bridge, which will automatically perform the required linear analysis. For each analysis case, the program will find the elastic critical buckling load as a multiple of all applied loads. Figure 5.13 shows a representative buckling analysis screen for the Marcy bridge.

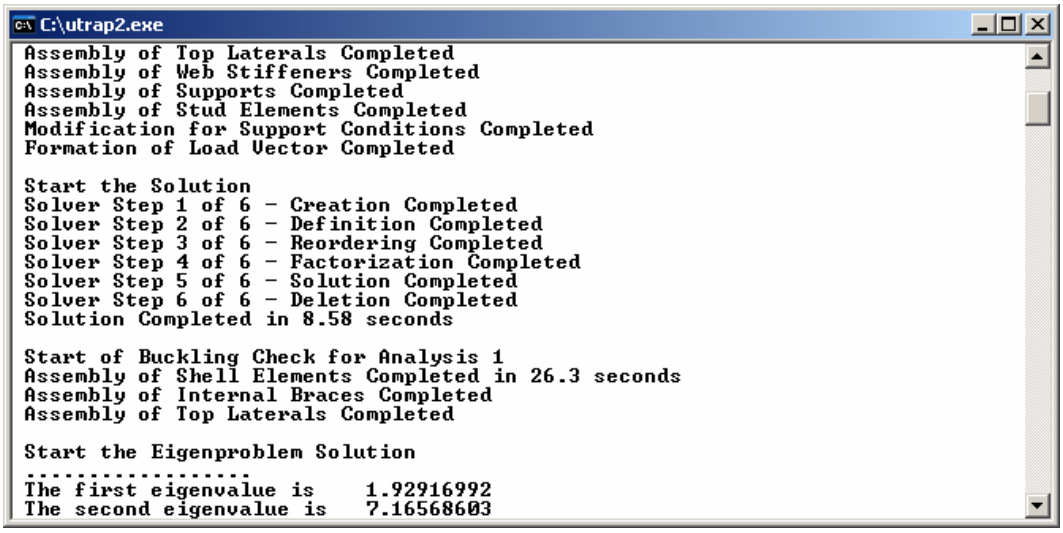

Figure 5.13 Buckling Analysis screen

Results Menus: The following eight submenus are used to visualize the output. Details of the submenus will be given in the following sections along with figures obtained from the solution of the example bridge.

Deflections/Cross-Sectional Rotations Submenus: These submenus are used to visualize the vertical deflections and cross-sectional rotations of the bridge. Because they have identical properties, both menus will be explained together in this section. Deflection values are the vertical deflection of the center of the bottom flange. Rotation values correspond to the rotation of the bottom flange. For twin girder systems, only the deflections and rotations of the outer girder are reported. Both tabulated and graphical output can be displayed. In the tables, deflection and rotation values at two-foot increments along the length of the bridge are shown. The user can request incremental deflection and rotation values for each analysis or cumulative values after each case. The Deflections form and Cross-Sectional Rotations form have four buttons to control the display of results. Functions of the buttons are explained below.

Tabulate Incremental Deflections/Rotations: This button tabulates the incremental deflections or rotations every two feet along the bridge. Values are presented for all analysis cases and are not summed. Figure 5.14 shows a sample of the deflections for the Marcy bridge.

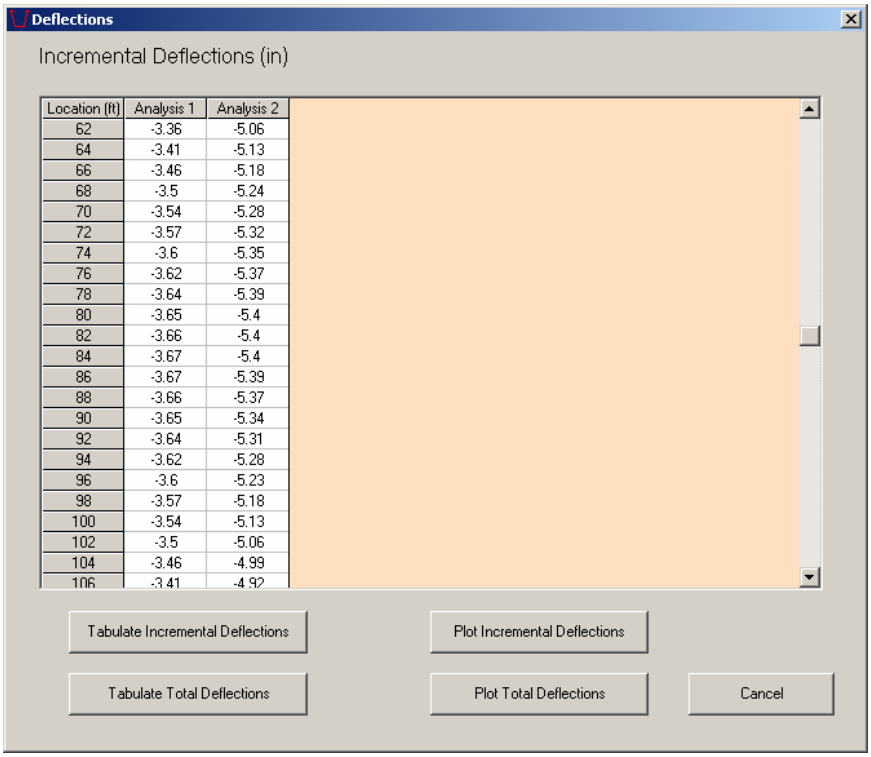

Figure 5.14 Table of incremental deflections

Tabulate Total Deflections: This button displays the total deflections or rotations every two feet along the bridge in tabular form. Cumulative deflection and rotation values are presented for each analysis. For example, the values in column two would be the summation of deflections or rotations resulting from the first and second analyses.

Plot Incremental Deflections/Rotations: This button displays the incremental deflections or rotations for all analyses on one graph. Figure 5.15 shows the incremental deflection diagram for the example bridge.

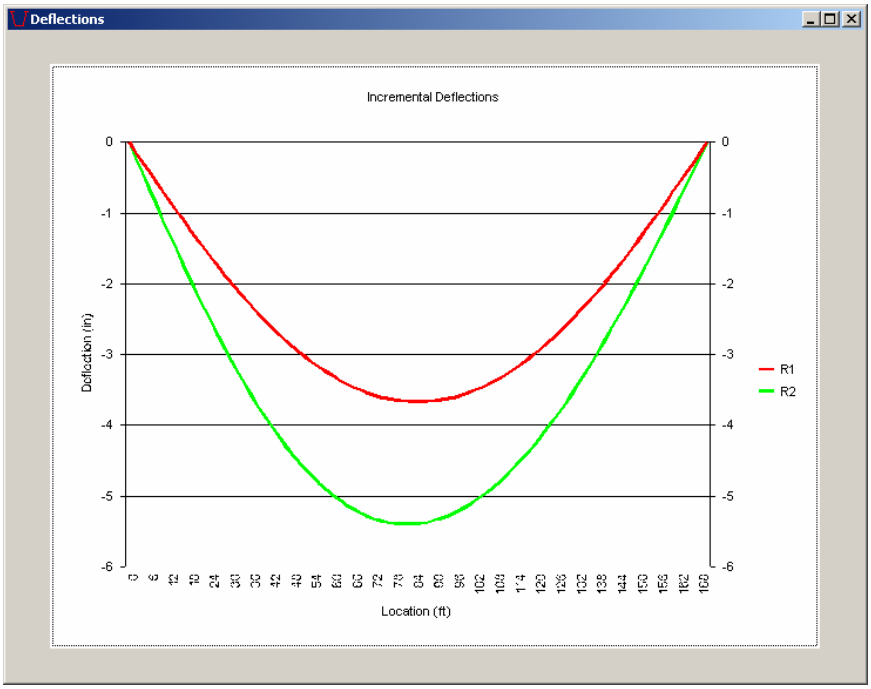

Figure 5.15 Diagram of incremental deflections

Plot Total Deflections/Rotations: This button displays the cumulative deflection or rotation diagram. Each curve represents the summation of the deflections or rotations from all previous analysis cases.

Cross-Sectional Forces Submenu: This submenu displays the values of the shear, moment, and torsion acting on the bridge at specified cross-sections. Data can be displayed in both tabular and graphical forms. Tabulated output consists of shear, moment, and torsion values every two feet along the bridge length. The same values can be displayed graphically. For twin-girder bridges, quantities are summed for the two girders. The Cross-Sectional Forces form has six buttons to control the display of results. Functions of the buttons are explained below.

Tabulate Shear: This button tabulates the shear every two feet along the bridge length. Incremental values are presented for all analysis cases. Figure 5.16 shows the Cross-Sectional Forces form with the results for the Marcy bridge.

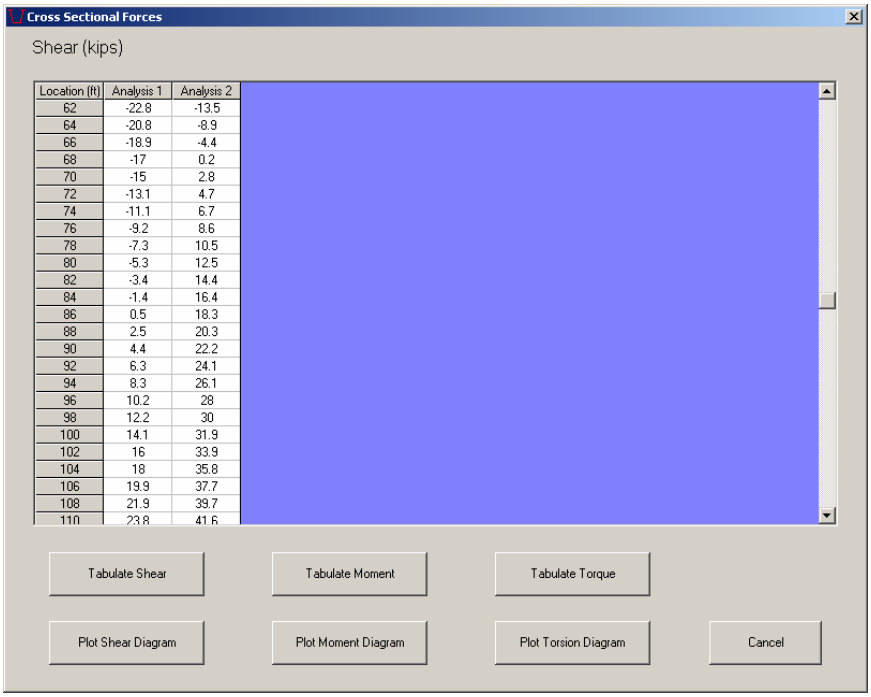

Figure 5.16 Table of incremental shear values

Tabulate Moment: This button tabulates the internal bending moment at locations every two feet along the bridge length. Incremental values are presented for all analysis cases.

Tabulate Torque: This button tabulates the incremental torque every two feet along the bridge length for all analysis cases.

Plot Shear Diagram: This button plots incremental shear values for all analyses on one graph. Figure 5.17 shows the shear diagram for the Marcy bridge.

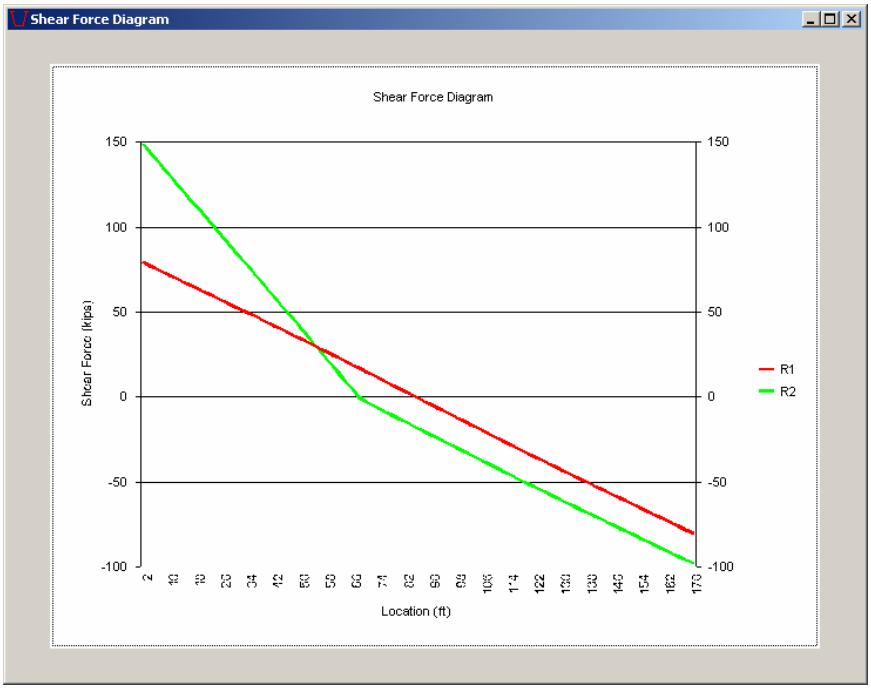

Figure 5.17 Diagram of incremental shear values

Plot Moment Diagram: This button displays the moment diagram. Incremental moment values for all analyses are displayed on one graph.

Plot Torsion Diagram: This button shows the incremental torsion values for all analyses on one graph.

Stresses Submenu: This submenu is used to visualize the cross-sectional stresses. The analysis module calculates normal and shear stresses at locations on the cross section denoted "section points" every two feet along the bridge length. There are 26 and 52 section points on the cross section for the single and dual girder systems, respectively. The Stresses form is used to tabulate the stress values along the length of the bridge for all section points. Both shear and normal stress can be tabulated in incremental or cumulative format. Radio buttons are placed on the form to select between shear and normal stress and between

incremental and cumulative values. This form is also used to display the stress diagram. Variation of normal or shear stress along the bridge length can be plotted for a specified section point. Additionally, this form can be used to display stresses at all section points at a specified cross section. The Stresses form has three buttons that interact with three scroll boxes. Functions of the buttons are explained below.

Tabulate Stresses: This button tabulates the stress values along the bridge length at all section points. Normal or shear stress can be tabulated depending on the user's selection. An analysis case must be selected using the scroll boxes. In addition, total or incremental values can be displayed. Figure 5.18 shows a stress output table.

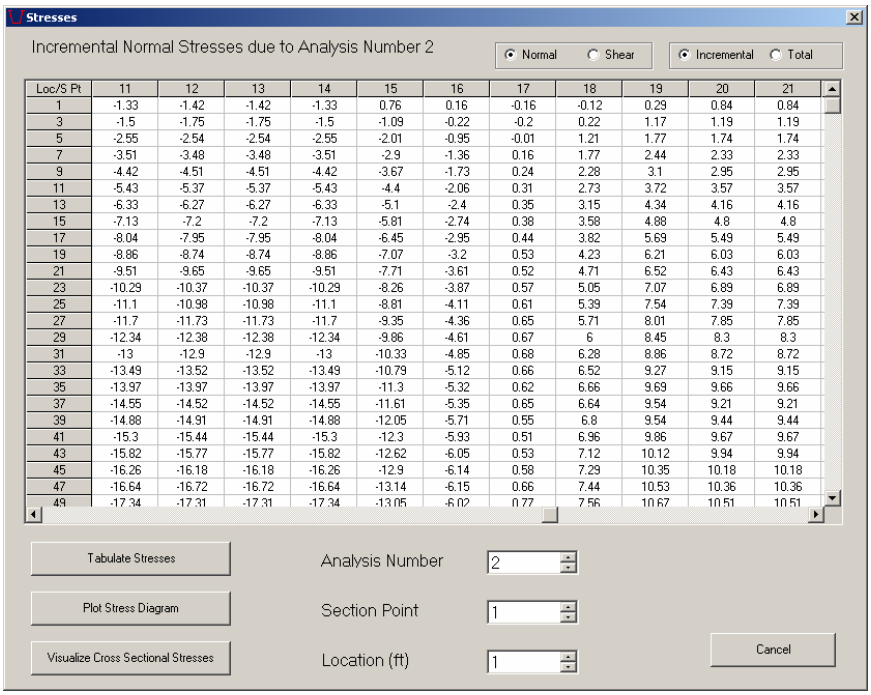

Loc/S Pt	11	12	13	14	15	16	17	18	19	20	21
1	-1.33	-1.42	-1.42	-1.33	0.76	0.16	-0.16	-0.12	0.29	0.84	0.84
3	-1.5	-1.75	-1.75	-1.5	-1.09	-0.22	-0.2	0.22	1.17	1.19	1.19
5	-2.55	-2.54	-2.54	-2.55	-2.01	-0.95	-0.01	1.21	1.77	1.74	1.74
7	-3.51	-3.48	-3.48	-3.51	-2.9	-1.36	0.16	1.77	2.44	2.33	2.33
9	-4.42	-4.51	-4.51	-4.42	-3.67	-1.73	0.24	2.28	3.1	2.95	2.95
11	-5.43	-5.37	-5.37	-5.43	-4.4	-2.06	0.31	2.73	3.72	3.57	3.57
13	-6.33	-6.27	-6.27	-6.33	-5.1	-2.4	0.35	3.15	4.34	4.16	4.16
15	-7.13	-7.2	-7.2	-7.13	-5.81	-2.74	0.38	3.58	4.88	4.8	4.8
17	-8.04	-7.95	-7.95	-8.04	-6.45	-2.95	0.44	3.82	5.69	5.49	5.49
19	-8.86	-8.74	-8.74	-8.86	-7.07	-3.2	0.53	4.23	6.21	6.03	6.03
21	-9.51	-9.65	-9.65	-9.51	-7.71	-3.61	0.52	4.71	6.52	6.43	6.43
23	-10.29	-10.37	-10.37	-10.29	-8.26	-3.87	0.57	5.05	7.07	6.89	6.89
25	-11.1	-10.98	-10.98	-11.1	-8.81	-4.11	0.61	5.39	7.54	7.39	7.39
27	-11.7	-11.73	-11.73	-11.7	-9.35	-4.36	0.65	5.71	8.01	7.85	7.85
29	-12.34	-12.38	-12.38	-12.34	-9.86	-4.61	0.67	6	8.45	8.3	8.3
31	-13	-12.9	-12.9	-13	-10.33	-4.85	0.68	6.28	8.86	8.72	8.72
33	-13.49	-13.52	-13.52	-13.49	-10.79	-5.12	0.66	6.52	9.27	9.15	9.15
35	-13.97	-13.97	-13.97	-13.97	-11.3	-5.32	0.62	6.66	9.69	9.66	9.66
37	-14.55	-14.52	-14.52	-14.55	-11.61	-5.35	0.65	6.64	9.54	9.21	9.21
39	-14.88	-14.91	-14.91	-14.88	-12.05	-5.71	0.55	6.8	9.54	9.44	9.44
41	-15.3	-15.44	-15.44	-15.3	-12.3	-5.93	0.51	6.96	9.86	9.67	9.67
43	-15.82	-15.77	-15.77	-15.82	-12.62	-6.05	0.53	7.12	10.12	9.94	9.94
45	-16.26	-16.18	-16.18	-16.26	-12.9	-6.14	0.58	7.29	10.35	10.18	10.18
47	-16.64	-16.72	-16.72	-16.64	-13.14	-6.15	0.66	7.44	10.53	10.36	10.36
49	-17.34	-17.31	-17.31	-17.34	-13.05	-6.02	0.77	7.56	10.67	10.51	10.51

Figure 5.18 Table of incremental normal stress values

Plot Stress Diagram: This button is used to display the variation of normal or shear stress along the bridge length at a specified section point. The

analysis case and section point must be selected using the scroll boxes. Figure 5.19 shows a plot of incremental normal stress along the bridge length for analysis number 2 at section point 11, located in the left top flange. The discontinuities in the graph are due to changes in the top flange thickness.

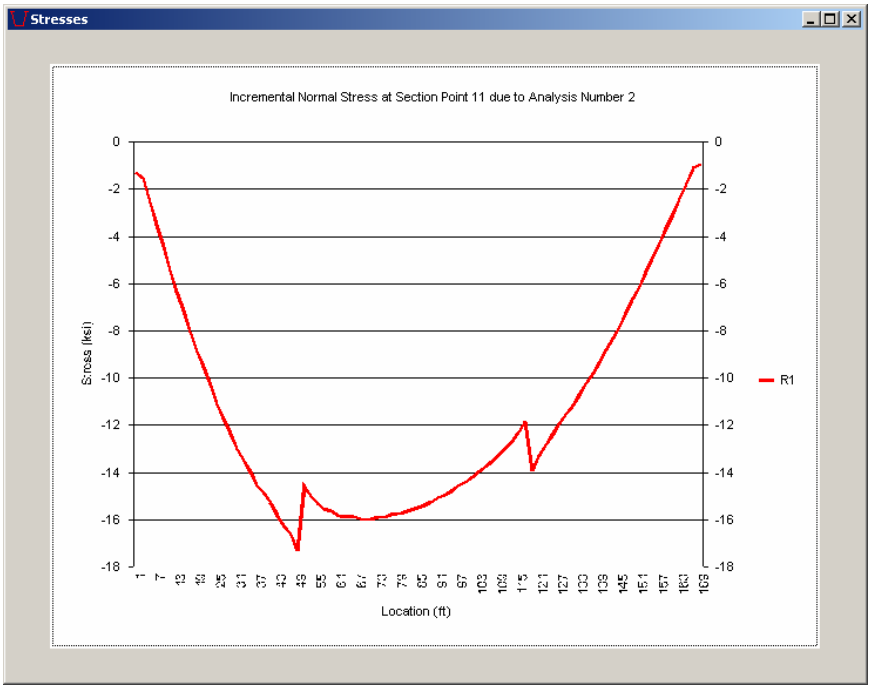

Figure 5.19 Diagram of incremental normal stresses

Visualize Cross-Sectional Stresses: This button is used to display the stresses at all section points on a specified cross section for an analysis case and location selected using the scroll boxes. Figure 5.20 shows the incremental normal stress distribution due to the second analysis in a cross section that is at midspan, 85 feet from the start end. Section points and stress values are shown on the diagram. The arrow in the figure points toward the center of radius for the bridge, which for a straight bridge is at a distance of infinity.

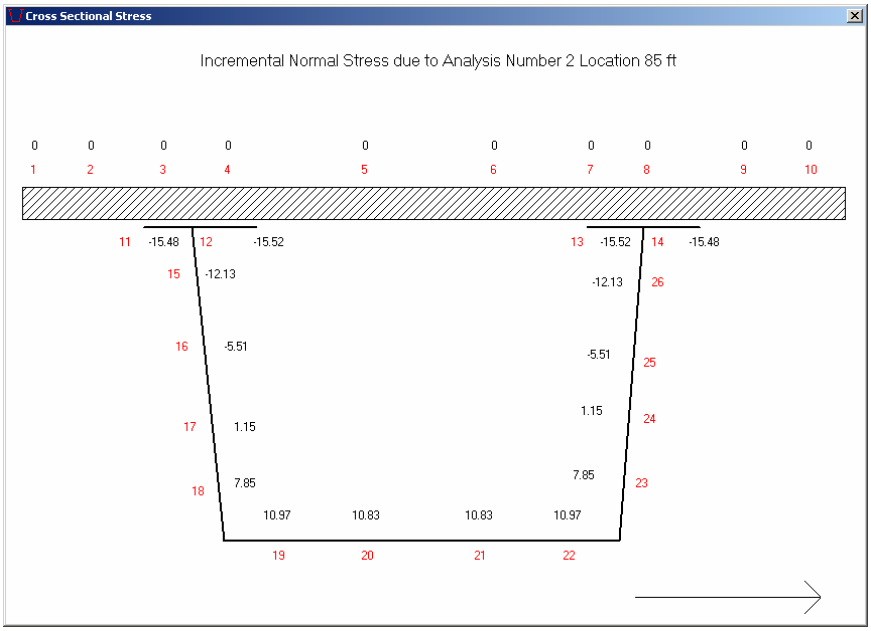

Figure 5.20 Visualization of incremental normal stresses on cross-section

Internal Brace Forces/External Brace Forces Submenus: These submenus are used to display the member axial forces for internal and external braces. Because they have identical properties, both menus will be explained in this section. Axial force values can be tabulated or displayed on a bar graph. Incremental axial forces due to each analysis or cumulative axial forces after each analysis can be displayed. Four buttons and a scroll box are used to control the output in these forms. Functions of these buttons are explained below.

Tabulate Incremental Forces: This button tabulates the forces in brace members due to each analysis case. Results for a certain member of the brace, selected using the scroll box, are displayed. Positive values represent tension forces in the brace members, and negative values represent compression forces. This convention is used throughout the program. The internal and external brace configurations and the corresponding

member numbers were presented previously in Figure 5.3. Figure 5.21 shows the Internal Brace Forces form together with the table of axial force values for member 2 of all internal braces.

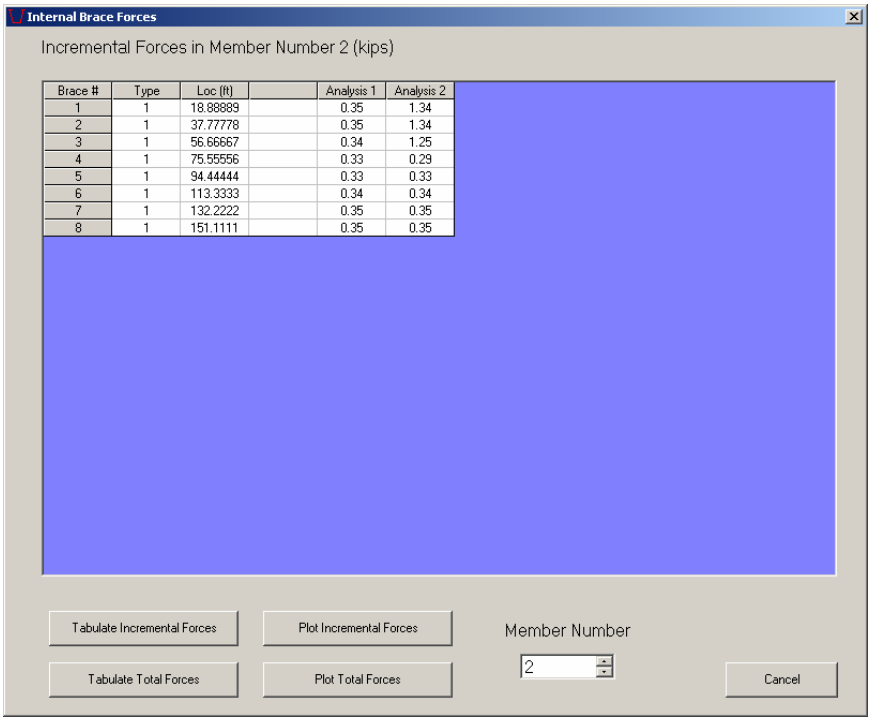

Figure 5.21 Table of incremental axial forces in internal braces

Tabulate Total Forces: Similar to the Tabulate Incremental Forces button, this button tabulates the cumulative forces after each analysis.

Plot Incremental Forces: This button displays a bar chart of axial forces in the braces for the member number selected using the scroll box. Figure 5.22 shows a bar chart of incremental axial forces in member two of the internal braces.

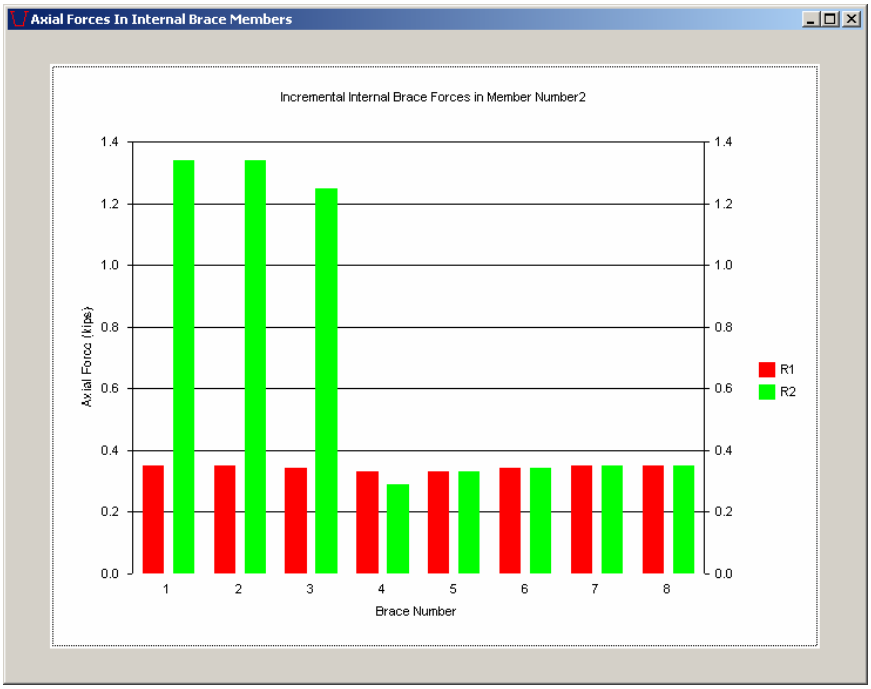

Figure 5.22 Chart of incremental axial forces in internal braces

Plot Total Forces: This button, similar to the Plot Incremental Forces button, is used to display the cumulative forces after each analysis.

Top Lateral Brace Forces Submenu: This submenu displays the forces in the top lateral braces. Values can either be tabulated or visualized as a bar graph. Incremental forces due to each analysis or cumulative forces after each analysis case can be displayed. The four buttons explained below are used to control the output.

Tabulate Incremental Forces: This button tabulates the forces in the top lateral members due to each analysis case.

Tabulate Total Forces: This button tabulates the cumulative forces in the top lateral members after each analysis case.

Plot Incremental Forces: This button plots a bar chart showing the incremental top lateral brace forces due to each analysis.

Plot Total Forces: This button shows a bar chart of the cumulative top lateral brace forces after each analysis.

Analysis Summary Submenu: This option displays the maximum values of significant quantities for each analysis, including maximum deflections, moments, shear forces, and axial stresses. The Analysis Summary form is shown in Figure 5.23.

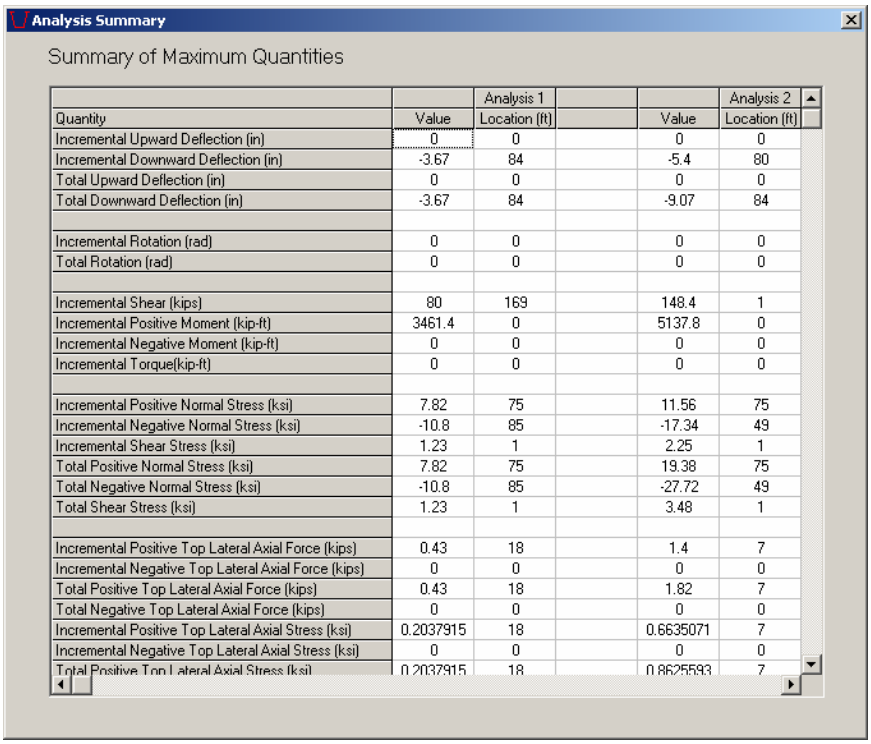

		Analysis 1			Analysis 2
Quantity	Value	Location (ft)		Value	Location (ft)
Incremental Upward Deflection (in)	0	0		0	0
Incremental Downward Deflection (in)	-3.67	84		-5.4	80
Total Upward Deflection (in)	0	0		0	0
Total Downward Deflection (in)	-3.67	84		-9.07	84
Incremental Rotation (rad)	0	0		0	0
Total Rotation (rad)	0	0		0	0
Incremental Shear (kips)	80	169		148.4	1
Incremental Positive Moment (kip-ft)	3461.4	0		5137.8	0
Incremental Negative Moment (kip-ft)	0	0		0	0
Incremental Torque(kip-ft)	0	0		0	0
Incremental Positive Normal Stress (ksi)	7.82	75		11.56	75
Incremental Negative Normal Stress (ksi)	-10.8	85		-17.34	49
Incremental Shear Stress (ksi)	1.23	1		2.25	1
Total Positive Normal Stress (ksi)	7.82	75		19.38	75
Total Negative Normal Stress (ksi)	-10.8	85		-27.72	49
Total Shear Stress (ksi)	1.23	1		3.48	1
Incremental Positive Top Lateral Axial Force (kips)	0.43	18		1.4	7
Incremental Negative Top Lateral Axial Force (kips)	0	0		0	0
Total Positive Top Lateral Axial Force (kips)	0.43	18		1.82	7
Total Negative Top Lateral Axial Force (kips)	0	0		0	0
Incremental Positive Top Lateral Axial Stress (ksi)	0.2037915	18		0.6635071	7
Incremental Negative Top Lateral Axial Stress (ksi)	0	0		0	0
Total Positive Top Lateral Axial Stress (ksi)	0.2037915	18		0.8625593	7

Figure 5.23 Analysis Summary form

5.2.3 Buckling Analysis Output

The preceding discussion of UTrAp 2.0 output has been limited to linear analysis, which is the same as in the original version of UTrAp. The focus in this section is on the output given by the revised version of the program. There are two types of output given by UTrAp 2.0 buckling analyses: the results just prior to buckling and the buckled shape.

5.2.3.1 Results Just Prior to Buckling

The response of the bridge just before it reaches the critical load is found by simply multiplying the displacement vector from the original applied load by the first eigenvalue. Because the analysis is linear and elastic, the eigenvalue is simply a scale factor increasing each response quantity. For example, if the midspan vertical deflection of a girder is one inch and the eigenvalue is 2.0, the results from the buckling analysis would indicate a midspan deflection of two inches. These results are equivalent to those from an elastic analysis with an applied load equal to the original load multiplied by the first eigenvalue.

This information is useful for two purposes: determining whether the bridge will buckle elastically, and determining the forces and displacements just prior to buckling. The UTrAp buckling analysis is valid only if the stresses at all points in the girder are below the yield stress of the material. The analysis is not valid if the stresses exceed yield, because linear-elastic material behavior is assumed. If the bridge remains elastic, the forces and displacements can be used to check local buckling of individual members. The forces in the brace members just prior to buckling are included in the output, and these quantities must be checked to ensure that they are below the buckling loads of the respective individual members.

As the response quantities just prior to buckling are obtained linearly, they are identical to the quantities that would be obtained from a linear analysis using a load that is scaled by the critical eigenvalue. The response quantities can therefore be output using the same Results menu as for elastic analysis, with one critical difference: the incremental results cannot be summed to give the total results because a buckling analysis cannot rely on elastic superposition of successive analyses. The load vector in the buckling analysis is cumulative: each new loading is added to the loadings from previous analyses. The buckling analyses are independent, each being done for all loads on the structure at that time. Each incremental response quantity displayed is therefore equivalent to the cumulative linear response for that analysis multiplied by the eigenvalue for that analysis, and represents the maximum value possible prior to buckling. For this reason, the display of total results is disabled for buckling analyses.

The results just prior to buckling may be slightly counter-intuitive upon initial inspection. For the Marcy bridge example, the first analysis case involves only the dead weight of the girder, forms, and diaphragms. The second analysis adds the weight of the wet concrete over the first 68 feet of the span, leading to greater forces and deflections throughout the girder. However, the results just prior to buckling are just the opposite. The first analysis has an eigenvalue of 1.93, which means the response quantities are increased by nearly a factor of two over the linear elastic analysis results. The second analysis case, chosen to result in imminent failure, has an eigenvalue of 1.00, which means the results just prior to buckling are equal to the results from the linear case. These results, however, are consistent with the eigenproblem. Thus, in order for the girder to become unstable for the first analysis, almost twice the load of the pattern specified for this analysis would be required. For the second case, the applied loads increase, and the load factor or eigenvalue associated with buckling is lower than the first

case. Though the eigenvalue is lower, the total applied loads are greater than in Analysis 1.

The two results are illustrated in Figure 5.24. The deflections just prior to buckling in Analysis 1 are greater than those in Analysis 2, implying that the second analysis is the more critical loading case. The bridge under the second loading case will buckle at lower levels of stress than it will under the first loading case. As explained above, the response quantities from each analysis must be individually examined to ensure that the bridge remains elastic.

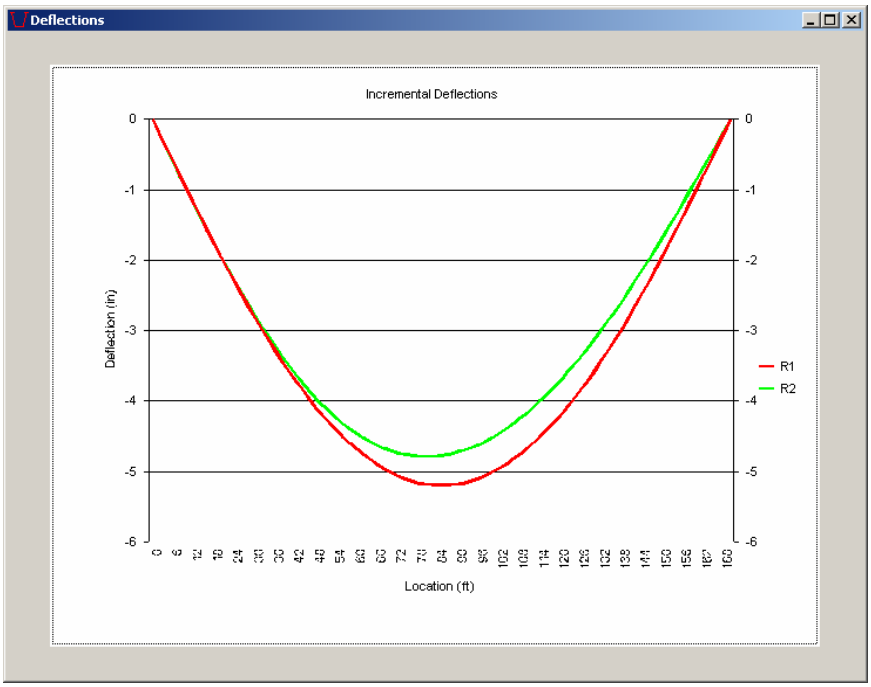

Figure 5.24 Deflections just prior to buckling

5.2.3.2 Buckled Shape

The buckled shape is also output by UTrAp 2.0 and is used to determine the type of buckling failure exhibited by the bridge. The displacements and rotations shown in the buckled shape are obtained from the eigenvector

corresponding to a particular eigenvalue, and thus are not related to the linear deformations of the girder. Because the displacements are based on the eigenvector, which was shown in Chapter 3 to have only relative values, no units can be assigned to the deformations. Some experience with the program and knowledge of stability is necessary to be able to interpret the failure modes predicted by the buckled shape. Examples of buckled shapes were given in Chapter 4, and more are given in this chapter.

Buckled Shape Submenu: Within the graphical user interface, the buckled shapes for a given analysis can be seen by using the Buckled Shape submenu. Buckled shapes are shown by two-dimensional cross-sections every two feet along the length of the bridge. The user specifies which mode shape and the location along the bridge by using the scroll boxes on the form. The Buckled Shape form in Figure 5.25 shows a typical first mode buckled shape of the Marcy bridge.

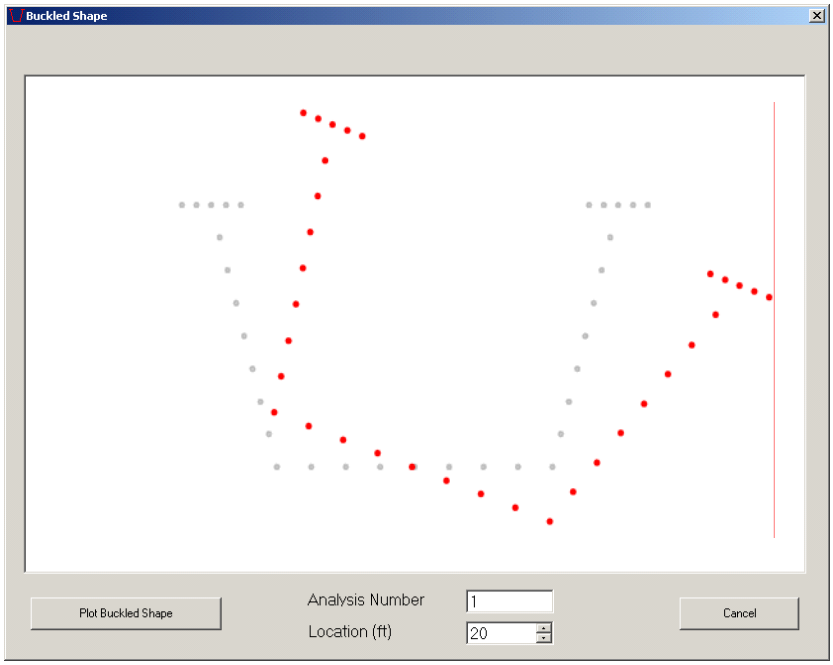

Figure 5.25 Buckled Shape form

5.3 OTHER ISSUES

UTrAp 2.0 operates with Windows 98, Windows 2000, and Windows XP. A physical memory of at least one gigabyte is recommended, particularly for buckling analyses. If the available physical memory is insufficient, virtual memory will be used, greatly increasing the analysis time.

5.4 SUMMARY

A user's guide for UTrAp 2.0 has been presented in this chapter. Capabilities and limitations of the program were discussed, and the graphical user interface was explained. Little or no knowledge of finite element modeling is required to obtain accurate results for both linear and buckling analyses of trapezoidal box-girder bridges.

CHAPTER 6
Global Instability

"To buckle, or not to buckle: that is the question."

- adapted from Shakespeare

Stability is a primary concern in the design of slender structures. With thin-walled members such as steel trapezoidal box girders, stability often governs the design. While current design specifications for steel box-girder bridges guard against local forms of buckling, they provide little guidance for considering the overall stability of the structure. This oversight has lead to one fatal collapse during construction, as well as other less serious problems.

In this chapter, global instability of a steel trapezoidal girder is investigated both theoretically and with UTrAp 2.0. A derivation of the lateral torsional buckling critical stress for a simple trapezoidal girder is developed and compared with the UTrAp results. Recommendations are given that provide the designer with methods for determining the overall stability of a trapezoidal girder.

6.1 BUCKLING

In design, all applicable limit states for each portion of a structure must be considered. The limit states for the compression flanges of a steel girder include both local buckling and lateral torsional buckling, which occurs when lateral buckling of the compression elements is accompanied by torsional rotation of the member. This form of buckling depends on the laterally unbraced length of the member, and can happen at relatively low stresses compared to the local buckling stresses, which depend only on the flange dimensions.

For I-section girders in composite construction, each compression flange may be checked for these limit states independently, as each girder behaves independently before the concrete deck has been placed. When considering trapezoidal sections with two top flanges per girder, it has been assumed that each top flange behaves independently and can be treated as part of an I-section for buckling considerations. Only local buckling and lateral torsional buckling of one top flange are checked, but lateral torsional buckling of the entire girder is not considered.

For a doubly-symmetric section such as an I-girder, lateral torsional buckling can only occur when the member is bent about the strong axis. The AISC LFRD Specifications specifically state that "the lateral-torsional buckling limit state is not applicable to members subject to bending about the minor axis" (2003). Because trapezoidal box girders are commonly bent about their minor axis, code provisions have assumed that lateral torsional buckling of the entire girder cannot occur. As Buhagiar et al. (1994) pointed out, though, thin-walled beams bent about their minor axis can undergo lateral torsional buckling. Steel trapezoidal girders fall into this category, meaning that they can fail in this manner. The results of this oversight are dramatically illustrated in the collapse of the Marcy pedestrian bridge. It is clear that lateral torsional buckling of the entire girder must be addressed in the design of steel trapezoidal box girders.

6.2 LATERAL TORSIONAL BUCKLING OF A TRAPEZOIDAL SECTION

A typical steel trapezoidal box-girder cross section as shown in Figure 6.1 is singly symmetric, being symmetric only about its vertical axis. The moment of inertia about the vertical axis of the section is often larger than that about the horizontal axis, meaning that the section is primarily bent about its weak axis. This fact, however, does not imply that it cannot fail in lateral torsional buckling.

In reality, this section is more prone to lateral instability, because the top flanges are smaller than the bottom flange. Additionally, the shear center for open sections and most sections with top lateral bracing is below the bottom flange, increasing the potential for instability.

Given in this section is a derivation of an approximate critical moment for the limiting case of lateral torsional buckling. The basic derivation makes several simplifying assumptions, including a uniform moment loading and the absence of a top lateral system. Corrections are presented to account for these simplifications.

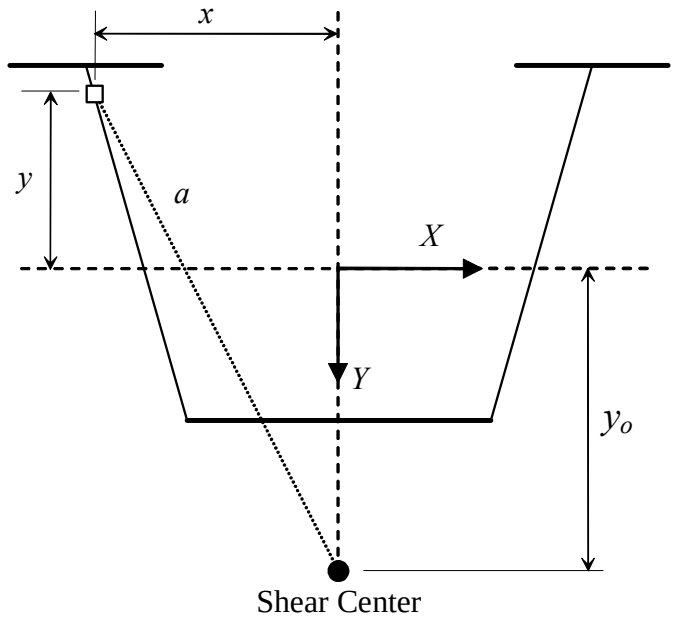

Figure 6.1 Shear center of a trapezoidal cross-section

The normal stress at any point on a cross-section is a function of the applied moment about the X (centroidal) axis and the distance from that axis:

$$\sigma = \frac{M_x y}{I_x} \tag{6.1}$$

where y as defined in Figure 6.1 is negative above the X axis, resulting in negative stresses in the compression flanges under positive moment. A new property can be defined:

$$\overline{K} = \int_A \sigma \; a^2 dA \tag{6.2}$$

which is substituted into the first equation, giving

$$\overline{K} = \int_A \frac{M_x y}{I_x} a^2 dA = \frac{M_x}{I_x} \int_A y a^2 dA \tag{6.3}$$

As shown in Figure 6.1, a is the distance between the shear center and the point where σ acts.

$$a^2 = x^2 + (y_o - y)^2 \tag{6.4}$$

Therefore

$$\overline{K} = \frac{M_x}{I_x} \left(\int_A x^2 y dA + y_o^2 \int_A y dA - 2 y_o \int_A y^2 dA + \int_A y^3 dA \right) \tag{6.5}$$

Observing that

$$\int_A y dA = 0 \quad \text{and} \quad \int_A y^2 dA = I_x$$

and using the relationship

$$\overline{K} = M_x \beta_x \tag{6.6}$$

a new cross-sectional property is defined:

$$\beta_x = \frac{1}{I_x} \int_A y\left(x^2 + y^2\right) dA - 2 y_o \tag{6.7}$$

This property is used in the formula given by Galambos (1968) for the critical moment of a singly-symmetric section subject to lateral torsional buckling:

$$M_{cr} = \frac{\pi^2 EI_y \beta_x}{2L^2}\left[1 \pm \sqrt{1 + \frac{4}{\beta_x^2}\left(\frac{GJL^2}{\pi^2 EI_y} + \frac{I_w}{I_y}\right)}\right] \tag{6.8}$$

The term β_x will be negative for trapezoidal cross-sections because the top flange area is less than the bottom flange area. This observation implies a decreased lateral torsional stiffness, just as one would expect from an I-section with a reduced top flange area. The integrals in the formulation of β_x can be evaluated separately for each portion of the cross-section as described below. Dimensions used in flange integrations are shown in Figure 6.2.

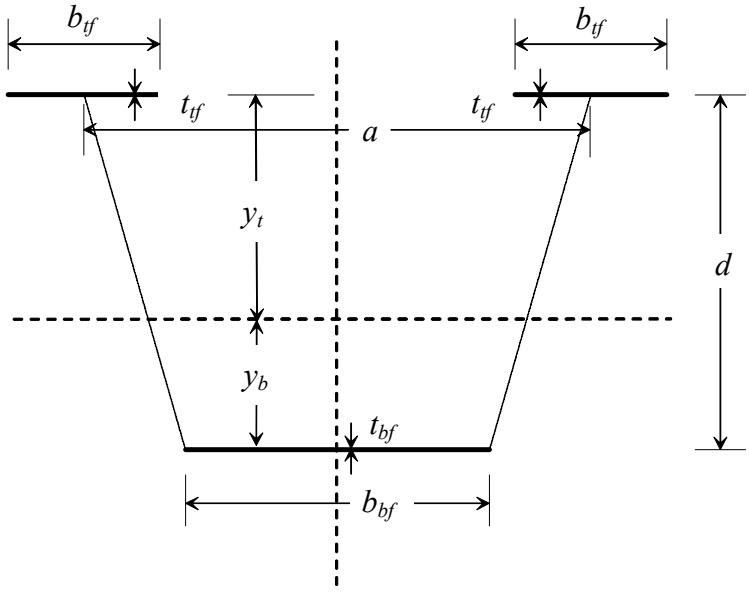

Figure 6.2 Notation for flange integration

Top flanges

$$\int_A yx^2 dA = 2y_t \int_A x^2 dA = 2y_t I_{yf} = 2y_t \left(\frac{1}{12} t_{tf} b_{tf}^3 + t_{tf} b_{tf} \left(\frac{a}{2} \right)^2 \right)$$

$$\int_A y^3 dA = 2y_t \int_A y^2 dA = 2y_t I_{xf} = 2y_t \left(\frac{1}{12} b_{tf} t_{tf}^3 + b_{tf} t_{tf} y_t^2 \right)$$

Bottom Flange

$$\int_A yx^2 dA = y_b \int_A x^2 dA = y_b I_{yf} = y_b \left(\frac{1}{12} t_{bf} b_{bf}^3 \right)$$

$$\int_A y^3 dA = y_b \int_A y^2 dA = y_b I_{xf} = y_b \left(\frac{1}{12} b_{bf} t_{bf}^3 + b_{bf} t_{bf} y_b^2 \right)$$

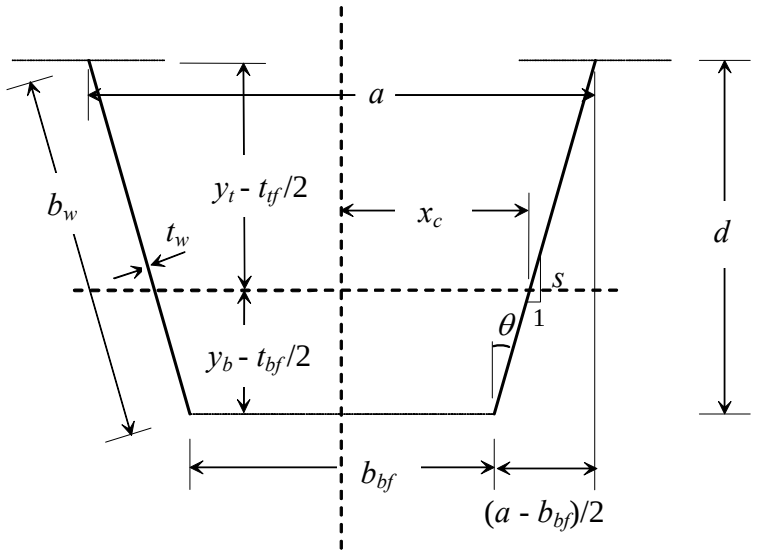

Figure 6.3 Notation for web integration

Using Figure 6.3, the following relationships for the web are formed:

$$\tan(\theta) = \left(\frac{a - b_{bf}}{2} \right) / \left(d - \frac{t_{tf}}{2} - \frac{t_{bf}}{2} \right) \tag{6.9}$$

$$x = x_c - y \tan(\theta) \tag{6.10}$$

$$y = \frac{x_c - x}{\tan(\theta)} \tag{6.11}$$

$$dA = t_w ds = \frac{t_w dx}{\sin(\theta)} = \frac{t_w dy}{\cos(\theta)} \tag{6.12}$$

The integrals can then be evaluated:

$$\int_A yx^2 dA$$

$$= 2 \int_A \frac{x_c - x}{\tan(\theta)} x^2 \frac{t_w dx}{\sin(\theta)}$$

$$= \frac{2t_w}{\tan(\theta)\sin(\theta)}\left[\int_{b_{bf}/2}^{a/2} x_c x^2 dx - \int_{b_{bf}/2}^{a/2} x^3 dx\right]$$

$$= \frac{2t_w}{\tan(\theta)\sin(\theta)}\left\{\frac{x_c}{24}\left[a^3 - b_{bf}^3\right] - \frac{1}{64}\left[a^4 - b_{bf}^4\right]\right\}$$

$$\int_A y^3 dA$$

$$= 2\int_A y^3 \frac{t_w dy}{\cos(\theta)}$$

$$= \frac{2t_w}{\cos(\theta)}\left[\int_{y_t+\frac{t_{tf}}{2}}^{y_b-\frac{t_{bf}}{2}} y^3 dx\right]$$

$$= \frac{t_w}{2\cos(\theta)}\left\{\left(y_b - \frac{t_{bf}}{2}\right)^4 - \left(y_t + \frac{t_{tf}}{2}\right)^4\right\}$$

Summing these contributions, Eq. (6.7) can be written:

$$\beta_x = \frac{1}{I_x}\left[2y_t\left(\frac{1}{12}t_{tf}b_{tf}^3 + t_{tf}b_{tf}\left(\frac{a}{2}\right)^2\right) + 2y_t\left(\frac{1}{12}b_{tf}t_{tf}^3 + b_{tf}t_{tf}y_t^2\right) + y_b\left(\frac{1}{12}t_{bf}b_{bf}^3\right)\right.$$
$$+ y_b\left(\frac{1}{12}b_{bf}t_{bf}^3 + b_{bf}t_{bf}y_b^2\right) + \frac{2t_w}{\tan(\theta)\sin(\theta)}\left\{\frac{x_c}{24}\left[a^3 - b_{bf}^3\right] - \frac{1}{64}\left[a^4 - b_{bf}^4\right]\right\}$$
$$\left. + \frac{t_w}{2\cos(\theta)}\left\{\left(y_b - \frac{t_{bf}}{2}\right)^4 - \left(y_t + \frac{t_{tf}}{2}\right)^4\right\}\right] - 2y_o \qquad (6.13)$$

Now that β_x has been determined, the remaining quantities in Eq. (6.8) must be found. E and G are the elastic modulus and the shear modulus of steel, respectively. The moment of inertia about the vertical axis I_y can be found by

typical methods knowing that the centroidal axis is at the center of the section. The pure torsional constant J_{open} for an open section is calculated as follows:

$$J_{open} = \frac{1}{3}\sum_{i=1}^{n} b_i t_i^3 \tag{6.14}$$

Finding the warping moment of inertia I_w of a trapezoidal cross-section is a complicated process. Widianto (2003) outlines a procedure for finding I_w in his thesis.

With these parameters known, Eq. (6.8) can be used to find the critical moment. The equation can be rewritten

$$M_{cr} = \frac{\pi^2 EI_y}{L^2}\left[\frac{\beta_x}{2} + \sqrt{\frac{\beta_x^2}{4} + \frac{GJ}{EI_y}\left(\frac{L}{\pi}\right)^2 + \frac{I_w}{I_y}}\right] \tag{6.15}$$

The plus sign is used in front of the radical for moment causing compression in the top flanges. To find the stress at which lateral buckling will occur, the critical moment can be divided by the section modulus:

$$F_{cr} = \frac{M_{cr}}{S_{xc}} \tag{6.16}$$

which leads to the following expression for critical stress in the top flanges:

$$F_{cr} = \frac{\pi^2 EI_y y_c}{L^2 I_x}\left[\frac{\beta_x}{2} + \sqrt{\frac{\beta_x^2}{4} + \frac{GJ}{EI_y}\left(\frac{L}{\pi}\right)^2 + \frac{I_w}{I_y}}\right] \tag{6.17}$$

6.2.1 Example of Determining Critical Stress

As an example of the above procedure, the lateral torsional buckling stress will be calculated for a typical trapezoidal cross-section. The properties as shown in Figure 6.4 are from the Model 1 girder discussed in Chapter 4, originally from Widianto (2003). Cross-section properties including I_w are given in his thesis, allowing the focus here to be on the above expressions.

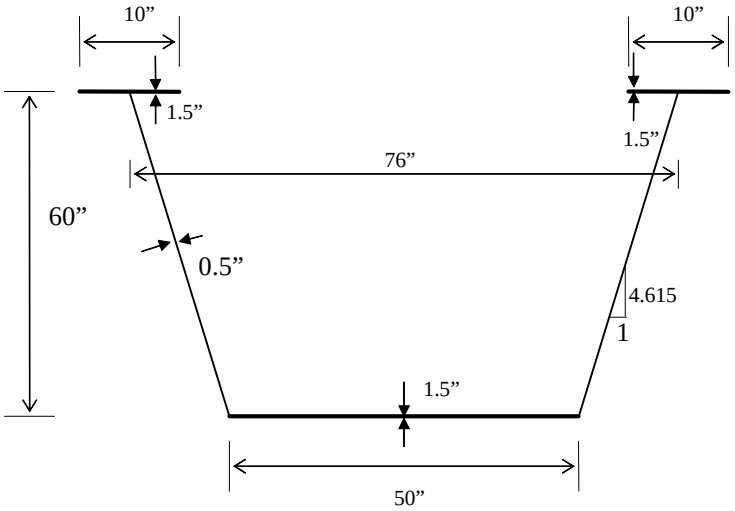

r_{bw} = 59.86 in
y_c = 38.19 in
y_o = 48.7 in
I_{XC} = 100535 in^4
I_{YC} = 119390 in^4
I_w = 2.74 x 10^7 in^6
J_{open} = 83.74 in^4

Figure 6.4 Properties of Model 1 girder

Considering each term inside the brackets in Eq. (6.13) separately, the following values for the area integrals are obtained:

Top Flanges

$$2y_t\left(\frac{1}{12}t_{tf}b_{tf}^3 + t_{tf}b_{tf}\left(\frac{a}{2}\right)^2\right) = 2(-38.19)\left(\frac{1}{12}(1.5)(10)^3 + 1.5(10)\left(\frac{76}{2}\right)^2\right) = -1663890\,\text{in}^5$$

$$2y_t\left(\frac{1}{12}b_{tf}t_{tf}^3 + b_{tf}t_{tf}y_t^2\right) = 2(-38.19)\left(\frac{1}{12}(10)(1.5)^3 + 10(1.5)(38.19)^2\right) = -1671046\,\text{in}^5$$

Bottom Flanges

$$y_b\left(\frac{1}{12}t_{bf}b_{bf}^3\right) = 21.81\left(\frac{1}{12}(1.5)(50)^3\right) = 340799\,\text{in}^5$$

$$y_b\left(\frac{1}{12}b_{bf}t_{bf}^3 + b_{bf}t_{bf}y_b^2\right) = 21.81\left(\frac{1}{12}(50)(1.5)^3 + 50(1.5)(21.81)^2\right) = 778512\,\text{in}^5$$

Webs

$$\frac{2t_w}{\tan(\theta)\sin(\theta)}\left\{\frac{x_c}{24}\left[a^3 - b_{bf}^3\right] - \frac{1}{64}\left[a^4 - b_{bf}^4\right]\right\}$$

$$= \frac{2(0.5)}{(0.222)(0.217)}\left\{\frac{29.68}{24}\left[(76)^3 - (50)^3\right] - \frac{1}{64}\left[(76)^4 - (50)^4\right]\right\} = -733111\,\text{in}^5$$

$$\frac{t_w}{2\cos(\theta)}\left\{\left(y_b - \frac{t_{bf}}{2}\right)^4 - \left(y_t + \frac{t_{tf}}{2}\right)^4\right\}$$

$$= \frac{0.5}{2(0.976)}\left\{\left(21.81 - \frac{1.5}{2}\right)^4 - \left((-38.19) + \frac{1.5}{2}\right)^4\right\} = -452763\,\text{in}^5$$

With these values, β_x can be calculated as follows:

$$\beta_x = \frac{1}{100535}\left[-1663890 - 1671046 + 340799 + 778512 - 733111 - 452763\right] - 2(48.7)$$

$$\beta_x = -131.2\,\text{in}$$

and finally, Eq. (6.17) is employed to find the buckling stress:

$$F_{cr} = \frac{\pi^2 E I_y y_c}{L^2 I_x}\left[\frac{\beta_x}{2} + \sqrt{\frac{\beta_x^2}{4} + \frac{GJ}{EI_y}\left(\frac{L}{\pi}\right)^2 + \frac{I_w}{I_y}}\right]$$

$$= \frac{\pi^2(29600)(119390)(38.19)}{(2160)^2(100535)}\left[\frac{-131}{2} + \sqrt{\frac{131^2}{4} + \frac{(11400)(83.74)}{(29600)(119390)}\left(\frac{2160}{\pi}\right)^2 + \frac{27400000}{119390}}\right]$$

$$F_{cr} = 7.58\,\text{ksi}$$

Thus, a 180-foot trapezoidal girder with the dimensions of Model 1 will exhibit lateral torsional buckling at a top-flange compressive stress of 7.58 ksi. The dead weight of the girder, however, is 0.56 kips/foot, which results in a midspan top-flange stress of 10.36 ksi. This would suggest that without a top lateral bracing

system to prevent lateral torsional buckling, the girder will fail under its own self-weight.

The same girder was analyzed using UTrAp 2.0, which predicted a failure in lateral torsional buckling at a stress of 7.70 ksi, only 1.6% higher than the value predicted using Eq. (6.17). To further verify the agreement between the two predictions, the length of the Model 1 girder was varied between 100 and 200 feet, and buckling stresses were compared. The values predicted using Eq. (6.17) and those by UTrAp for the critical buckling stresses are shown in Figure 6.5.

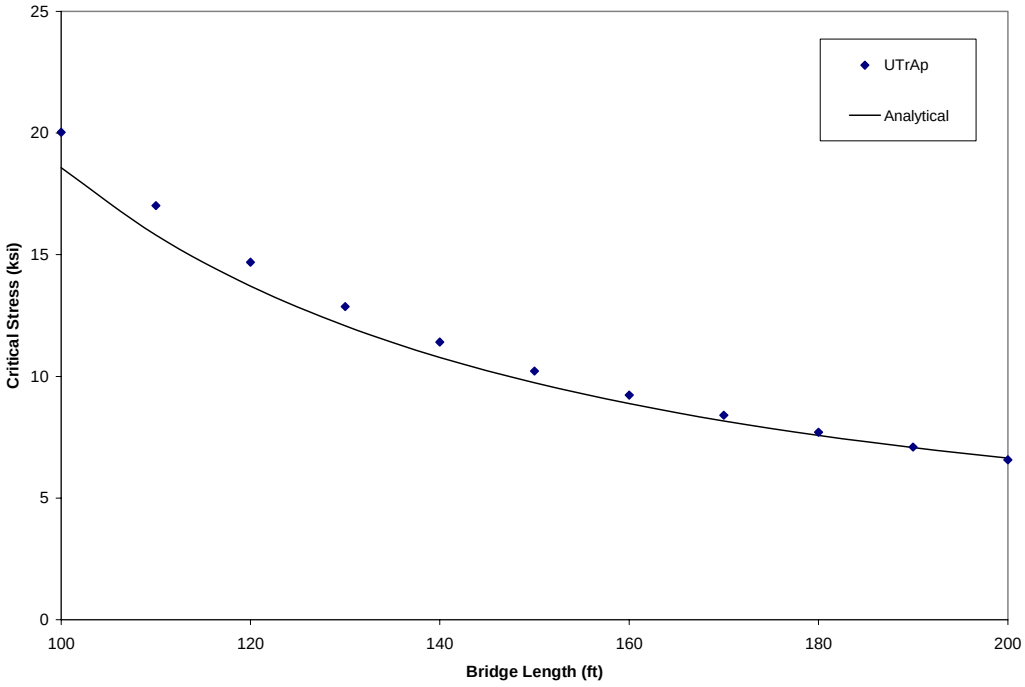

Figure 6.5 Predicted critical buckling stresses versus length for Model 1 girder

The results from UTrAp 2.0 agree very well with the predicted stresses over the range of lengths. Because the theoretical solution and the UTrAp model incorporate slightly different boundary conditions, the predicted values diverge somewhat for shorter lengths, where the effect of support conditions becomes

more pronounced. Overall, however, the agreement between the two methods of obtaining the critical buckling stress shows that results are in agreement.

6.2.2 Non-uniform Moment Loading

The lateral torsional buckling critical stress prediction shown in Equation (6.17) is derived for a simply-supported member with uniform moment along the span. This condition represents a worst-case scenario because other loading cases and end conditions will result in higher buckling stresses. To account for other girder loading and boundary configurations, the lateral torsional buckling stress can be multiplied by C_b, a multiplication factor based on the shape of the moment diagram along the member. For lateral torsional buckling, the AASHTO LRFD (2003) expression for this factor is given by Equation 6.10.8.2.3-7:

$$C_b = 1.75 - 1.05\left(\frac{f_1}{f_2}\right) + 0.3\left(\frac{f_1}{f_2}\right)^2 \tag{6.18}$$

in which f_2 is the larger of the flexural stresses at either end of the unbraced length and f_1 is calculated from Equation 6.10.8.2.3-11:

$$f_1 = 2f_{mid} - f_2 > f_0 \tag{6.19}$$

Here f_{mid} is the stress at the middle of the unbraced length and f_0 is the stress at the opposite end of the unbraced length from f_2. If f_{mid} is greater than both f_0 and f_2, or in the case of a simply-supported unbraced length where f_0 and f_2 are both zero, C_b is taken to be 1.0. For the case of a simply-supported member braced only at the ends and midspan, C_b from Eq. (6.18) is 1.3, which matches the value from the AISC LRFD specifications. For an unbraced, simply-supported member with a uniform load, the value given for C_b from Eq. (6.18) is 1.0, which is less than the value from the AISC LRFD Specifications (2003) of 1.14.

The equations for C_b given in the AASHTO Specifications are developed for doubly-symmetric I-sections. The accompanying commentary makes provisions for singly-symmetric I-sections, but trapezoidal or box sections are not mentioned. For non-symmetric sections, the increase in the critical stress due to non-uniform moment can depend on the position of the loading with respect to the shear center as well as on the moment diagram. Because the shear center of a trapezoidal girder can be below the bottom flange, the position of the load can be extremely critical.

To investigate the effect of non-uniform moment on the critical buckling stress of trapezoidal girders, models were analyzed using both uniform loading of the top flanges and uniform moment. A uniform moment loading was achieved by applying equal and opposite axial forces to the top and bottom flanges on each end of the girder. The magnitude of the forces was determined so as to make the constant moment equal to the maximum midspan moment for a uniformly loaded girder. The ratio of the buckling loads for the two cases was then found. Table 6.1 shows the C_b factors obtained.

Table 6.1 C_b factors for trapezoidal box-girder bridges

Span	Model 1	Marcy Pedestrian Bridge
100 feet	0.9741	-
160 feet	0.9945	-
170 feet	0.9973	0.987
180 feet	1.0002	-

Using the AASHTO expression shown in Eq. (6.18) for an unbraced section with uniform loading gives a C_b value of 1.0. The values in Table 6.1 are

very close to this number, suggesting that the AASHTO expression, which was developed for symmetric sections, would be only slightly unconservative for use with straight trapezoidal sections. Thus, for the simple cases considered, the critical buckling stress for a typical steel trapezoidal girder under a uniform loading can be approximated by Eq. (6.17) without additional modification factors.

It must be noted that other cases, including curved girders and girders with changing cross-sections along the length, have not been studied. The results for the simple case of a straight uniform girder may or may not be applicable to more complex cases. Further investigation is warranted. Additionally, due to the fact that a trapezoidal section is unsymmetric, the effect of loading position will influence the critical stress. The values obtained above were for loading along the top flanges; loading along the centroid of the section and along the bottom flange would also be of interest.

6.3 TOP LATERAL BRACING

The formula for critical stress shown in Eq. (6.17) is derived for a trapezoidal girder with an open section, that is, a girder without top lateral bracing, as shown in Figure 6.6. Top lateral bracing is defined as any bracing that extends along the length of a bridge, and thus does not include diaphragms, internal braces, or struts. Typical top lateral bracing configurations are X-type, alternating-diagonal, and single-diagonal, each shown in Figure 6.7.

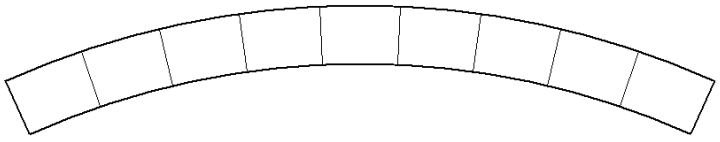

Figure 6.6 Open section girder with struts

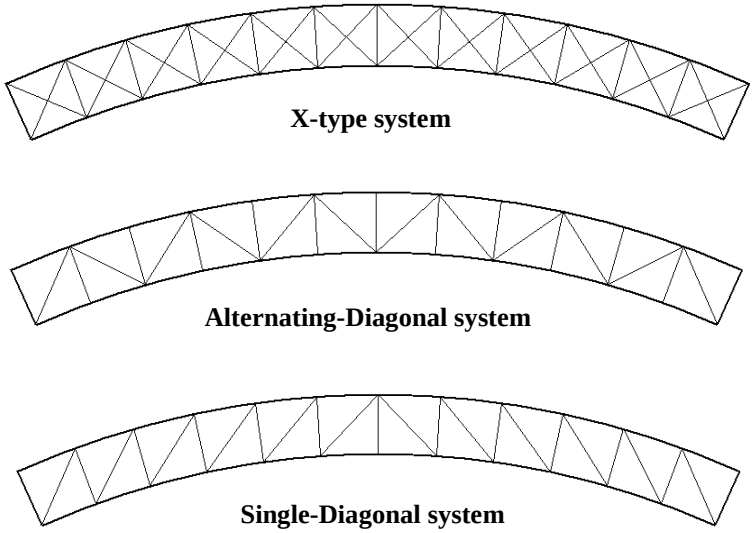

Figure 6.7 Top lateral bracing systems

A top lateral bracing system contributes to the overall stability of a trapezoidal girder in several ways. The presence of top lateral bracing allows for shear flow across the top of the girder, forming what is known as a pseudo-closed section. The torsional constant *J* is increased by several orders of magnitude with the addition of a top lateral system.

In addition to increasing the torsional stiffness of the girder, the top lateral bracing system adds stability to a trapezoidal box girder by joining the two top flanges, effectively bracing both. With only struts or internal diaphragms between the top flanges, they may both displace in the same direction. A top lateral bracing system forms a truss in the plane of the top flanges, which resists lateral movement much better than the individual flanges.

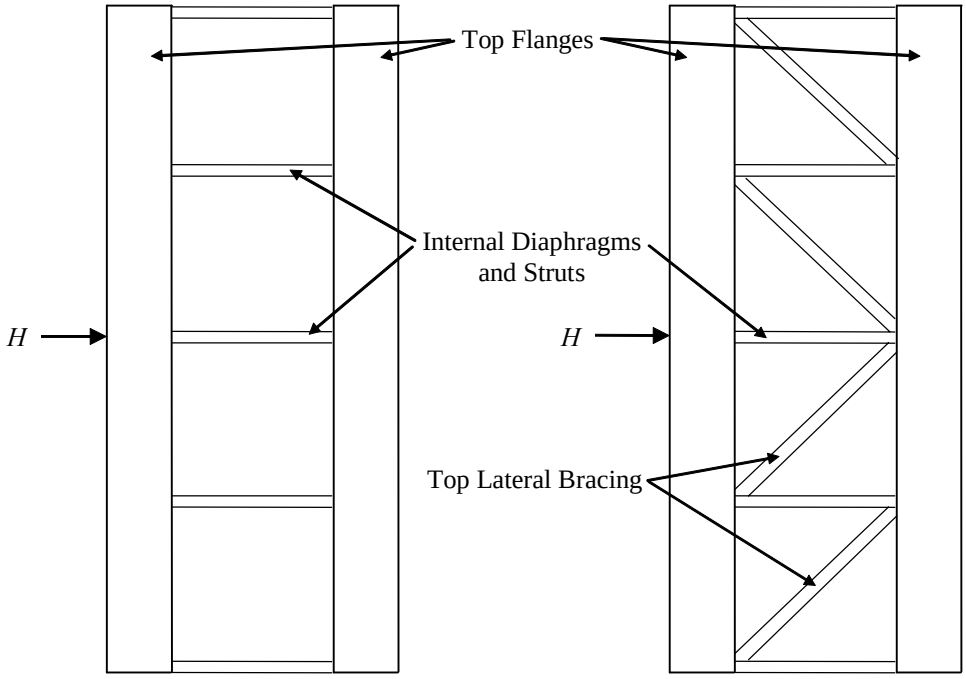

Figure 6.8 Trapezoidal girder plan view with and without top lateral bracing

Figure 6.8 illustrates the truss action made possible by the presence of a top lateral bracing system. A box girder without top lateral bracing, shown in Figure 6.8a, must resist lateral forces on the top flanges (represented by point load *H*) by flange bending only. When a top lateral system is added as shown in Figure 6.8b, the force *H* is resisted by a combination of truss action and top flange bending, resulting in a greatly increased lateral stiffness.

To incorporate top lateral bracing into the derived formula for the lateral torsional buckling critical stress, the bracing can be treated as an equivalent plate between the top flanges. This approach, known as the equivalent plate method, was developed by Kollbrunner and Basler (1969), and is applied specifically to trapezoidal sections by Widianto (2003). The equations for the equivalent plate thicknesses for the three lateral bracing systems in Figure 6.7 are repeated below.

For an X-type system, the equivalent plate thickness is:

$$t_{eq} = \frac{E}{G}\frac{as}{\frac{d^3}{2A_d} + \frac{s^3}{6A_{tf}}} \tag{6.20}$$

Similarly for an alternating diagonal system,

$$t_{eq} = \frac{E}{G}\frac{as}{\frac{d^3}{A_d} + \frac{2s^3}{3A_{tf}}} \tag{6.21}$$

and for a single-diagonal top lateral bracing system,

$$t_{eq} = \frac{E}{G}\frac{as}{\frac{d^3}{A_d} + \frac{a^3}{A_s} + \frac{s^3}{6A_{tf}}} \tag{6.22}$$

In Eqs. (6.20) through (6.22) above, E and G are the elastic and shear moduli, respectively, a is the top width of the girder, s is the strut spacing, and d is the length of the diagonal brace members. A_d, A_s, and A_{tf} are the areas of the diagonal brace members, the struts, and the top flanges, respectively.

These equivalent plate thicknesses can be used in the calculation of the section properties. The procedure followed to evaluate Eq. (6.7) for the webs and flanges can be followed for the equivalent plate between the top flanges, as shown below:

$$\int_A yx^2 dA = y_t \int_A x^2 dA = y_t I_y = y_t\left(\frac{1}{12} t_{eq} a^3\right) \tag{6.23}$$

$$\int_A y^3 dA = y_t \int_A y^2 dA = y_t I_x = a t_{eq} y_t^3 \tag{6.24}$$

Along with the additional terms within the integral in Eq. (6.7), both I_x and y_0 change with the presence of a top lateral system and must be calculated for the pseudo-closed section.

6.3.1 Example of Determining Critical Stress with Top Lateral Bracing

To illustrate the effect of top lateral bracing, the previous example for an open-section girder is modified to include the effect of top lateral bracing. The bracing configuration is taken from Widianto (2003), who gives the necessary section properties in his thesis. An alternating diagonal system is chosen with WT 7x24 structural tee diagonal members with a cross-sectional area of 7.07 in^2 and L5x3½x½ angle strut members with an area of 4 in^2, as shown in Figure 6.9. The strut spacing is 10 feet.

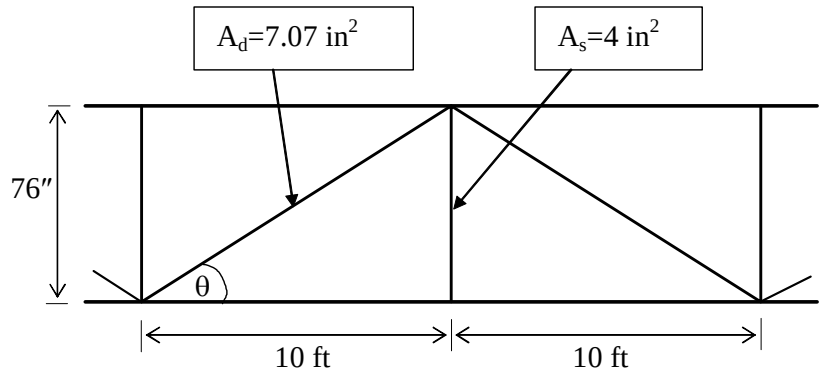

Figure 6.9 Top lateral bracing for Model 1 girder

Using Eq. (6.22) to find the equivalent plate thickness gives

$$t_{eq} = \frac{E}{G}\frac{as}{\dfrac{d^3}{A_d}+\dfrac{a^3}{A_s}+\dfrac{s^3}{6A_{tf}}} = \frac{29600}{11400}\frac{(76\,\text{in})(120\,\text{in})}{\dfrac{(142\,\text{in})^3}{7.07\,\text{in}^2}+\dfrac{(76\,\text{in})^3}{4\,\text{in}^2}+\dfrac{(120\,\text{in})^3}{6(15\,\text{in}^2)}} = 0.0443\,\text{in}$$

Equations (6.23) and (6.24) provide the integrals for use in the calculation of β_x:

$$y_t\left(\frac{1}{12}t_{eq}a^3\right) = (-38.13\,\text{in})\left(\frac{1}{12}(0.0443\,\text{in})(76\,\text{in})^3\right) = -61819\,\text{in}^5$$

$$at_{eq}y_t^3 = (76\,\text{in})(0.0443\,\text{in})(-38.13\,\text{in})^3 = -186723\,\text{in}^5$$

The values of I_x and y_0 for the pseudo-closed section are calculated following the procedure given by Widianto (2003), resulting in:

$$I_x = 100909\,\text{in}^4$$

$$y_0 = 38.619\,\text{in}$$

Equation (6.7) can now be used to find β_x:

$$\beta_x = \frac{1}{100909}\left[-3401499 - 61819 - 186723\right] - 2(38.619)$$

$$\beta_x = -110.7\,\text{in}$$

This value of β_x is approximately 16% smaller than for the open section, which by itself leads to only an 18% increase in the critical stress.

The main factor in increasing the critical stress, however, is the increase in the torsional constant *J*. Adding top lateral bracing closes the section, greatly increasing the torsional stiffness. The pure torsional constant can be calculated for a pseudo-closed section as follows:

$$J_{pseudo-closed} = \frac{4A_o^2}{\sum_{i=1}^{4}\frac{b_i}{t_i}} \tag{6.25}$$

which for this example becomes

$$J_{pseudo-closed} = \frac{4(3780\,\text{in}^2)^2}{2\left(\frac{61.39\,\text{in}}{0.5\,\text{in}}\right) + \frac{50\,\text{in}}{1.5\,\text{in}} + \frac{76\,\text{in}}{0.0443\,\text{in}}} = 28756\,\text{in}^4$$

The torsional constant for the pseudo-closed section in this example is 343 times greater than the open-section torsional constant.

Equation (6.17) gives the critical buckling stress:

$$F_{cr} = \frac{\pi^2 E I_y y_c}{L^2 I_x}\left[\frac{\beta_x}{2} + \sqrt{\frac{\beta_x^2}{4} + \frac{GJ}{EI_y}\left(\frac{L}{\pi}\right)^2 + \frac{I_w}{I_y}}\right]$$

$$= \frac{\pi^2 (29600)(119390)(38.13)}{(2160)^2 (100909)}\left[\frac{-111}{2} + \sqrt{\frac{111^2}{4} + \frac{(11400)(28756)}{(29600)(119390)}\left(\frac{2160}{\pi}\right)^2 + \frac{13070419}{119390}}\right]$$

$$F_{cr} = 456.2 \text{ ksi}$$

which is sixty times greater than the critical buckling stress of the open section girder. It is clear that lateral torsional buckling will not occur in this case because the critical stress is much greater than the typical yield stress of steel. The girder will become inelastic and fail in another manner long before lateral torsional buckling becomes possible.

6.4 SUMMARY

This chapter has discussed global instability of steel trapezoidal box girders, focusing on the phenomenon of lateral torsional buckling. It has been shown that the presence of even a small top lateral bracing system will prevent lateral torsional buckling. Because a curved girder experiences torsion, it must have a top lateral bracing system, which will prevent lateral torsional buckling of the entire cross-section. Curved girders were therefore not considered in this chapter. Straight girders, on the other hand, are not designed for torsion, and thus are currently allowed to have no top lateral bracing system. The Marcy pedestrian bridge is an example of a straight girder without a top lateral bracing system, and its performance suggests a need for improved understanding of lateral torsional buckling for these systems.

Two approaches to the design of straight trapezoidal girders can be taken. The decision of whether to use top lateral bracing can be left to the designer, who would be required only to ensure stability during construction. If the designer decides not to use a top lateral bracing system, the equations derived in this chapter could be used to determine the stability of the open-section girder. Construction methods such as temporary bracing could be used to increase the stability of the open-section girder during the concrete pour. Alternatively, a top lateral bracing system could be required by the code for all steel trapezoidal girders, whether straight or curved. In any case, the current code specifications for a straight trapezoidal box girder appear to be insufficient and should be modified to account for stability effects.

CHAPTER 7
Conclusions and Future Research

"A poem is never finished, only abandoned."

- Paul Valery

The goal of this research was to develop a program that would determine the buckling characteristics of steel trapezoidal box-girder bridges. This task has been accomplished, but the application of the program to actual problems has only begun to be explored. What has been learned and what is yet to be learned are discussed in this concluding chapter.

7.1 CONCLUSIONS

Motivating this research was the general lack of knowledge on the stability characteristics of steel trapezoidal box girders, particularly during the construction stage. Numerous local failures have been observed, and several global stability failures have occurred, most notably that of the pedestrian bridge near Marcy, New York. The need for a method to predict these sorts of failures was clear.

To address these problems, a buckling analysis capability was added to an existing finite element analysis program for steel trapezoidal box girders. The existing program, UTrAp, was developed at The University of Texas at Austin, to perform linear analyses of box girder bridges during the construction stage, accounting for partially composite action between the deck and the girder. The revised program, named UTrAp 2.0, performs linearized buckling analyses of steel box-girder bridges.

The following observations can be made concerning the program:

1. UTrAp 2.0 gives accurate and valuable information on the buckling characteristics of steel trapezoidal box-girder bridges. The output from the program has been verified by comparison with theory, with commercial finite-element software, and with the failure of the Marcy pedestrian bridge.
2. UTrAp 2.0 is practical for design use. Commercial finite element programs such as ABAQUS and ANSYS can perform similar analyses, but due to the cost and time involved, they are rarely if ever used for design. Because it is designed specifically for the analysis of box-girder bridges, UTrAp 2.0 can analyze in minutes what could take hours or days to model in commercial software.
3. UTrAp 2.0 provides information not readily available from other sources. As mentioned above, the stability of steel box-girder bridges during construction is not currently well-understood. Due to this lack of information, code provisions for stability tend to treat box girders as two independent I-girders, which may not be a conservative approach in some situations. UTrAp 2.0 enables designers to directly determine stability characteristics of box-girder bridges, without reliance on design codes.
4. The finite element methods implemented in UTrAp 2.0 can be applied to other buckling analysis problems. The shell element geometric stiffness derived in this thesis can be useful in other thin-shell buckling problems. The eigensolver techniques utilized in UTrAp could also find application in other analysis problems.

7.1.1 Lateral Torsional Buckling

To complement the program, an analytical approach for predicting lateral torsional buckling in straight girders has been developed. The theoretical predictions agree closely with answers from UTrAp 2.0. Current code provisions do not consider lateral torsional buckling of the entire cross-section, the failure mode of the Marcy bridge. The equations given in chapter six provide guidance for ensuring the stability of straight steel box-girder bridges.

7.2 FURTHER RESEARCH

While UTrAp 2.0 has been shown to give accurate results for simple cases, the program has several limitations. Material behavior is assumed to be elastic, which does not allow for yielding of the steel prior to buckling. Inelastic behavior of the girder is therefore not captured by UTrAp. An improved version of the program could include material nonlinearity. Additionally, brace members in UTrAp are currently modeled as truss elements, which carry only axial forces. The element geometry is defined as a straight line between two points, which does not allow for buckling of the individual member. In reality, braces can carry moments in addition to the axial forces and will buckle under high compression forces. To accurately model this behavior, beam elements would have to be used for the brace members in UTrAp.

Using the current UTrAp program, however, much can be determined about the behavior of steel trapezoidal box-girder bridges. The investigation of global stability in this thesis addressed only straight, simply-supported girders. This is clearly a small subset of possible bridges, and actual designs will almost always be more complex. Using UTrAp 2.0, a study to determine buckling characteristics of different types of box-girder bridges could be performed.

Curved bridges require top lateral bracing, which would prevent the type of lateral torsional buckling illustrated in chapter six. Thus, curved bridges would exhibit a different type of buckling failure, which should be examined. Buckling behavior of straight and curved multiple-span bridges can also be investigated. This study could determine characteristics of negative moment section buckling behavior.

With more complicated bridge configurations and loading patterns, the availability of a validated software tool that can readily assess performance is needed because hand-based solutions under such conditions are not practical. Thus, software such as UTrAp 2.0 provides engineers with tools that allow for the safe design of desirable bridge structures.

APPENDIX A EIGENSOLVER RESOURCES

ARNCHEB

http://www.cerfacs.fr/algor/Softs/ARNCHEB/arncheb.html

ARPACK

http://www.caam.rice.edu/software/ARPACK/

IRBL

http://www.math.uri.edu/~jbaglama/

JDQR

http://www.math.uu.nl/people/sleijpen/index.html

LANCZOS

http://www.cs.ucdavis.edu/~bai/ET/lanczos_methods/lanczos_methods.html

LASO

http://www.netlib.org/laso/

LOBPCG

http://www-math.cudenver.edu/~aknyazev/software/CG/

SRRIT

http://www.cs.ucdavis.edu/~bai/ET/MVI_methods/overview_SRRIT.html

SVDpack

http://www.netlib.org/svdpack/

References

AASHTO (2003). "Guide specifications for horizontally curved steel girder highway bridges." American Association of State Highway and Transportation Officials, Washington, D.C.

AISC. (2003). *Manual of Steel Construction: Load & Resistance Factor Design.* American Institute of Steel Construction, Chicago, Illinois.

Ahmad, S., Irons, B.M., and Zienkiewicz, O.C. (1970). "Analysis of thick and thin shell structures by curved finite elements." *International Journal for Numerical Methods in Engineering*, Vol. 2, No. 3, pp. 419-451.

Bostic, S. W. (1993). "Lanczos algorithm for vibration, buckling, and thermal analysis." *Collection of Technical Papers – AIAA/ASME Structures, Structural Dynamics and Materials Conference*, Part 5, pp. 2904-2911.

Branco, F. A. and Green, R. (1985). "Composite box girder behavior during construction." *Journal of Structural Engineering*, ASCE, Vol. 111, No. 3, pp.577-593.

Buhagiar, D., Chapman, J.C., and Dowling, P.J. (1994). "Lateral torsional buckling of thin-walled beams subject to bending about the minor axis." *The Structural Engineer*, Vol. 72, No. 6, pp. 93-99.

Chen, B. S. (1999). "Top flange lateral bracing of steel U-shaped girders." Thesis presented to The University of Texas at Austin, in partial fulfillment of the requirements for the degree of Master of Science in Engineering.

Corrado, J. A., and Yen, B. T. (1973). ‘‘Failure tests of rectangular model steel box girders.’’ *Journal of the Structural Division*, ASCE, Vol. 99, No. 7, pp. 1439–1455.

Craig, R. (2000). *Mechanics of Materials*. Second Edition. John Wiley & Sons, New York.

Dabrowski, R. (1968). *Curved Thin-Walled Girders – Theory and Analysis*. Translation, Cement and Concrete Association, London.

Dongarra, J.J., Duff, I.S., Sorensen, D.C., and van der Vorst, H.A. (1998). *Numerical Linear Algebra for High-Performance Computers*. SIAM, Philadelphia.

Dowling, P. J. (1975). “Strength of Steel Box-Girder Bridges.” *Journal of the Structural Division*, ASCE, Vol. 101, No. 9, pp.1929-1947.

Ericsson, T., and Ruhe, A. (1980). “The spectral transformation Lanczos method for the numerical solution of large sparse symmetric eigenvalue problems.” Mathematics of Computation, Vol. 35, No. 152, pp. 1251-1268.

Galambos, T. V., ed. (1998). *Stability Design Criteria for Metal Structures*. Fifth edition. John Wiley & Sons, New York.

Galambos, T.V. (1968). *Structural Members and Frames*. Prentice-Hall, Englewood Cliffs, N.J.

Gilchrist, C.L. (1997). “Buckling Behavior of U-Shaped Girders.” Thesis presented to The University of Texas at Austin, in partial fulfillment of the requirements for the degree of Master of Science in Engineering.

Golub, G. H. and van der Vorst, H. A. (2000). "Eigenvalue Computation in the 20th Century." *Journal of Computational and Applied Mathematics*, Vol. 123, No. 1, pp. 35-65.

Grimes, R. G., Lewis, J. G., and Simon, H. D. (1994). "A shifted block Lanczos algorithm for solving sparse symmetric generalized eigenproblems." *SIAM Journal on Matrix Analysis and Applications*, Vol. 15, No. 1, pp. 228-272.

Kollbrunner, C.F. and Basler, K. (1969). *Torsion in Structures*. Springer-Verlag, Berlin, Germany.

Lehoucq, R.B., Sorensen, D.C., and Yang, C. (1998). *ARPACK User's Guide: Solution of Large Scale Eigenvalue Problems with Implicitly Restarted Arnoldi Methods*. SIAM, Philadelphia.

McDonald, R. E., Chen, Y., Yilmaz, C., and Yen, B. T. (1976). "Open steel box sections with top lateral bracing." *Journal of the Structural Engineering Division*, ASCE, Vol. 102, No. 1, January, pp. 35-49.

McGuire, W., Gallagher, R.H., and Ziemian, R.D. (2000). *Matrix Structural Analysis*. Second Edition. John Wiley and Sons, New York.

Parlett, B. N. (1998). *The Symmetric Eigenvalue Problem*. Society for Industrial and Applied Mathematics, Philadelphia.

Salahuddin, A. (1994). ''Design of box girder bridges by nonlinear theory.'' *Proceedings of Structures Congress '94*, ASCE, New York, pp. 491-496.

Sennah, K. M. and Kennedy, J. B. (2001). "State-of-the-art in design of curved box-girder bridges." *Journal of Bridge Engineering*, ASCE, Vol. 6, No. 3, pp. 159-167.

Sorensen, D.C. (2002). "Numerical methods for large eigenvalue problems." *Acta Numerica*, Vol. 11, pp. 519-584.

Sorensen, D.C. (1995). *Implicitly Restarted Arnoldi/Lanczos Methods for Large Scale Eigenvalue Calculations*. Rice University, Houston.

Thimmhardy, E. G. (1991). ''Nonlinear analysis of buckling behavior of steel box-girder components.'' *Computers and Structures*, Pergamon Press, Vol. 40, No. 2, pp. 469–474.

Topkaya, C. and Williamson, E.B. (2003). "Development of computational software for analysis of curved girders under construction loads." *Computers and Structures*, Vol. 81, pp. 2087-2098.

Topkaya, C., Yura, J.A., Williamson, E.B., and Frank, K.H. (2002). UTrAp: Finite-element-based Software for the Analysis of Curved Trapezoidal Girders under Construction Loads. *Report No. FHWA/TX-03/1898-3.* Texas Department of Transportation, Research and Technology Implementation Office, Austin, Texas.

Topkaya, C. (2002). "Behavior of curved steel trapezoidal box girders during construction." Dissertation presented to The University of Texas at Austin, in partial fulfillment of the requirements for the degree of Doctor of Philosophy in Engineering.

United States Steel. (1978). *Steel / Concrete Composite Box-Girder Bridges: A Construction Manual*. United States Steel, United States.

Widianto. (2003). "General Behavior of a Steel Trapezoidal Box-Girder during Construction." Thesis presented to The University of Texas at Austin, in partial

fulfillment of the requirements for the degree of Master of Science in Engineering.

Zienkiewicz, O.C. (1977). *The Finite Element Method*. Third Edition. McGraw Hill, London.

Vita

Daniel Ray Popp was born in Jefferson City, Missouri, to Richard and Debbie Popp on June 10th, 1981. After graduating from Jefferson City High School in 1999, he entered the University of Missouri in Columbia, Missouri. In 2002, the ACI Missouri Chapter recognized him with the Outstanding Undergraduate Award. During the summer of 2002, he worked at Consulting Structural Engineers, Inc. in Colorado Springs, Colorado. He received the degree of Bachelor of Science in Civil Engineering with Highest Honors on December 22nd, 2002.

In January 2003, he enrolled in the structural engineering graduate program at The University of Texas at Austin. He has been employed as a Graduate Research Assistant while pursuing his graduate degree. After graduation, he will work as a structural engineer in Honolulu, Hawaii.

Permanent Address: 4915 State Highway 94
Tebbetts, MO 65080

This thesis was typed by the author.